The Hashemite Kingdom of Jordan
Scientific Research Support Fund
The Hashemite University

# JJEES

## Jordan Journal of Earth and Environmental Sciences

Volume (10) Number (4)

Cover photo © Dr. Ahmed Gharaibeh

JJEES is an International Peer-Reviewed Research Journal

ISSN 1995-6681 jjees.hu.edu.jo December 2019

# Jordan Journal of Earth and Environmental Sciences (JJEES)

JJEES is an International Peer-Reviewed Research Journal, Issued by Deanship of Scientific Research, The Hashemite University, in corporation with, the Jordanian Scientific Research Support Fund, the Ministry of Higher Education and Scientific Research.




## Submission address:

Manuscripts should be submitted electronically to the following e-mail:

**jjees@hu.edu.jo**

For more information and previous issues:

**www.jjees.hu.edu.jo**

Hashemite Kingdom of Jordan

Scientific Research Support Fund

Hashemite University

# Jordan Journal of Earth and Environmental Sciences

# JJEES

*An International Peer-Reviewed Scientific Journal*

*Financed by the Scientific Research Support Fund*

Volume 10 Number (4)

http:// jjees.hu.edu.jo/

ISSN 1995-6681

Cover page photo: Dead Sea Salt crystallization, by the Dr. Ahmed Gharaibeh

المجلة الأردنية لعلوم الأرض والبيئة
Jordan Journal of Earth and Environmental Sciences (JJEES)
http://jjees.hu.edu.jo

# Hashemite University

## Deanship of Scientific Research

## TRANSFER OF COPYRIGHT AGREEMENT

**Journal publishers and authors share a common interest in the protection of copyright: authors principally because they want their creative works to be protected from plagiarism and other unlawful uses, publishers because they need to protect their work and investment in the production, marketing and distribution of the published version of the article. In order to do so effectively, publishers request a formal written transfer of copyright from the author(s) for each article published. Publishers and authors are also concerned that the integrity of the official record of publication of an article (once refereed and published) be maintained, and in order to protect that reference value and validation process, we ask that authors recognize that distribution (including through the Internet/WWW or other on-line means) of the authoritative version of the article as published is best administered by the Publisher.**

**To avoid any delay in the publication of your article, please read the terms of this agreement, sign in the space provided and return the complete form to us at the address below as quickly as possible.**

**Article entitled:----------**

**Corresponding author: ----------**

**To be published in the journal: Jordan Journal of Earth & Environmental Sciences (JJEES)**

**I hereby assign to the Hashemite University the copyright in the manuscript identified above and any supplemental tables, illustrations or other information submitted therewith (the "article") in all forms and media (whether now known or hereafter developed), throughout the world, in all languages, for the full term of copyright and all extensions and renewals thereof, effective when and if the article is accepted for publication. This transfer includes the right to adapt the presentation of the article for use in conjunction with computer systems and programs, including reproduction or publication in machine-readable form and incorporation in electronic retrieval systems.**
**Authors retain or are hereby granted (without the need to obtain further permission) rights to use the article for traditional scholarship communications, for teaching, and for distribution within their institution.**

☐ **I am the sole author of the manuscript**

☐ **I am signing on behalf of all co-authors of the manuscript**

☐ **The article is a 'work made for hire' and I am signing as an authorized representative of the employing company/institution**

**Please mark one or more of the above boxes (as appropriate) and then sign and date the document in black ink.**

**Signed:**_____ **Name printed:** _____

**Title and Company (if employer representative) :** _____

**Date:** _____

**Data Protection: By submitting this form you are consenting that the personal information provided herein may be used by the Hashemite University and its affiliated institutions worldwide to contact you concerning the publishing of your article.**

**Please return the completed and signed original of this form by mail or fax, or a scanned copy of the signed original by e-mail, retaining a copy for your files, to:**

**Deanship of Scientific Research**
**The Hashemite University P.O. Box 150458, P.C.13115, Zarqa, Jordan**
**Tel.: 00962 53903333/ Ext. 4235**
**Fax: 00962 53826823**
**E-mail: jjees@hu.edu.jo**

Subscription

Jordan Journal of Earth & Environmental Sciences (ISSN 1995-6681)
An International Peer- Reviewed Research Journal
Published by the Deanship of Scientific Research - The Hashemite University

| | |
|---|---|
| Name: ..... | الاســـــــــــم: |
| Specialty:..... | التخصـــــــــص: |
| Address:..... | العنـــــــــوان: |
| P.O. Box:..... | صنـــدوق البريـــــد: |
| City & Postal Code: ..... | المدينة: الرمز البريدي: |
| Country:..... | الـــــــــــدولة: |
| Phone:..... | رقـــم الهاتـــــف: |
| Fax No:..... | رقـــم الفاكـــــس: |
| E-mail:..... | البريـــد الإلكترونـــي: |
| Method of payment: ..... | طريقـــــة الدفـــع: |
| Amount Enclosed:..... | المبلـــغ المرفـــق: |
| Signature:..... | التوقيـــــــــع: |

Cheques should be paid to Deanship of Research - The Hashemite University

I would like to subscribe to the Journal:

**For**

- ☐ One year
- ☐ Two years
- ☐ Three years

One year Subscription Rates

| | Inside Jordan | Outside Jordan |
|---|---|---|
| Individuals | 10JD | 70$ |
| Students | 5JD | 35$ |
| Institutions | 20JD | 90$ |

Correspondence

**Subscriptions and sales:**

Professor Fayez Ahmad
Deanship of Scientific Research
The Hashemite University P.O. Box 150458, P.C.13115, Zarqa, Jordan
Tel.: 00962 53903333/ Ext. 4235
Fax: 00962 53826823
E-mail: jjees@hu.edu.jo

JJEES
Jordan Journal of Earth and Environmental Sciences

JJEES

JJEES (2019) 10 (4): 187-193
ISSN 1995-6681

Jordan Journal of Earth and Environmental Sciences

# Potential Artificial Recharge to a Semi-arid Basin: A Case Study in a Shallow Groundwater Aquifer, South of West Bank, Palestine

Abdelhaleem Khader*, Radwan El-Kelani, Sameer Shadeed

*An-Najah National University, Faculty of Engineering, Department of Civil Engineering, Palestine*

*Received 17 December 2017; Accepted 23 February 2019*

**Abstract**

Groundwater is the main source of fresh water for domestic and agricultural uses in Palestine. Increased dependence on groundwater demonstrates the dire need to improve aquifer management in terms of understanding and controlling recharge and discharge issues. An artificial groundwater recharge feasibility study was proposed as one of the viable options to halt the decline of groundwater storage in Wadi Abu Al-Qamrah (WAAQ) area located in Hebron, south of the West Bank. Artificial recharge provides natural storage with minimum surface area requirements. It also minimizes evaporation loss, improves water quality, and utilizes surplus surface water runoff. The geology, soil, land cover, and natural streams were mapped using GIS and spatial analysis techniques. Geologic, hydrologic, and piezometric analyses were performed to support the decision. The geological investigation shows that there are two dominant geological formations in the study area: The Cenomanian formation at the foothills east and west, and the lower Cenomanian formation down in the valley. The hydrological analysis using the SCS-CN method indicates that the annual runoff generation in the catchment is estimated at about 0.33 MCM, among which, 70% comes from the upper urbanized part. The piezometric analysis obtained from monitoring the water level in thirty-three dug wells showed that in a short period of time, three months after the end of the rainy season, water table elevation was being declined at about 8 meters. This can be attributed to excessive abstraction. Based on the results of these analyses, several artificial recharge methods were proposed to check their suitability for the study area. The injection wells method was found to be the most suitable for WAAQ. This will enhance the sustainable groundwater management in the West Bank. To achieve this objective, a design well for the injection process is proposed. The potential locations the injection wells have been suggested based on the hydrological and geological analyses.



**Keywords:** Artificial recharge, Geographical Information System, Piezometric maps, Hydrological modeling, West Bank, Palestine

## 1. Introduction

The artificial groundwater recharge aims at modifying the natural movement of surface water by utilizing proper structures, to replenish depleted groundwater aquifers due to excessive pumping. In the West Bank, groundwater is the main source of water for domestic and agriculture uses, and provides more than 90% of all water supplies (PWA, 2013). Recently, the increasing demand on groundwater to satisfy the increasing water needs for domestic and agricultural uses, makes Palestine suffers from the limited water resources. Moreover, the problem of water shortages is exacerbated by the fact that shared water resources in Palestine are controlled by the Israelis, a situation that fuels tensions over water rights and makes water a significant political issue (Haddad and Mizyed, 1996; El-Fadel et al., 2001). In arid and semi-arid regions of the world, the shortage of water is a major limiting factor for economic and social development. In such regions including Palestine, almost any development of the aquifers constitutes over-abstraction conditions. This is due to the fact that groundwater is the only reliable and renewable source of fresh water for human life and development in the absence of perennial surface water (Abdin, 2006; Al-Assa'd and Abdulla, 2009; Shadeed, 2012). Thus, increased dependence on groundwater needs improved aquifer management with respect to understanding recharge and discharge issues (Tompson et al., 1999). Rainfall is the main source of groundwater recharge. In the West Bank, rainfall is characterized by high temporal and spatial variations. This can be attributed to the variable topographic features and climatic conditions. On the other hand, the amount of groundwater available for domestic and agricultural uses has been declining, and its quality has been deteriorating due to excessive pumping and the improper disposal of untreated wastewater (Shadeed et al., 2016). Therefore, comprehensive water management strategies have to be adopted to bridge the increasing water supply-demand gap for both domestic and agricultural uses. Hence, artificial groundwater recharge is one of the potential water management options aiming at bridging the gap between the very limited available water resources and the increased water demand resulting from the expanding human activities. This technique had been used since the eighteenth century and has started to be in use, recently on a large scale as a new non-conventional water resource (Helweg, and Smith, 1978; Asano, 1985; Pyne, 1994). Consequently, artificial recharge in arid and semi-arid regions including Palestine can play an important role in

* Corresponding author e-mail: a.khader@najah.edu

conserving its water resources and avoiding the depletion of the existing aquifers (Al-Assa'd and Abdulla, 2009; Ghanem, 2011; Shadeed et al., 2011; Hamdan, 2012; El Arabi, 2012)

The main objective of this research is to assess the feasibility of adopting artificial groundwater recharge techniques in order to enhance groundwater resources. The methodology of the research will be applied in Wadi Abu Al-Qamrah (WAAQ) located in the southern part of the West Bank as part of the eastern aquifer basin (Figure 1).

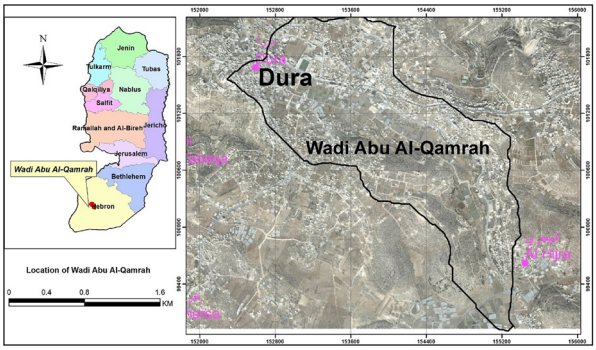


**Figure 1.** Location map of the study area.

## 2. Study area

### *2.1. Geography and Topography*

WAAQ is located in the city of Dura (Figure 1), about 7 Km west of the city of Hebron in the southern part of the West Bank. With an area of about 4.3 km$^2$, the Wadi lies within 35$^o$ 03' 21"and 35$^o$ 01' 42" longitude, and within 31$^o$ 29' 09" and 31$^o$ 30' 34" latitude (between 152-156 E and 99-102 N referenced on the Palestinian grid). This Wadi is a sub-catchment of Besor-Nar catchment, which drains into the Mediterranean Sea (Shadeed and Almasri, 2010). Figure 2 shows that the land surface elevation in WAAQ varies between 897 and 738 m AMSL (above mean sea level).

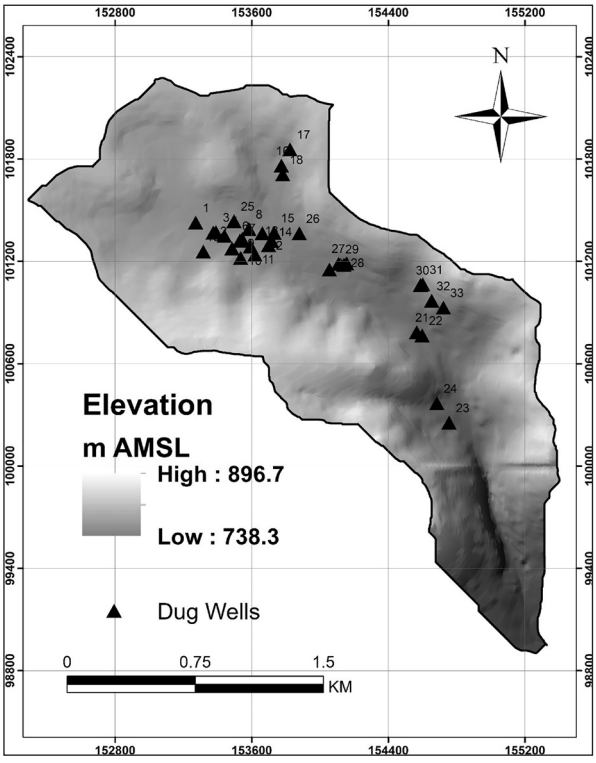


**Figure 2.** Topographic map of the study area (GeoMOLG 2016).

### *2.2. Geology and Soil*

The geological map of WAAQ (Figure 3) shows that there are two dominant geological formations: The Cenomanian formation at the foothills east and west, and the lower Cenomanian formation down in the valley (Abed and Wishahi, 1999). The Cenomanian (Hebron) Formation is composed of brittle karistified gray dolomite, dolomitic limestone, and gray limestone. At its base, it is formed of hard dolomite and dolomitic limestone with some silicification. The lithology is uniform since dolomite and dolomitic limestone are found throughout the sequence of Hebron Formation. The porosity of this Formation is mainly secondary because the rocks are well jointed and karistified. The Hebron Formation is, without doubt, the most important aquifer within the West Bank. Its Vertical thickness ranges between 70 and 120 m. On the other hand, the Lower Cenomanian (Yatta) Formation, 86 m to128, acts generally as an aquiclude, and separates the Cenomanian aquifer from the Albian aquifer underlying it.

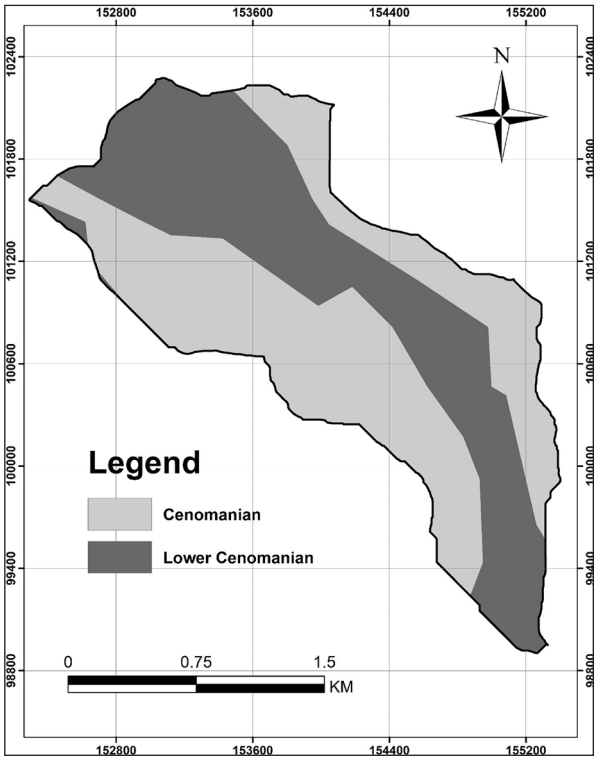


**Figure 3.** Geological map (GeoMOLG 2016).

The study area has only one soil class which is clay, in particular Terra Rossa Clay, stemming from dolomite and hard limestone. The soil cover has a reddish brown color and its depth varies between 0.5 and 2 meters (Abed and Wishahi, 1999).

### *2.3. Climate and Hydrology*

The area of Hebron Governorate including WAAQ has a Mediterranean climate with hot and dry summers and mild and wet winters. The average daily mean temperature ranges from 22 °C in summer to 7 °C in winter. Average daily maximum temperatures range from 27 °C to 10 °C and minimum temperatures from 17 °C to 4 °C in the summer and winter respectively. The daily relative humidity fluctuates between 48% and 75%. The average wind speed ranges from 4 m/s to 6.4 m/s. The typical potential evaporation ranges

from 62 mm in December to 225 mm in August (PMD, 2017).

Based on the available rainfall data at Dura rainfall station for the last 10 years (Table 1), the annual rainfall varies from 284 mm to 587 mm, with an average of 507 mm. Most of the rainfall occurs in the period from October to April, the rest of the year being completely dry.

**Table 1.** Annual rainfall in Dura, Hebron

| Rainy Season | Total Rainfall (mm) |
|---|---|
| 2004/2005 | 587 |
| 2005/2006 | 357 |
| 2006/2007 | 570 |
| 2007/2008 | 284 |
| 2008/2009 | 342 |
| 2009/2010 | 508 |
| 2010/2011 | 315 |
| 2011/2012 | 568 |
| 2012/2013 | 456 |
| 2013/2014 | 514 |

### *2.4. Land Cover*

The land cover map of WAAQ (Figure 4) shows that the higher areas at the foothills are mainly occupied by urban built-up zones. The valley and the southern part of the study area are mainly used for different types of agriculture. Politically, WAAQ is divided into three sovereignty zones according to Oslo Accord (Figure 5).

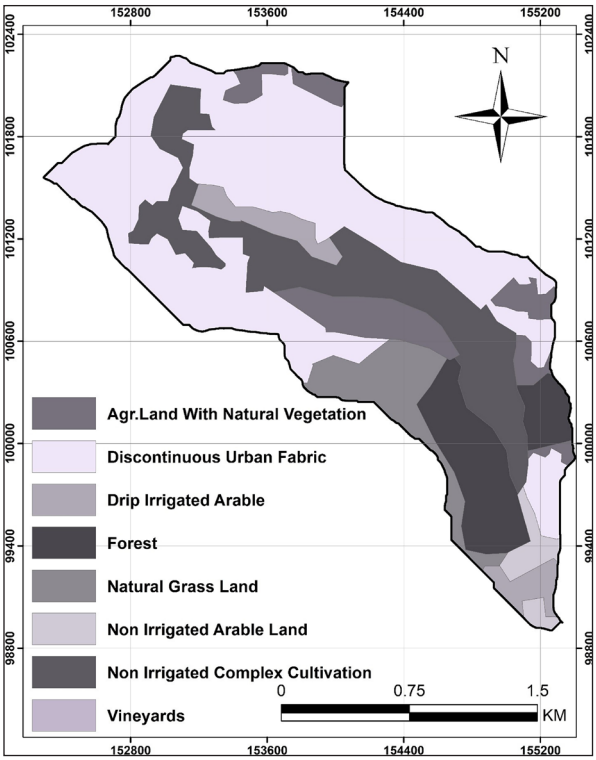


**Figure 4.** Land cover map of the study area.

## 3. Results and discussion

### *3.1. Borehole Logs*

Six boreholes were selected to be drilled in the study area; the borehole locations (Figure 5) were chosen to facilitate the drawing of a geological cross section (Figure 6a) and a profile (Figure 6b) in order to understand the geological layers along and across the valley. Based on the aerial photograph, the locations should be easily accessible; meanwhile, sovereignty zones according to Oslo Accord (Figure 5) causes constrains concerning the selection of the sites.

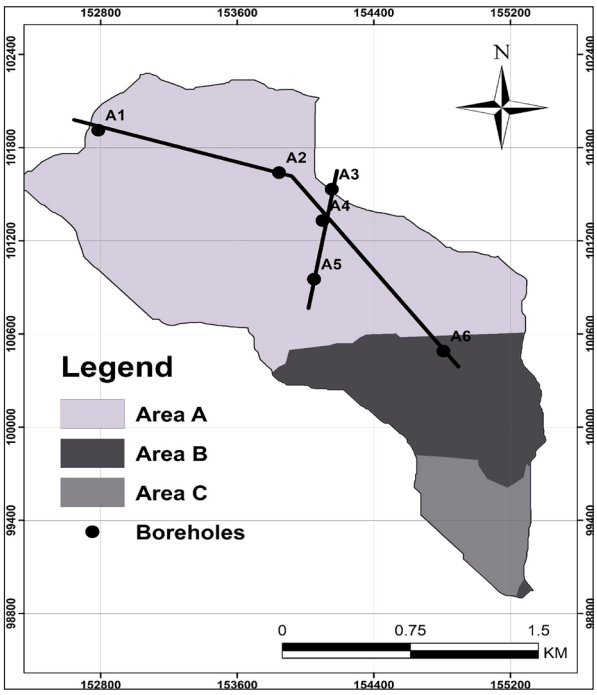


**Figure 5.** Borehole locations and 2 Sovereignty borders in the study area according to Oslo Accord; zone A: land of Palestinian administrative control and security authority zone B: land of Palestinian administrative control and Israeli security control zone C: land of full Israeli administrative and security control (GeoMOLG 2016).

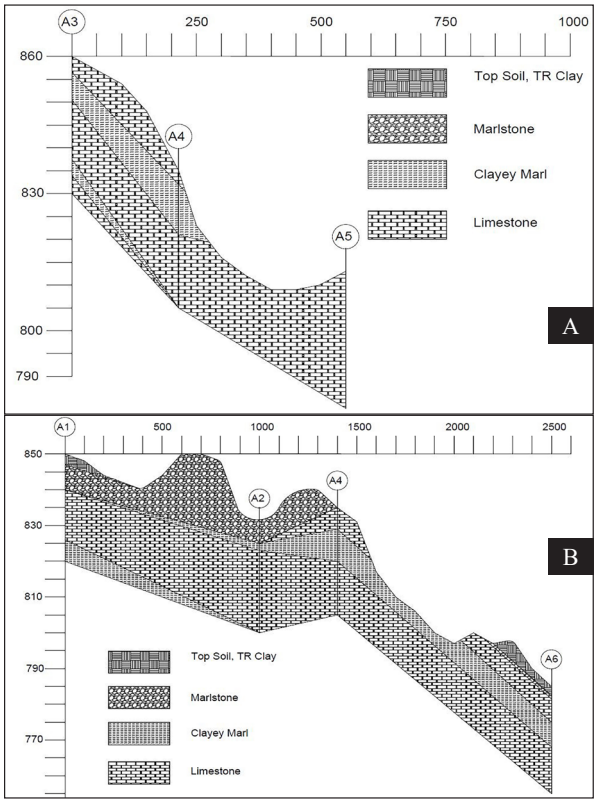


**Figure 6.** Geological Cross Section (a), and Geological Profile (b).

### *3.2. Hydrological analysis*

#### *3.2.1. Catchment delineation*

Before conducting any hydrological study of the catchment, first, the catchment needs to be delineated. The availability of a digital elevation model (DEM), with adequate spatial resolution to cover the whole area of interest, is a basic requirement to achieve the delineation (Bertolo, 2000). The required DEM for this study was obtained from GeoMOLG, 2016. State of the art ArcHydro Tools 2.0, which is an extension of ArcGIS 10.1, was used to delineate the catchment and sub-catchments, and to define the drainage networks (natural streams). Figure 7 shows the distribution of these streams and sub-catchments.

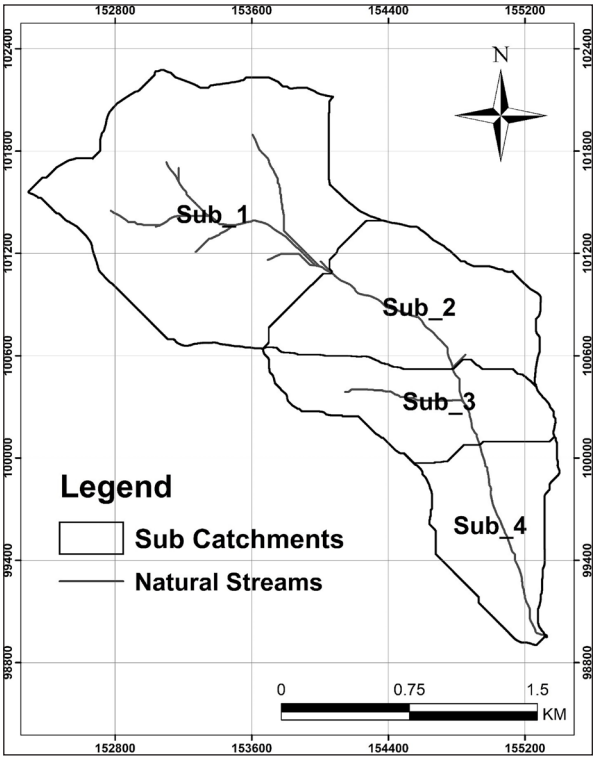


**Figure 7.** Natural streams and sub-catchments of WAQ.

#### *3.2.2. Hydrological Modelling*

The objective of this step is to estimate the surface water runoff from each sub-catchment. To do so, the SCS-CN method was used. The SCS-CN method is one of the most popular methods for computing the volume of surface runoff in catchments for a given rainfall event (Schulze et al., 1992; Shadeed and Almasri, 2010). This approach involves the use of a simple empirical formula and readily available tables and curves. A high curve number means high runoff and low infiltration (urban areas); whereas a low curve number means a low runoff and high infiltration (dry soil). The curve number is a function of land use and hydrologic soil group (HSG). It is a method that can incorporate land use for the computation of runoff from rainfall. The SCS-CN method provides a rapid way to estimate the change in the runoff due to changes in land use.

The standard SCS-CN method is based on the following relationship between rainfall, P (mm), and runoff, Q (mm):

$$Q = \begin{cases} \dfrac{(P - I_a)^2}{P - I_a + S} & P > I_a \\ 0 & P \le I_a \end{cases} \quad \ldots\ldots\ldots\ldots\ldots\ldots\ldots\ldots (1)$$

where S (mm) is the potential maximum retention after runoff begins. Through the studies of many small agricultural catchments, $I_a$ was found to be approximated by empirical equations such as

$I_a = 0.2 \times S.$

The variable S, which varies with antecedent soil moisture and other variables, can be estimated as:

$$S = \frac{25\,400}{CN} - 254. \quad \ldots\ldots\ldots\ldots\ldots\ldots\ldots\ldots (2)$$

where CN is a dimensionless catchment parameter ranging from 0 to 100. A CN of 100 represents a limiting condition of a perfectly impermeable catchment with a zero retention, in which all rainfall becomes runoff. Conceptually, a CN of zero represents the other extreme, with the catchment abstracting all rainfall and with no runoff regardless of the rainfall amount.

For WAAQ, CN values for the four sub-catchments were obtained by modifying the CN value for Besor-Nar catchment to take into account the percentage of built-up areas in each sub-catchment. Table 2 shows the CN value and the area of each sub-catchment.

**Table 2.** Sub-catchment characteristics

| Sub-catchment | CN Value | Area (Km$^2$) |
|---|---|---|
| Sub-1 | 78 | **2.024** |
| **Sub-2** | 65 | **0.956** |
| **Sub-3** | 52 | **0.674** |
| **Sub-4** | 65 | **0.636** |

To apply the SCS-CN method to WAAQ in order to estimate surface water runoff from each sub-catchment, daily rainfall values are needed.

Table 3 shows the results of applying the SCS-CN method to WAAQ sub-catchments for the 2015/2016 rainfall (which is a typical rainy season with 604.4 mm of rainfall). As shown in the results, Sub-1 has the highest runoff/rainfall ratio and the largest volume of runoff. This is due to the large percentage of built-up areas (higher CN value) in this sub-catchment and its large area compared to the other sub-catchments.

**Table 3.** Runoff values using SCS-CN method

| Sub-catchment | Runoff Depth (mm) | Runoff Volume (1000 m$^3$) | Runoff/Rainfall Ratio% |
|---|---|---|---|
| **Sub-**1 | 113.2 | 229.2 | **18.7** |
| **Sub-2** | 55.1 | 52.7 | **9.1** |
| **Sub-3** | 20.5 | 13.8 | **3.4** |
| **Sub-4** | 55.1 | 35.1 | **9.1** |
| **Total** | | **330.8** | |

A high runoff/rainfall ratio in an area indicates a higher runoff and a lower natural recharge in that area, and vice versa. Sub-1 has the highest Runoff/Rainfall ratio in the study area, which indicates that this sub-catchment is more suitable for artificial recharge infrastructure. This is because natural recharge in this sub-catchment is lower, most likely as there is more "room" available for artificial recharge, and because of the availability of more water for recharge from surface runoff.

### 3.3. Piezometric Analysis

There are forty-six dug wells in WAAQ from which around 170,000 $m^3$of water is being extracted annually; data are available for thirty-three of these wells. Figure 2 shows the locations of these dug wells along the valley. The piezometric water levels in the thirty-three dug wells were monitored seven times between 18/5/2016 and 15/8/2016. The data were interpolated using the inverse distance weighted (IDW) method. The piezometric surface elevation was calculated by subtracting the interpolated depth-to-water surface readings from the surface elevations obtained from the DEM. The piezometric level was the highest on May, 18th, only one month following the rainy season. It started to decline after that. Figure 8 shows that this decline could reach up to 10 meters especially in the southern part of the valley. It is also noted from Figure 8 that the decline in some of the dug wells is significantly higher compared to others. This variability in decline may be attributed to the variability in actual abstraction rates from these dug wells.

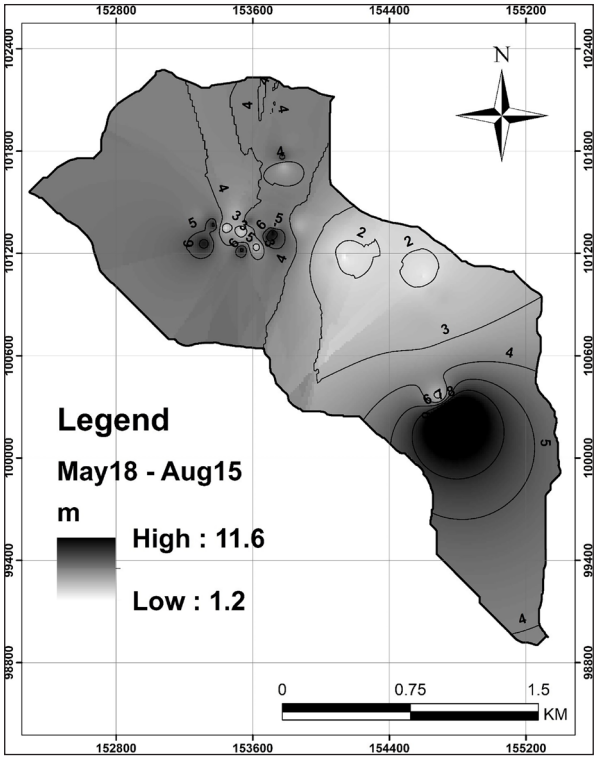


**Figure 8.** The decline in Piezometric level between May 18th and August 15th 2016.

### 3.4. Groundwater Recharge Scenarios

Due to variation in rainfall and the limited surface water resources, groundwater has become the main source of freshwater in many parts of the world including Palestine. However, the amount of water that percolates to groundwater varies greatly from region to region and from place to place within the same region depending on the amount and pattern of rainfall (i.e. number and duration of rainy days, rainfall amount and intensity), the characteristics of soils and rocks (i.e. porosity, cracks and loose joints in rocks etc.), the nature of terrain (i.e. hills, plateaus, plains, valleys etc.), as well as other climatic factors including temperature and humidity. As a result, the availability of groundwater varies considerably from place to place.

In order to improve the groundwater situation, it is necessary to artificially recharge the depleted groundwater aquifers. The advantages of artificial recharge are listed below (Ravichandran et al., 2011):

- No need for large storage structures to store water. The structures required are small and cost-effective
- Enhancement of the dependable yield of wells
- Negligible losses compared to losses in surface storages
- Improved water quality due to dilution of harmful chemicals/salts
- No adverse effects such as the inundation of large surface areas and loss of crops
- No displacement of local populations
- Reduction in the cost of energy for lifting water especially where rise in groundwater level is substantial
- Utilization of the surplus surface runoff which, otherwise, drains off

Artificial groundwater recharge is usually applied where groundwater level is declining and where groundwater quality is poor. The source of water for recharge includes rainfall, surface runoff, and properly-treated wastewater. However, there are factors that should be taken into consideration in order to assess the source of water such as quantity, quality, timing, and convenience (Kumar, 1997).

Another factor that should be considered is the infiltration capacity rate of the soil, which governs the rate of recharge. In addition to that, the aquifer characteristics such as storage coefficient, availability of storage space, and permeability, are important factors to assess the suitability of the aquifer for artificial recharge.

Furthermore, the unsaturated thickness of rock formations occurring beyond 3 meters below the ground level should be considered for recharge. Usually, the upper 3 meters of the unsaturated zone are not considered for recharge, since it may cause adverse environmental impacts such as water logging and soil salinity (Kumar, 1997).

There are various methods for artificial recharge ranging from simply modifying the land surface to the technically advanced injection wells (Ravichandran et al., 2011). After investigating these methods, recharge shafts have been found to be the efficient alternative to be considered. But the problem concerning this is that the shaft needs to be drilled exactly in a fracture in the aquifer which is almost impossible to locate in advance. This means that injection wells are the most effective method for confined aquifers and fractured hard rocks, which is the case in this study area.

## 4. Conclusions and recommendations

As mentioned earlier, injection wells are the most effective method for confined aquifers and fractured hard rocks, which is the case in WAAQ. Thus, the following strategies are proposed:

1- A design well for the injection process, as shown in Figure 9, can be adopted for the artificial recharge mechanism. The estimated cost of one well of this proposed design is detailed in Table 4.

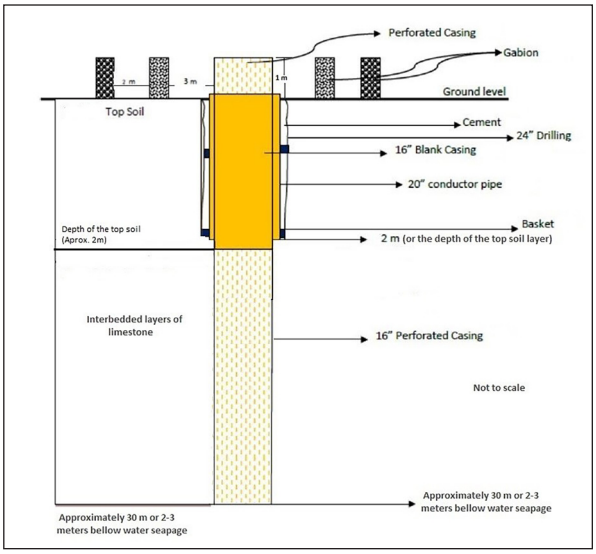


**Figure 9.** Proposed injection well design.

**Table 4.** Estimated cost details for the proposed design

| Item | Unit | Unit Cost ($US) | Quantity | Cost ($US) |
|---|---|---|---|---|
| 24" drilling | m | 300 | 30 | 9,000 |
| Gabion 1 (15-20 cm stones) | m | 200 | 20 | 4,000 |
| Gabion 2 (7-15 cm stones) | m | 200 | 12 | 2,400 |
| Cement grouting | $m^2$ | 100 | 5 | 500 |
| 16" blank casing | m | 150 | 2 | 300 |
| 20" conductor pipe | m | 100 | 2 | 200 |
| Pump (injection well) | unit | 700 | 1 | 700 |
| Screen (perforated casing) | m | 200 | 30 | 6,000 |
| **Total** | | | | 23,100 |

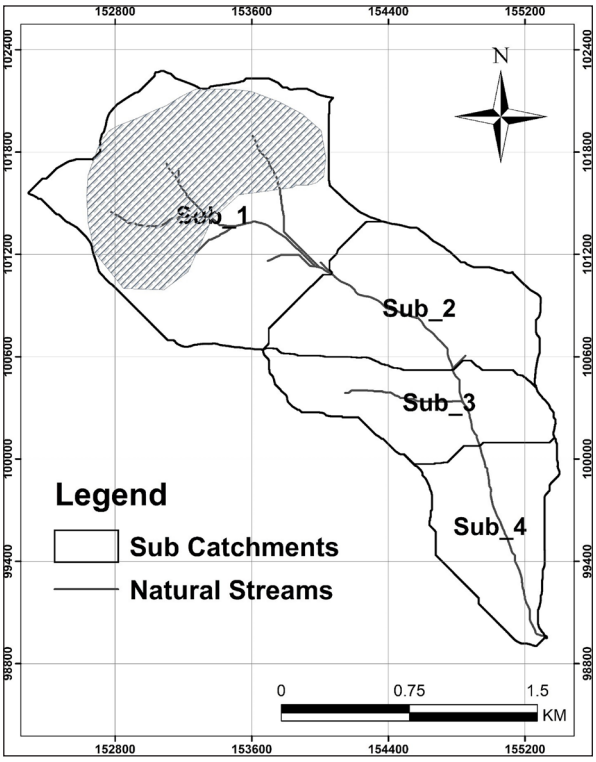


**Figure 10.** Proposed locations (shaded area) for injection wells.

2- Based on the hydrological and geological analysis, the suggested locations of the proposed injection wells are in the shaded area of Figure 10. The justification of choosing this approximate area is that it is located in sub- 1 (see the hydrological Analysis in Section 3.2), and it is in the upper area where the confining clayey marl layer is thinning (see Figure 6). It should be noted here that the injection wells could be theoretically located anywhere in the study area, but in the suggested area they are closer to the source of water (runoff in Sub-1).

**Acknowledgement**

The authors would like to acknowledge the Union of Agricultural Work Committee (UAWC), Ramallah, Palestine for providing the relevant information needed for this research. The authors also would like to thank the French decentralized cooperation for sponsoring the field work.

**References**

Abdin, S. (2006). Qantas a unique groundwater management tool in arid regions, the case of Bam Region in Iran. International symposium on groundwater sustainability.

Al-Assa'd, T., and Abdulla F. (2009). Artificial groundwater recharge to a semi-arid basin: case study of Mujib aquifer, Jordan. Environmental Earth Sciences, 60: 845–859.

Abed, A., and Wishahi, S. (1999). Geology of palestine: the West Bank and Gaza Strip, Palestine. Palestine Hydrology Group (PHG), Ramallah, West Bank, Palestine

Asano, T. (1985). Artificial recharge of groundwater. Butter worth Publishers, Boston, 767 p.

Bertolo, F. (2000). Catchment delineation and characterization, a Review. Space Applications Institute. An Activity of the Euro Landscape Project.

British Geological Survey (2005). A New Map for the West Bank, NERC.

Dura Municipality (2016). Unpuplished report.

El Arabi, N. (2012). Environmental management of groundwater in Egypt via artificial recharge extending the practice to soil aquifer treatment (SAT). International Journal of Environment and Sustainability, 1(3): 66–82.

El-Fadel, M., Quba'a, R., Al-Hougeiri, N., Hashisho, Z. Jamali, D. (2001). The Israeli Palestinian Mountain Aquifer: A Case Studyin Ground Water Conflict Resolution J. Nat. Resour. Life Sci. Educ. 30: 50–61.

GeoMOLG. (2016). The Integrated Spatial Information System of the Palestine Ministry of Local Government. Accessed 2016

Ghanem, M., Marei, A., Hoetzl, H., Wolf, L., Ali, W., Assi, A. (2011). Assessment of artificial recharge test in Jeftlik-Faria area, West Bank. Journal of Water Resource and Protection, 3: 186–191.

Haddad, M., and Mizyed, N. (1996). Water resources in the Middle East: conflict and solutions. p. 3.17. In J.A. Allan (ed.) Water, peace and the Middle East: Negotiating resources in the Jordan basin. Taurus Academic Studies, New York.

Hamdan, S. (2012). Artificial recharge of groundwater with stormwater as a new water resource-case study of the Gaza Strip, Palestine. PhD Thesis, Institute of Applied Geosciences, Berlin Technical University, Berlin.

Helweg, O., and Smith, G. (1978). Appropriate technology for artificial aquifers, Groundwater, 16(3): 144–148.

Kumar, C.P. (1997). Estimation of natural ground water recharge. ISH Journal of Hydraulic Engineering 3(1): 61–74.

PHG, Palestinian Hydrological Group (2013). Groundwater Artificial Recharge, The Marj Sanour Watershed.

Palestinian Meteorological Department (2016). www.pmd.ps, Accessed 2016

Pyne, R. (1994). Groundwater Recharge and Wells: A Guide to Aquifer Storage and Recovery, Lewis Publishers, Florida.

PWA, Palestinian Water Authority (2013). Status report of water resources in the occupied state of Palestine, year of flood water harvesting, Annual Report. Ramallah, Palestine.

Qannam, Z. (2003). A hydrogeological, hydrochemical and environmental study in Wadi Al Arroub drainage basin, south West Bank, Palestine. Freiberg On-line Geosciences. Vol.9

Ravichandran, S., Sathish Kumar, S., Singh, L. (2011). Selective techniques in artificial ground water recharge through dug well and injection well methods .International Journal of ChemTech Research, 3(3): 1050–1053.

Schulze, R.E., Schmidt, E.J., Smithers, J.C. (1992). SCS-SA User Manual PC Based SCS Design Flood Estimates for Small Catchments in Southern Africa. Pietermaritzburg: Department of Agricultural Engineering, University of Natal.

Shadeed, S., and Almasri, M. (2010). Application of GIS-based SCS-CN method in West Bank catchments, Palestine.Water Science and Engineering, 3(1): 1–13.

Shadeed, S. (2012). Spatio-temporal drought analysis in arid and semi-arid regions: A case study from Palestine, The Arabian Journal for Science and Engineering. 38: 2303–2313, doi: 10.1007/s13369-012-0504-y.

Shadeed, S., Sawalhah, M., Abu Jaish, A., Haddad, M., Alawneh, A., Abboushi, A., Doraidi, D., Homeidan, M. (2011). Overview of quantity and quality of water resources in the Faria catchment, Palestine. International Graduate Conference on Science, Humanities and Engineering. An-Najah National University, Nablus, Palestine. 38–51.

Shadeed, S., Sawalhah, M., Haddad, M. (2016). Assessment of groundwater quality in the Faria catchment, Palestine. An - Najah Univ. J. Res. (N. Sc.), 30: 81–100.

Tompson, A., Carle, F., Rosenberg D., Maxwell, M. (1999). Analysis of groundwater migration from artificial recharge in a large urban aquifer: a simulation perspective. Water Resour. Res. 35 (10): 2981-2998.

JJEES

JJEES (2019) 10 (4): 194-203
ISSN 1995-6681

Jordan Journal of Earth and Environmental Sciences

# Depositional Environment and Storage Capacity of Eocene Carbonate Rocks, South Western Sinai, Egypt

Atef Ibrahim[1], Asha Abou El Ezz[2],
Tarek El Hariri[2*], Ahmed Mousa[2], Ahmed Abd El-Ghany[2]

[1]Al Azhar University, Faculty of Science, Geology Department, Egypt
[2]Egyptian Petroleum Research Institute, Exploration Department, Egypt

Received 15 January 2019; Accepted 23 February 2019

**Abstract**

The main objective of the present study is to shed light on the lithostratigraphy, microfacies association, depositional environment, and the petrophysical characteristics of the Eocene carbonate rocks in southwestern Sinai, Egypt. The study area is represented by two examined sections, namely Wadi Tayiba and Wadi Feiran (from older to younger): Thebes, (Samalute equivalent Darat), Khaboba and Tanka. In this study, five microfacies were identified. These microfacies are: pellitiferous micrite, micrite, foraminiferal biomicrite, argillaceous micrite, and fossiliferous micrite. These are deposited in a platform and an open marine occurrence on the inner ramp. The obtained petrophysical results show that the Darat Formation at the Wadi Tayiba area and the Thebes Formation at the Wadi Feiran area possess the best storage capacity of the Eocene carbonate rocks in the studied area.



**Keywords:** Microfacies associations, Depositional environments, Petrophysical characteristics, Eocene carbonate rocks, Southwestern Sinai, Egypt.

## 1. Introduction

The present study deals with petrography, the paleo-depositional, environmental, and petrophysical characteristics of the Eocene carbonate rocks exposed at Southwestern Sinai along the Western side of the Gulf of Suez. The study area lies between latitudes 28º 40' 00" and 29º 10' 00" N. and longitudes 33º 00' 00" and 33º 30' 00" E. (Fig 1). The Eocene succession had been studied by several authors. Said (1990) suggested that the Eocene sediments along the Eastern side of the Gulf of Suez which are correlated with the observed sub-group, are of a limited distribution. They are represented by the deposits of Khaboba Formation. Abul-Nasr (1993 a) re-evaluated the middle upper Eocene biostratigraphy of the successions exposed at Wadi Tayiba, Wadi Matulla and Wadi Nukhul. He differentiated between the Thebes, Darat, Khaboba, and Tayiba Formations. Abul-Nasr (1993 b) recorded, for the first time, the Globigerintheka semiinvoluta zone in the Upper part of the Khaboba Formation at Wadi Warden which he assigned to the presence of the Upper Eocene in Sinai. Magdy (1997) studied the Eocene rocks in Southwest Sinai, and concluded that the conditions which prevailed during their deposition varied rapidly from South to North especially during the Middle Eocene. Ibrahim et al. (2016 a) suggested that the Eocene limestone rocks were mostly deposited under relatively warm alkaline conditions. However, the pH degrees of alkalinity during the deposition for the Darat Formation (Wadi Tayiba area) and the Thebes and Samalut Formations (Wadi Reiran area) (less in $SiO_2$ content) were higher than those which prevailed during the times of the Thebes, Khaboba, and Tanka Formations (Wadi Tayiba area). Ibrahim et al. (2016 b) concluded that the Eocene marine basin of deposition was relatively alkaline, close to the landmass that supplied the basin of deposition by quartz and clay.

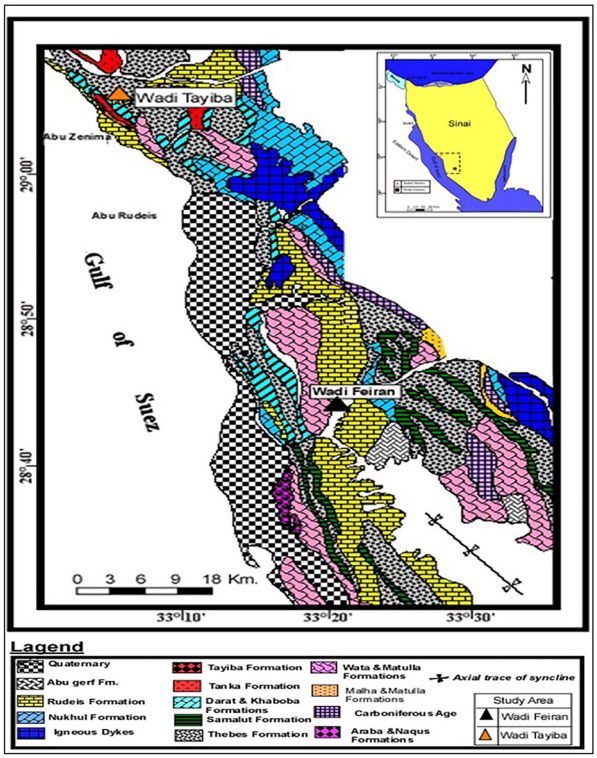


**Figure 1.** Location and geological maps of the study area (After Conoco, 1992).

* Corresponding author e-mail: el_hariri@yahoo.com

## 2. Materials and methods

The present work is focused on petrography, paleo-depositional, environmental and petrophysical characteristics of the Eocene carbonate rocks at Wadi Tayiba and Wadi Feiran areas to determine the best storage capacity. The samples were prepared and measured in the Egyptian Petroleum Research Institute (EPRI) as follows:

Sixty three thin sections were prepared (twenty six samples from Wadi Tayiba and thirty seven from Wadi Feiran) for the petrographic studies of Eocene carbonate rocks, to determine the mineralogical composition, microfacies, and paleo-depositional environment.

Forty-nine samples (sixteen samples from Wadi Tayiba) and thirty-three samples from Wadi Feiran area were examined to determine the petrophysical characteristics. The studied samples were measured using plugs of a 2.5 cm diameter and a 5cm length. All samples were cleaned and dried in an electric oven at 110 C° as maximum temperature. Bulk and grain densities, porosity, and permeability were measured using the method introduced by Dakhanova (1977). Other parameters are calculated from them. The packing index is defined by El-Sayed (1993) and the reservoir quality index (RQI) is controlled by two parameters: porosity and permeability (Dibber et al., 1996.)

### *2.1 Lithostratigraphy*

The Eocene successions exposed in the Southwestern part of Sinai are dominated by carbonate rocks. The Eocene successions recorded in the study areas range in thickness from 152 meters (at Wadi Tayiba) to 408 meters (at Wadi Feiran), (Figs. 2 and 3) and Pl. I.

The Eocene rocks of the study areas are represented by five formations namely; Thebes (Lower to Middle Eocene), Darat and Samalut (Middle Eocene), Khaboba (Middle to Late Eocene) and Tanka (Late Eocene).

The Thebes Formation is well exposed in the study areas. It attains an average thickness of 48 meters in the Tayiba area and 268 meters in the Feiran area. Also, the Thebes Formation is characterized mainly by yellow to pale brown colored, thin–bedded, moderately-hard, and argillaceous limestones.

| Age | Rock unit | Bed No. | S.No. | Thick in Meter | Lithic log. | Lithic Description |
|---|---|---|---|---|---|---|
| Upper Eocene | Tanka | 10 | 25,26 23,24 | 8 | | **Massive, grayish yellow, argillaceous, fine grained and fossiliferous (*G. index index*) limestone.** |
| | | 8 | 22 21 | 14 | | **Varicolored, calcareous and well banded shales.** |
| Middle Eocene | Khaboba | 7 | 20 19 | 11 | | **Massive, grayish yellow, argillaceous, fine grained and fossiliferous (*Tr. rohi*) limestone.** |
| | | 6 | 18 17 | 10 | | **Varicolored, calcareous and well banded shales.** |
| | Darat | 5 | 15,16 | 6 | | **Varicolored, calcareous and well banded shales.** |
| | | 4 | 14 13 12 11 | 39 | | **Massive, grayish yellow, argillaceous , fine grained and fossiliferous(*M. lehneri* And *Globigerina thekasubconglobata*) limestone.** |
| | | 3 | 9, 10 | 7 | | **Varicolored, calcareous and well banded shales.** |
| Lower Eocene | | 2 | 8 | 8 | | **Massive, grayish yellow, argillaceous , fine grained and fossiliferous(*Globigerina theka subconglobata*) limestone** |
| | Thebes | 1 | 7 6 5 4 3 2 1 | 48 | | **Massive, grayish yellow, argillaceous , fine grained and fossiliferous(*H. nttalli*) limestone** |

lagend: limestone, Shale

**Figure 2.** Idealized columnar Lithic Log of the Eocene Formations measured at Wadi Tayiba area.

The Darat Formation is well-exposed in the studied areas. It is recorded in the Tayiba area with a thickness of about 60 meters, and overlies conformably the Thebes Formation. The Darat Formation is composed mainly of yellowish brown colored limestones, that are argillaceous, moderately hard, and alternated with shale.

The Samalut Formation is well-exposed in the study areas. It attains an average thickness of 140 meters in the Feiran area. Samalut Formation is equivalent to the Darat Formation in the Tayiba section.

The Khaboba Formation is recorded in the Tayiba area with a thickness of about 21 meters, and overlies conformably the Darat Formation. The Khaboba Formation is composed mainly of fossiliferous limestones.

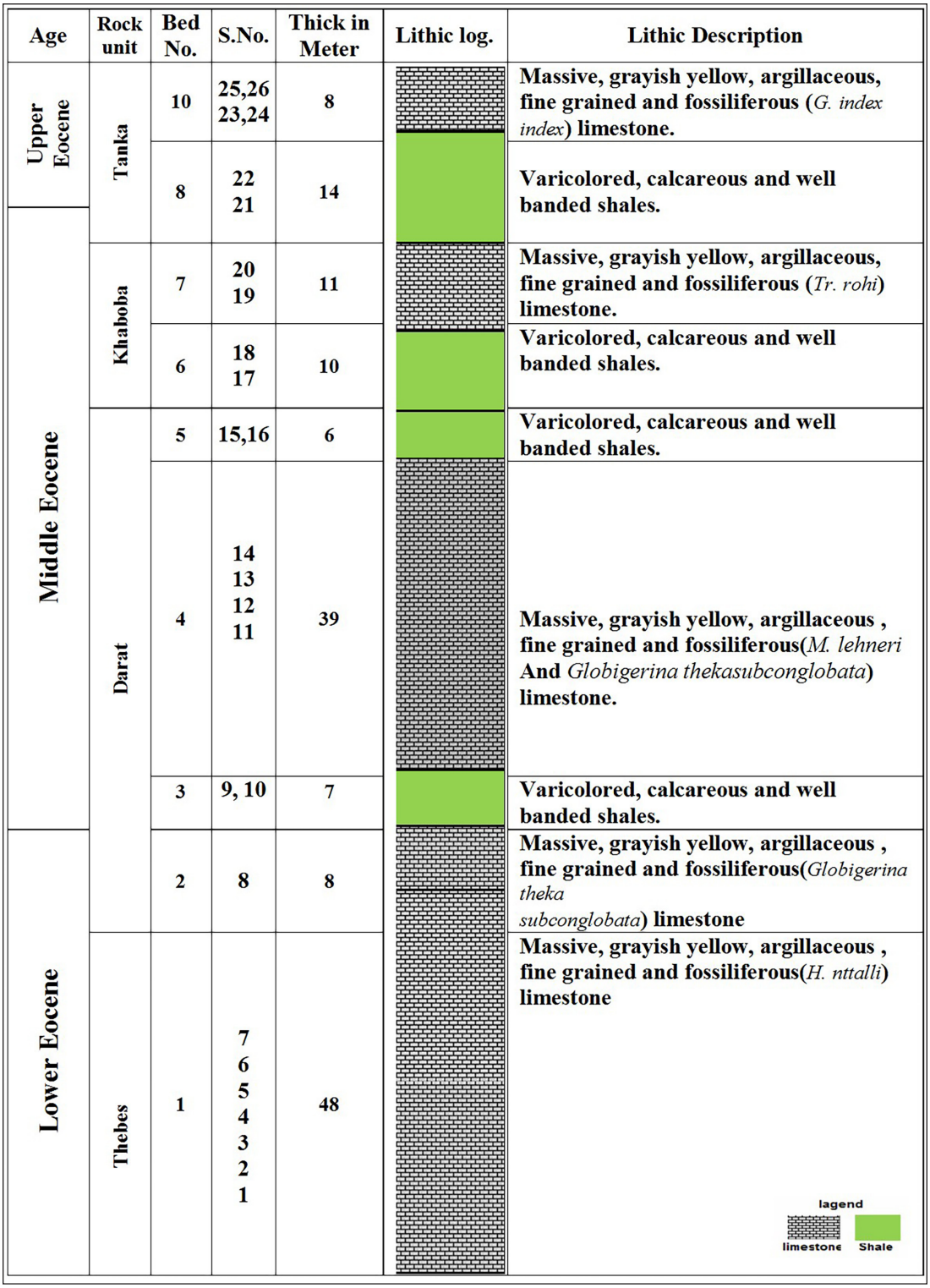


**Figure 3.** Idealized columnar Lithic Log of the Eocene Formations recorded at Wadi Feiran area.

The Tanka Formation in the Tayiba area attains a thickness of 22 meters. This formation conformably overlies the Khaboba Formation. The Tanka Formation is composed mainly of yellowish brown limestones that are argillaceous and moderately hard.

**Plate I**

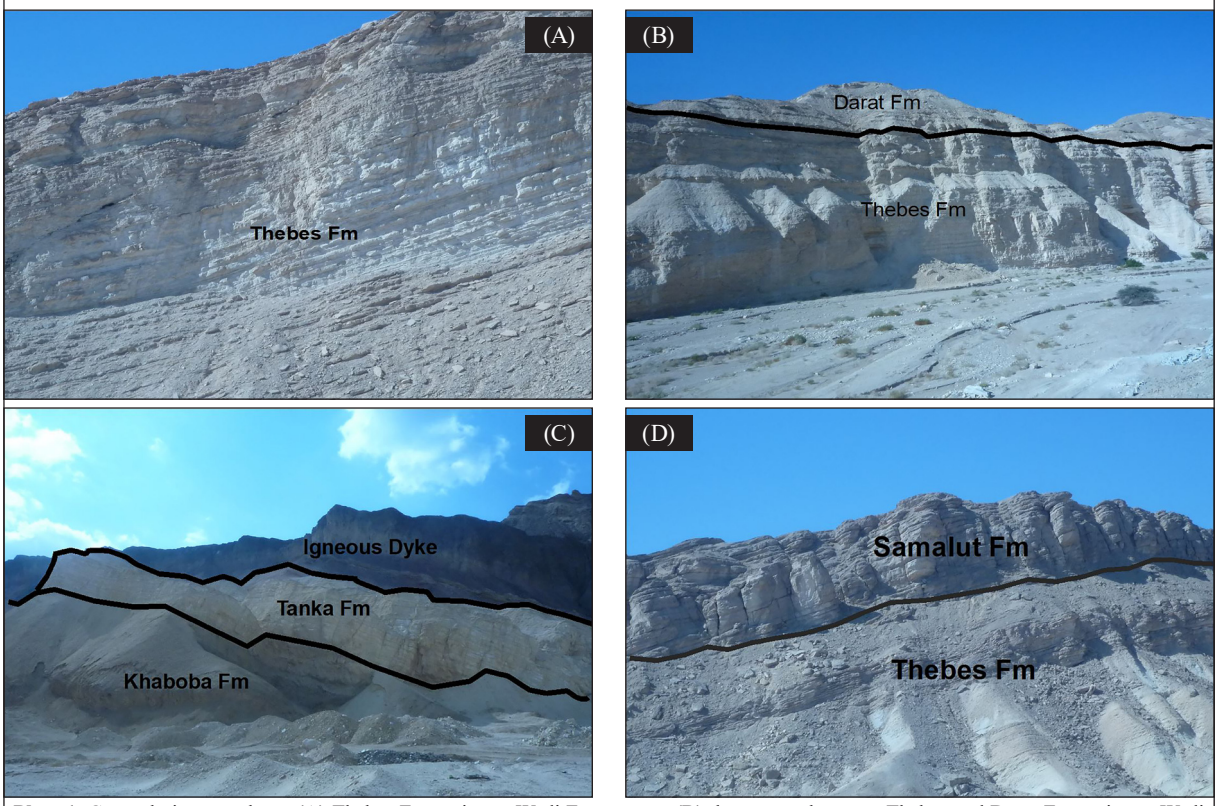


**Plate 1.** General views to show: (A) Thebes Formation at Wadi Ferran area, (B) the contact between Thebes and Darat Formation at Wadi Tiaba area, (C) the contact between Khaboba and Tanka Formation at Wadi Tiaba area, and (D) contact between Thebes and Samalut Formations at Wadi Ferran area.

***- Microfacies Association***

The study of microfacies associations was carried out to interpret the environmental conditions of deposition and to understand the digenetic processes affecting the consolidated rocks. For this purpose, the collected rock samples were thin-sectioned and examined petrographically, and the percentages of the matrix and the constituent allochems were estimated by point counting.

In the present study, the classifications of Folk (1959, 1962, and 1974), Dunham (1962) and Embry and Klovan (1972) were used. The identified microfacies associations of the studied rock sequences are shown in Fig. (4).

***-Fossiliferous Micrite (Fig. 4A).***

This microfacies association was detected at the Wadi Tayiba (S. No. 1, 2, 3, and 7) and Wadi Feiran (S. No. 1, 2, 4, 5, 17, 18, and 21) areas. It consists mainly of 92% carbonate for both of the Wadi Tiayba and Wadi Feiran areas. The bioclastic carbonate grains are represented by an inconsiderable amount of fossil tests and shell fragments. In this microfacies association, terrigenous materials are preset in the form of clay which is the main constituent (5%) for both of the wadi Tayiba and Feiran areas. Spary calcite cement was present in a considerable amount; it seems to be formed during restricted recrystallization process. Dolomite is represented by a few rhombs scattered in micrite matrix 1% for both Wadi Taybia and Feiran. Texturally, according to Dunham (1962) and Embry and Klovan (1972), these microfacies associations are considered as mudstones. The presence of fossiliferous micrite microfacies association indicates a deposition under shallow marine calm water conditions. Under this condition, micrite can be formed either by the action of bacteria-producing ammonia which reacts with the carbonates to form ammonium carbonates which in turn react with calcium sulphate of the seawater precipitate calcium carbonate. Consequently, this microfacies association indicates a deposition in the shallower setting of the inner neritic.

***-Arigillaceous Micrite (Fig. 4B).***

This microfacies association was detected at the Wadi Tayiba area (S. No. 4, and 6). It consists mainly of 75% carbonate. The presence of spary calcite cement in an inconsiderable amount favors the little pore space available for its formation in the micrite matrix. In this microfacies association, terrigenous materials are present in two forms; clay and silty grains up to 25%. Texturally, according to Dunham (1962) and Embry and Klovan (1972), this microfacies association is considered as mudstone, (Tables 1 and 2). The study of this microfacies association points to the lack of strong currents leading to a rapid rate of precipitation of micro-crystalline ooze (23). The terrigenous materials in the form of clay and silts, present in a considerable amount, can be attributed to the increase of terrigenous contents delivered into the site of deposition either by running water, fluctuation of sea level, or as a result of strong currents and turbulence in deeper waters.

***-Foraminiferal Biomicrite (Figs. 4 C and D).***

This is recorded in the Lower and Middle Eocene at Wadi Feiran area and was detected at Wadi Tayiba only in Middle Eocene. It consists of 90% carbonate, with a considerable proportion of allochems (more than 10%).

The bioclastic carbonate grains (allochems) are represented by foraminiferal tests of a small size and good sorting. Texturally, according to Dunham (1962) and Embry and Klovan (1972), this microfacies association is considered to be as a packstone. The study of this microfacies association suggests that currents were not sorting or persistent enough to winnow away the microcrystalline ooze which remained as a micrite matrix Folk, (1974). The presence of well-sorted foraminiferal tests, which have relatively small sizes and the nature of micrite, indicates the deposition in the marine environment at the middle part of the outer neritic zone Fig. 4 (C and D).

***-Micrite (Fig. 4E).***

This microfacies association was observed at the Wadi Feiran area. According to the classifications of limestone based on depositional texture, Dunham (1962) and Embry and Klovan (1972) believe this microfacies is to be considered as mudstone. The study of the microfacies association reveals a rapid rate of precipitation of the microcrystalline ooze with a lack of strong currents (Folk, 1959). Micrite was formed either by direct inorganic precipitation of aragonite, or by producing aragonite needles within the tissues of calcareous algae as shown in Fig. 4E. Consequently, this microfacies association was thought to be deposited under relatively shallow marine conditions in the deeper part of the inner neritic zone in quiet water.

***-Pellitiferous Micrite (Fig. 4F).***

This microfacies association was detected at the Wadi Tayiba area. The non- bioclastic carbonate grains are represented by homogeneous pellets, composed of aggregates of lime mud, well-rounded and embedded in a micrite matrix. The terrigenous material in this microfacies is present up to 5% only in the form of clay. It is clear that the packing of these rocks impose a certain maximum on the amount of pellets (less than 10%). Most pellets are formed in situ, whereas the hydraulic condition in deep waters may form from lime mud pellets. Texturally, according to Dunham (1962) and Embry and Klovan (1972), this microfacies association is considered as mudstone, as shown in Fig. 4 (F).

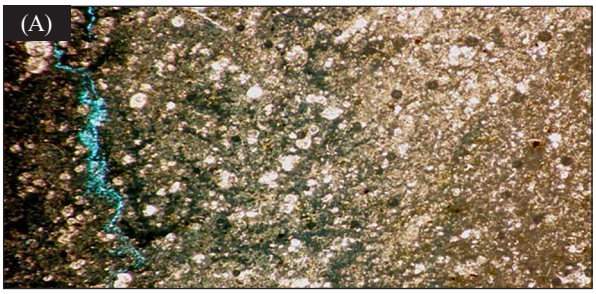


**(A):** Photomicrograph showing fossiliferous micrite microfacies association consists mainly of microcrystalline ooze with unconsiderable proportion of allochems. Thebes Formation, Wadi Tiaba area. Ordinary Light X 10.

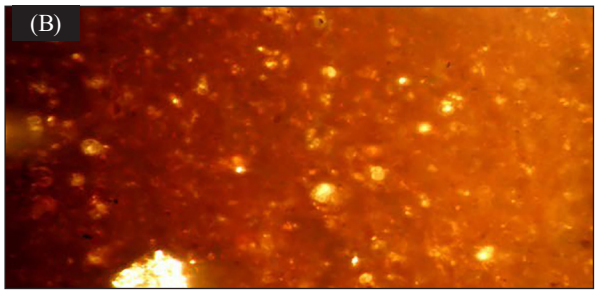


**(B):** Photomicrograph showing argillaceous micrite microfacies association consists mainly of microcrystalline ooze. Thebes Formation, Wadi Tiaba area. Ordinary Light X 10.

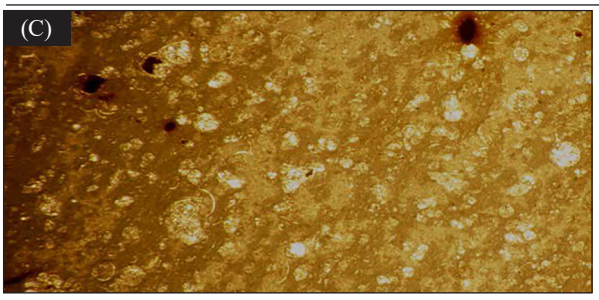


**(C):** Photomicrograph showing Foraminiferal biomicrite microfacies association, consists mainly of microcrystalline ooze with considerable proportion of allochems. Thebes Formation, Wadi Ferran area. Ordinary Light X 10.

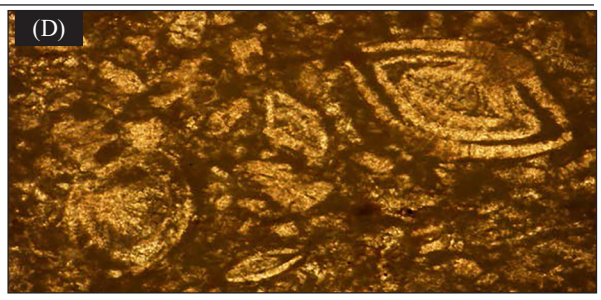


**(D):** Photomicrograph showing Foraminiferal biomicrite microfacies association consists mainly of microcrystalline ooze with considerable proportion of allochems. Samalut Formation, Wadi Ferran area. Ordinary Light X 10.

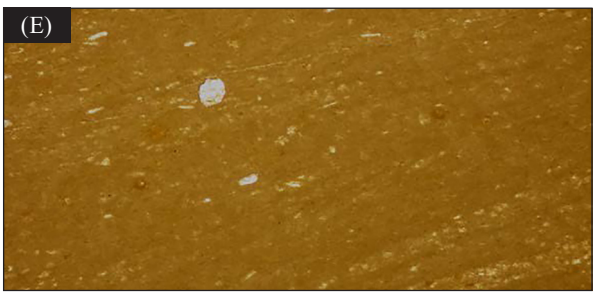


**(E):** Photomicrograph showing Micrite microfacies association consists mainly of microcrystalline ooze with unconsiderable proportion of allochems. Thebes Formation, Wadi Ferran area. Ordinary Light X 10.

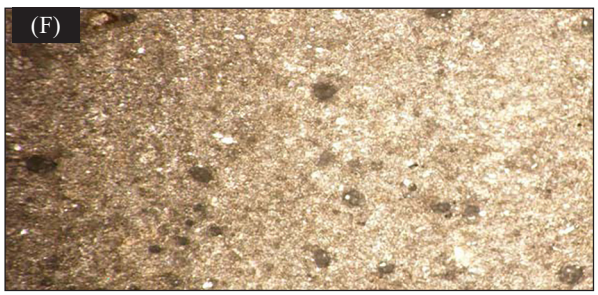


**(F):** Photomicrograph showing Pellitiferous micrite microfacies association consists mainly of microcrystalline ooze with un-considerable proportion of allochems. Darat Formation, Wadi Tiaba area. Ordinary Light X 10.

**Figure 4.** The Identified microfacies associations of studied Eocene rocks .

***-Depositional Environment.***

The petrographic studies on the Wadi Tayiba and Wadi Feiran areas reveal that several depositional environments which can be summarized according to Flugel (2004 and 2010). The depositional patterns of the Eocene microfacies associations recorded in the Wadi Tayiba and Wadi Feiran areas are characterized by shallow waters, generally a few to tens of meters deep. Salinity varies from essentially a normal marine to somewhat higher. Circulation is very moderate, and water conditions are favourable for organisms to live as shown in Tables (1 and 2).

**Table 1.** Microfacies association depositional patterns (Wadi Tiayba) area.

| Age | Formation | Described microfacies type | Microfacies association according to Embry and Klovan (1972) | Standard microfaccies SMF | Facies Zone (FZ) V | Occurrence on flat-top platform | Occurrence on ramp |
|---|---|---|---|---|---|---|---|
| Upper Eocene | Tanka | Agril. Micrite; S. No. 24 | Mudstone | 23 | 8 | Restricted plateform | Inner ramp |
| | Khaboba | Micrite; S. No. 23 | | 23 | 8 | | |
| Middle Eocene | | Agril. Micrite; S. No. 19, 20 | | 23 | 8 | | |
| | Darat | Foraminiferal biomicrite; S. No. 12 | Packstone | 9 | 7 | Open marine | |
| | | Foraminiferal micrite; S. No. 11, 13. 14 | Mudstone | 19 | 8 | Restricted platform | |
| Lower Eocene | | Pellitiferous micrite; S. No. 8 | | 19 | 8 | | |
| | Thebes | Agril. Micrite; S. No. 4, 5, 6 | | 19 | 8 | | |
| | | Fossiliferous micrite; S. No. 1, 2, 3, 7 | | 19 | 8 | | |

Texturally, the Eocene sediments in the Wadi Tayiba and Wadi Feiran areas vary but contain considerable amounts of lime mud. The prevailing rock types are variable limestones interbedded with a calcareous shale (marlstone). The grain types show a little variety of textures from a packstone to mudstone with little pelleting of micrite matrix. The terrigenous clastic is characterized by the presence of quartz silt, siltstone and calcareous shale intercalated with limestone in the lower segregated beds. Biota is represented by foraminifera. Consequently, according to Flugel (2004 and 2010), the depositional patterns of the Eocene microfacies associations in the Wadi Tayiba and Wadi Feiran areas show a sequence of both uniform and cyclically alternating, open and restricted marine and evaporate environments of the carbonate facies zone (7 and 8), on the inner ramp.

**Table 2.** Microfaciesassociation depositional patterns of (Wadi Feiran).

| Age | Formation | Described microfacies type | Microfacies association occurring to Embry and Klovan (1972) | Standard microfacies SMF | Facies zone (FZ) | Occurrence on flat-top platform | Occurrence on ramp |
|---|---|---|---|---|---|---|---|
| Middle Eocene | Samalute | Foraminiferal biomicrite; 31, 32, 33, 34, 35, 36, 37 | Packstone | 9 | 7 | Open marine | Inner ramp |
| | | Micrite; 24, 25, 26, 27, 28, 30 | Mudstone | 23 | 8 | Restricted platform | |
| Lower Eocene | Thebes | Micrite; 13, 14, 19, 20 | Wackstone | 19 | 8 | | |
| | | Foraminiferal biomicrite; 7, 8, 9, 10, 11, 15, 16 | Packstone | 9 | 7 | Open marine | |
| | | Fossiliferous micrite; 1, 2, 4, 5, 6, 17, 18, 21 | Mudstone | 19 | 8 | Restricted platform | |

***-Petrophysical Characterization***

The reservoir characterization of any hydrocarbon-bearing system depends on its petrophysical parameters (porosity, permeability, grain and bulk densities, packing index, porosity ratio, and quality reservoir index). To achieve this, the collected samples were studied to determine the storage capacity as shown in Tables (3 and 4).

In the present study, forty-nine samples were selected, (Sixteen samples) from the Wadi Tayiba area and (thirty-three samples) from the Wadi Feiran area to detect the petrophysical characteristic of these areas.

The petrophysical results reveal that the Wadi Tayiba, Darat Formation (T11, T12, T13, and T14) samples, have higher porosity and permeability values associated with a decrease in the grain density and the bulk density. The quality-reservoir index, packing index and porosity ratio increase as the porosity and permeability increase (Abd El-Hafez et al., 2015).

**Table 3.** Petrophysical parameters of the investigated samples (Wadi Tayiba area).

| Age | Form. | S. No. | Grain density | Bulk density | Porosity | Per. | Packing index | Porosity ratio | QRI |
|---|---|---|---|---|---|---|---|---|---|
| Upper Eocene | Tanka | T24 | 2.57 | 2.331 | 9 | 0.023 | 1.1025 | 0.09890 | 0.0008 |
| | | T23 | 2.66 | 2.3583 | 11 | 0.005 | 1.1279 | 0.12359 | 0.001 |
| | Khaboba | T20 | 2.55 | 2.1071 | 17 | 0.035 | 1.2101 | 0.20481 | 0.0006 |
| Middle Eocene | | T19 | 2.66 | 2.3673 | 11 | 0.02 | 1.1236 | 0.12359 | 0.0005 |
| | Darat | T14 | 2.53 | 2.0205 | 20 | .027 | 1.2521 | 0.25 | 0.0004 |
| | | T13 | 2.57 | 2.1145 | 18 | 0.052 | 1.2154 | 0.21951 | 0.009 |
| | | T12 | 2.44 | 1.4434 | 41 | 0.304 | 1.6904 | 0.69491 | 0.002 |
| | | T11 | 2.58 | 1.3476 | 48 | 0.556 | 1.9145 | 0.92307 | 0.003 |
| Lower Eocene | | T8 | 2.69 | 2.5089 | 7 | 0.009 | 1.0721 | 0.07526 | 0.004 |
| | Thebes | T7 | 2.68 | 2.2144 | 18 | 0.958 | 1.2102 | 0.21951 | 0.016 |
| | | T6 | 2.68 | 2.1518 | 20 | 1.203 | 1.2454 | 0.25 | 0.018 |
| | | T5 | 2.69 | 2.0245 | 25 | 0.26 | 1.3287 | 0.33333 | 0.003 |
| | | T4 | 2.56 | 1.6308 | 36 | 0.65 | 1.5697 | 0.5625 | 0.005 |
| | | T3 | 2.5 | 1.7472 | 30 | 0.625 | 1.4308 | 0.42857 | 0.006 |
| | | T2 | 2.61 | 1.4936 | 43 | 0.6 | 1.7474 | 0.75438 | 0.004 |
| | | T1 | 2.68 | 2.2211 | 17 | 0.575 | 1.2066 | 0.20481 | 0.010 |

The petrophysical results reveal that Wadi Feiran, Thebes Formation samples (F15, F16, F17 and F18) have higher porosity and permeability values associated with a decrease in the grain density and the bulk density.

**Table 4.** Petrophysical parameters of the investigated samples (Wadi Feiran area).

| Age | Form. | S. No. | Grain density | Bulk density | Porosity | Per. | Packing index | Porosity ratio | QRI |
|---|---|---|---|---|---|---|---|---|---|
| Middle Eocene | Samalut | F37 | 2.58 | 2.2822 | 12 | 0.006 | 1.1304 | 0.1304 | 0.065 |
| | | F36 | 2.61 | 2.3492 | 10 | 0.005 | 1.1110 | 0.11111 | 0.11111 |
| | | F35 | 2.62 | 2.5884 | 1 | 0.04 | 1.0122 | 0.01010 | 0.007 |
| | | F34 | 2.65 | 2.6226 | 1 | 0.06 | 1.0104 | 0.01010 | 0.005 |
| | | F33 | 2.59 | 2.5692 | 3 | 0.04 | 1.0080 | 0.030920 | 0.003 |
| | | F32 | 2.66 | 2.5853 | 0.5 | 0.01 | 1.0288 | 0.03092 | 0.066 |
| | | F31 | 2.67 | 2.572 | 3 | 0.02 | 1.0381 | 0.03092 | 0.065 |
| | | F30 | 2.39 | 2.5943 | 3 | 0.01 | 0.9212 | 0.0392 | 0.009 |
| | | F29 | 2.64 | 2.1405 | 11 | 0.007 | 1.233 | 0.12359 | 0.007 |
| | | F28 | 2.42 | 2.278 | 14 | 0.004 | 1.0623 | 0.16279 | 0.005 |
| | | F27 | 2.4 | 2.0912 | 13 | 0.003 | 1.1476 | 0.14942 | 0.003 |
| | | F26 | 2.47 | 1.916 | 22 | 0.432 | 1.2891 | 0.28205 | 0.038 |
| | | F25 | 2.48 | 1.7564 | 29 | 0.861 | 1.4119 | 0.40845 | 0.066 |
| | | F24 | 2.68 | 2.1814 | 19 | 1.29 | 1.2285 | 0.23456 | 0.065 |
| | Thebes | F21 | 2.73 | 1.91 | 30 | 1.72 | 1.4293 | 0.42857 | 0.102 |
| | | F20 | 2.69 | 2.2683 | 16 | 1.78 | 1.1859 | 0.19047 | 0.070 |
| | | F19 | 2.66 | 1.7307 | 35 | 6.17 | 1.5369 | 0.53846 | 0.137 |
| | | F18 | 2.68 | 1.8146 | 32 | 10.54 | 1.4769 | 0.47058 | 0.180 |
| | | F17 | 2.67 | 1.8225 | 32 | 5.41 | 1.4650 | 0.47058 | 0.146 |
| | | F16 | 2.69 | 2.0213 | 25 | 1.22 | 1.3308 | 0.33333 | 0.058 |
| Early Eocene | | F15 | 2.7 | 1.7579 | 35 | 9.62 | 1.5359 | 0.53846 | 0.212 |
| | | F14 | 2.69 | 2.1335 | 21 | 6.38 | 1.2608 | 0.26582 | 0.138 |
| | | F13 | 2.68 | 1.7852 | 33 | 3.12 | 1.5012 | 0.49253 | 0.127 |
| | | F11 | 2.62 | 2.1185 | 19 | 1.62 | 1.2367 | 0.2367 | 0.081 |
| | | F10 | 2.7 | 2.0621 | 24 | 0.13 | 1.3093 | 0.31578 | 0.022 |
| | | F9 | 2.7 | 2.0256 | 25 | 0.27 | 1.3329 | 0.33333 | 0.033 |
| | | F8 | 2.7 | 2.0135 | 24 | 0.14 | 1.3212 | 0.31578 | 0.023 |
| | | F7 | 2.71 | 2.0044 | 26 | 0.43 | 1.3520 | 0.351350 | 0.044 |
| | | F6 | 2.68 | 2.1211 | 21 | 0.5 | 1.2634 | 0.26582 | 0.043 |
| | | F5 | 2.7 | 1.981 | 26 | 0.66 | 1.3629 | 0.35135 | 0.052 |
| | | F4 | 2.65 | 2.0071 | 24 | 0.35 | 1.3203 | 0.31578 | 0.075 |
| | | F2 | 2.7 | 1.7442 | 35 | 0.55 | 1.5479 | 0.53846 | 0.041 |
| | | F1 | 2.68 | 1.8619 | 32 | 0.4 | 1.4393 | 0.47058 | 0.035 |

From the obtained petrophysical results, it can be concluded that the Wadi Tayiba area (samples T11, T12, T13, and T14 of Darat Formation) and the Wadi Feiran area (samples F15, F16, F17, and F18 of Thebes Formation) represent the best storage capacity (Figures 5 and 6).

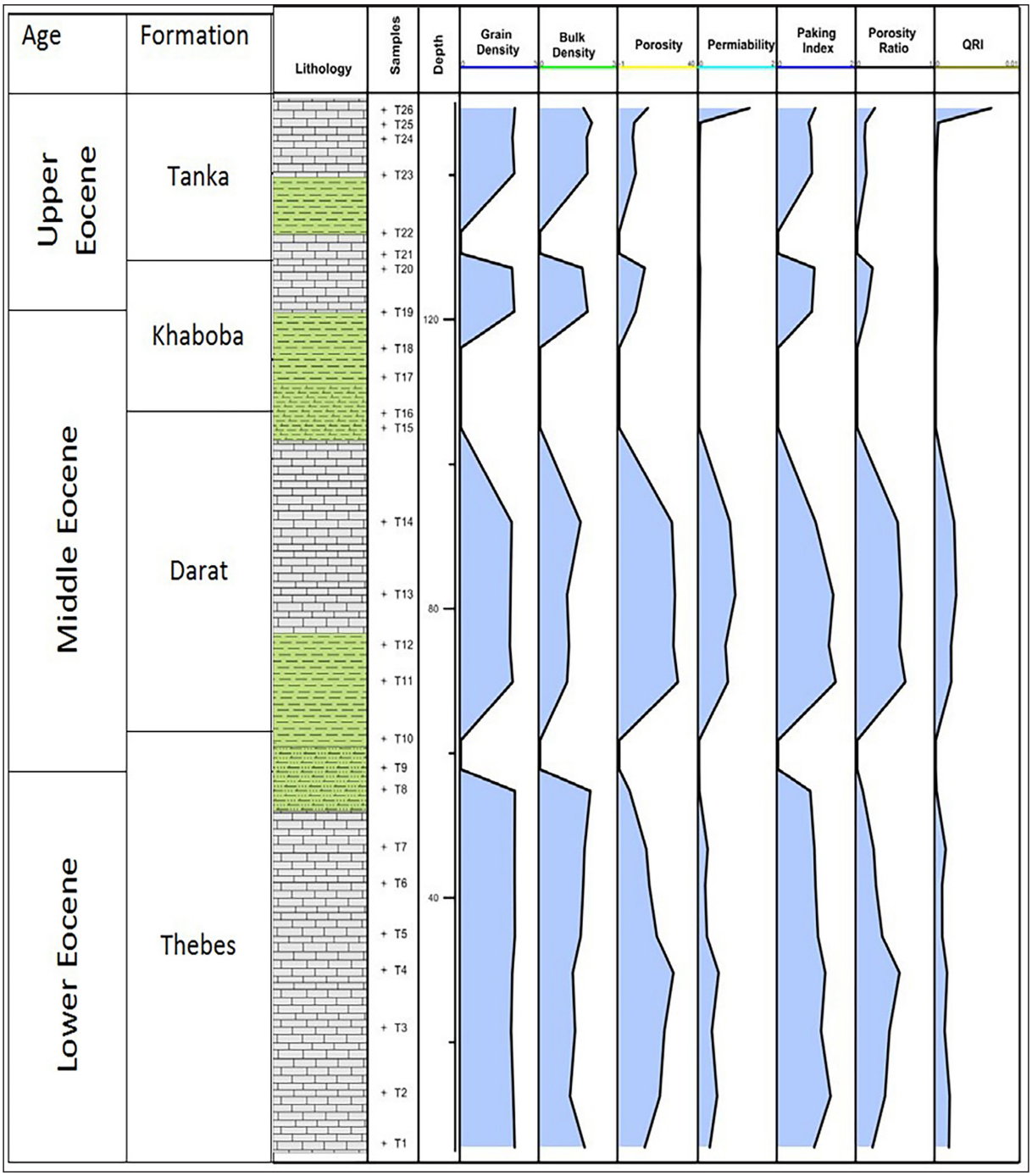


**Figure 5.** Vertical distribution of the petrophysical properties in Wadi Tiayba area, South western Sinai, Egypt.

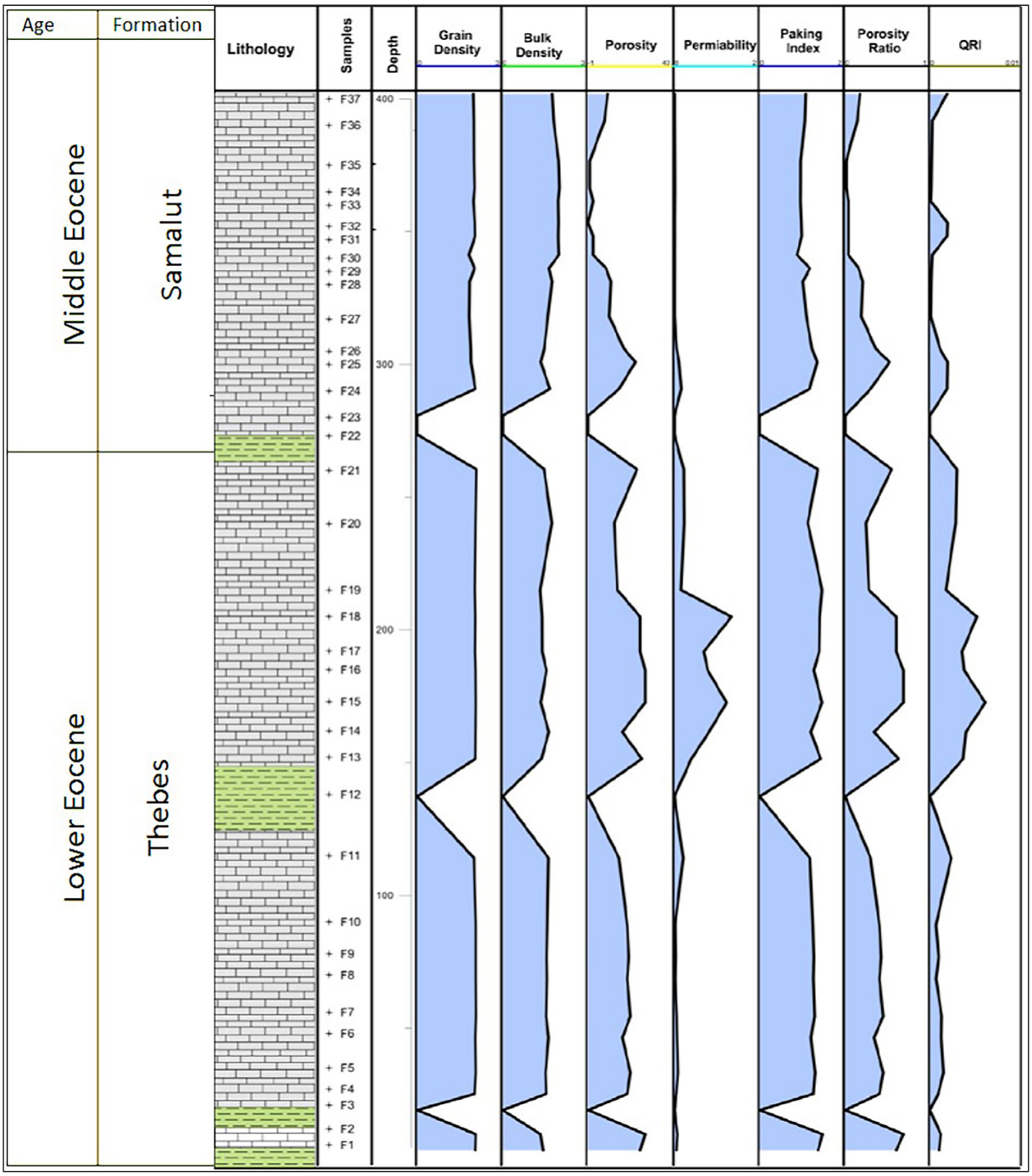


**Figure 6.** Vertical distribution of the petrophysical properties in Wadi Ferran area, South western Sinai, Egypt.

## 3. Conclusions

The Eocene successions exposed in the Southwestern part of Sinai are dominated by carbonate rocks. The Eocene successions recorded in the study areas range in thickness from 152 meters (at Wadi Tayiba) to 408 meters (at Wadi Feiran).

The petrographic study of the carbonate rocks reveals the following observations:

Lower Eocene: Fossiliferous micrite and argillaceous fossiliferous micrite were detected at the Wadi Tayiba area. At Wadi Feiran area, the detected microfacies associations are fossiliferous micrite Foraminiferal biomicrite and micrite.

Middle Eocene in the study areas is represented by the Darat and Khaboba formations (Wadi Tayiba area) and Samalut Formation (Wadi Feiran area). At Wadi Tayiba area Pellitiferous micrite, fossiliferous micrite and foraminiferal biomicrite were detected, while at the Wadi Feiran area, micrite and foraminiferal biomicrite were the main microfacies.

Upper Eocene: The Tanka Formation in (Wadi Tayiba area) is represented by Micrite and argillaceous micrite.

The obtained petrophysical results reveal that the Darat Formation at Wadi Tayiba area and The Thebes Formation at Wadi Feiran area showed the best storage capacity.

## References

Abd El-Hafez, N.A., Abd El Moghny, M.W., Mousa, A. S., El-Hariri, T.Y.M.A., Sharaka, H.K. (2015). Effect of diagensis processes on storage capacity of Lower Miocene rocks at Southwestern Sinai, Egypt. Inter. Jour. of Sci. Eng. and App. Scie., 1.9: 176-196.

Abul-Nasr, R.A. (1993a). Re-evaluation of Middle-Upper Eocene bio Stratigraphy of West Central Sinai: M.E.R.C. Ain Shams Univ., Earth Sc. Ser., 7, pp. 153-166, Cairo.

Abul-Nasr, R.A. (1993b). Contribution of the Eocene biostratigraphy in Sinai: M. E. R .C. Ain shams Univ., Earth Sc. Ser., 7, pp. 167-176, Cairo.

Conoco. (1992). Geological map of Egypt, Scale 1 : 500.000, 6 sheets with cooperation of Egyptian General Petroleum Corporation , Klitzsch, E. List, F. K. and Pohlmann, G. (Ed.), Berlin, Cairo, Egypt.

Dakhanova, N.V. (1977). Determination of the petrophysical characteristics of sample in Russian. Nedra. Moscow, 41.

Dunham, R.J. (1962). Classification of carbonate rocks according to depositional texture. In: classification of carbonate rocks (Ed. By W. E. Ham) Mem. Am.

El-sayed, A.M.A. (1993). Packing index and saturation parameters for limestone, Ain Shams Sci., Bull., 31: 411-424.

Embry, A.F., and Klovan, J.E. (1972). A late Devonian reef tract on north eastern Banks Islands, Northwest territories. Con. Petrol. Geology. Bull, 19 pp. 730-781.

Flugel, E. (2004). Microfacies of carbonate rocks analysis, 1st interpretation and application Springer- verlag, Berline Heideberg, New York, 956 pp.

Flugel, E. (2010). Microfacies of carbonate rocks analysis, 2nd interpretation and application Springer- verlag, Berline Heideberg, New York, 1006 pp.

Folk, R.L. (1959). Practical petrographic classification of limestone Bull. Am. Ass. Petrol. Geol., 43: 1-38.

Folk, R.L. (1962). Spectral subdivision of limestone types in Classification of carbonate rocks (Ed. By W. E. Ham.) Mem. Am. Assoc. Petrol. Geol., 1: 62-84.

Folk, R.L. (1974). The natural history of crystalline calcium carbonate effect of magnesium content and salinity. Jour. Sed. Petrol., 27: 3-26.

Ibrahim, A.M., Abou El Ezz, A.R., Mousa, A.S., El Hariri, T.Y., Abd El Ghany, A.A. (2016 b). Mineralogical and Geochemical of Eocene Carbonate rocks at Wadi Tayiba and Wadi Feiran areas, Southwestern Sinai, Egypt. Inter. Jour. of Sci. Eng. and App. Scie., 2.2: 279-304.

Ibrahim, A.M., Abou El Ezz, A.R., Mousa, A.S., El Hariri, T.Y., Abd El Ghany, A.A. (2016 b). Geochemical assessment and Clay Mineralogical Studies of Eocene at Wadi Tayiba and Wadi Feiran areas, Southwestern Sinai, Egypt. Inter. Jour. of Sci. Eng. and App. Scie., V. 2.3, pp. 119-136.

Magdy, S.N. (1997). Stratigraphy and Sediment logy of Eocene in South Western Sinai. Ph.D. Suez Canal Univ, Ismailia.

Said, R. (1990). The Geology of Egypt, Cenozoic: pp. 451-468, Balkema, Rotterdam, and Brook Field.

Tiab, D., and Donalson, E. (1996). Petrophysics, Theory and practice of measuring reservoir rock and fluid transport properties. Gulf Publishing Company, Houston, Taxes, USA, pp. 94-135.

JJEES

JJEES (2019) 10 (4): 204-214
ISSN 1995-6681

Jordan Journal of Earth and Environmental Sciences

# Nitrogen Mineralization Kinetics in some Tropical Soils Amended with Ashed and Un-ashed Animal Manures

Toyin Olowoboko[1*], Jamiu Azeez[1], Olanrewaju Olujimi[2], Oluwatoyin Babalola[1]

[1]Federal University of Agriculture Abeokuta, Department of Soil Science and Land Management, Nigeria
[2]Federal University of Agriculture Abeokuta, Department of Environmental Management and Toxicology, Nigeria

Received 19 March 2019; Accepted 23 July 2019

**Abstract**

This study is carried out to evaluate mineral nitrogen release of three animal manure ashes and dried animal manures by kinetic models under incubation, screen-house, and field conditions. Soils were treated with dried manures and manure ashes of cattle, goat, and poultry and NPK 15-15-15 at 120kg N $ha^{-1}$ after which the amended soil mixtures were taken fortnightly and analyzed for mineral nitrogen. The incorporation of manure ashes increased mineral N in the incubation experiment; there was a significant increase of 184%, 245%, 53%, and 65% in the screen-house and field experiments respectively with the cattle manure ash amendment compared to the control and dried manure. Mineral N release was in the following order: screen-house experiment > incubation experiment > field experiment. The first and second order was fit for N release only from the goat manure ash in the incubation and screen-house experiments. The relationship between N kinetics and time was polynomial.



**Keywords:** Nitrogen mineralization, nutrient release kinetics, rate order, recycled manure.

## 1. Introduction

Land application of animal manure seems to be an effective option in terms of management and disposal. It is considered as a valuable nutrient source when applied to the soil at rates and proportion to agronomic practices. Animal manure has been reported to significantly increase the soil physical properties such as soil aggregation, infiltration, and water holding capacity (Gilley and Risse, 2000) as well as the chemical properties including the cation exchange capacity and the soil buffering potential (Tisdale et al., 1993). Major nutrients like nitrogen and phosphorus have been recovered by the manure input to the soil. Despite all this importance of animal manure, its use is still limited due to bulkiness, nutrient heterogeneity, weed seed content, and low surface area; hence the recycling of manures becomes important. The incineration of animal manure is effective in reducing the volume and in concentrating the fertilizer nutrients. Thermal energy, which can be used for heating animal houses and electricity generation, is produced by incineration (Teppei et al., 2012). Beneficial uses of animal manure ash include its use in land application as an agricultural fertilizer, or a liming agent and a partial substitute for Portland cement in the cement and concrete industries (Demeyer et al., 2001). Furthermore, the nutrient-rich ash has the potential to increase the concentration of extractable plant nutrients in the amended soils. The calcium-rich alkaline ash from the poultry manure (Codling et al., 2002; Yusiharni et al., 2007) increases the pH of acidic soils and may increase the yield of barley, grass, white clover, rice, carrots, onions, beans, tomatoes, and wheat. Alkaline ash may, however, decrease the bioavailability of P, potassium (K), magnesium (Mg), copper (Cu), and iron (Fe) in soil (Yang et al., 2007).

The immediate impact of organic waste application is relevant to the availability of nitrogen to the subsequent crop, because of mineralization–immobilization processes (Hadas et al., 2004). However, the release of nutrients from the added organic substrate has proven to be difficult to predict, and this is to say that farmers often take inadequate account of the nutrient supply provided by various organic amendments (Domburg et al., 2000). The proportion of mineral N released from an added material may become part of the mineralized N pool; it may be immobilized by microbes and hence become part of a microbial biomass pool, or may be denitrified and lost as either nitrous oxide or dinitrogen (Calderon et al., 2005). Most recommendations on manure N application are blanket, with the assumption that N release is the same for all manures even though a large variability in manure qualities between manures from the same animal species has been reported (Chadwick et al., 2000). Abbasi et al. (2007) worked on the mineralization of three organic manures as nitrogen sources in a soil incubated under laboratory conditions. Teppei et al. (2012) worked on the chemical characteristics of ashes from cattle, swine, and poultry manure. Paulo et al. (2010) worked on the phosphorus availability and early corn growth response in soils amended with turkey manure ash. Information on the amount of N mineralized under incubation, screen-house, and field conditions in soils amended with animal manure ash and dried animal manure is not available.

Measuring the amount of mineral N ($NH_4^+$ + $NO_3^-$) released during a specified period under uniform conditions is an assessment of the mineralization potential of a soil or any organic substrate (Abbasi et al., 2003). Several approaches have been used to evaluate the N mineralization kinetics as

* Corresponding author e-mail: rachy_blare26@yahoo.com

indicators of N availability over time. Stanford and Smith (1972) proposed calculating the amount of N mineralized directly, while single exponential models have been successfully applied to describe N mineralization by relating the $N_0$ from a single compartment with the incubation time (Wang et al., 2003; Camargo et al., 2004; Pereira et al., 2005). In an incubation experiment Stanford and Smith (1972) estimated the N mineralization potential ($N_0$) and the rate constant (k) of the kinetic equation to be a first order using a logarithmic function. Smith et al. (1980) improved the model and reported that a nonlinear least-squares equation gave a more accurate estimation of k and $N_0$.

Azeez and Van Averbeke (2010) used the first order, second order, and power function model developed by Dang et al. (1994) for abiotic system to test the data on nitrogen mineralization kinetics of three animal manures. It was reported that the model did not capture the N kinetics, and the relationship between the amount of N release and time was not linear but polynomial to the power of three. The inconsistencies in the N mineralization kinetics could be attributed to the different systems used for testing the models. Hence, there is a need for re-evaluation of the model used by Azeez and Van Averbeke (2010) in order to acquire concrete information on the N kinetics of systems involving dried manures and manure ashes. This study is aimed at determining the mineral N release kinetics of three animal manure ashes and dried animal manures in incubation, screen-house and field experiments. It also evaluates the data by kinetic models. Moreover, it is aimed at determining the percentage of mineral N released and the effect of animal manure ashes, and dried animal manures on mineral N in the amended soils.

## 2. Materials and Methods

### *2.1 Soil, Manure Collection and Analysis*

The top soil samples (0-20 cm) were collected from four locations, which were chosen based on parent material (two locations from basement complex (Alabata, Osiele) and the other two from a sedimentary parent material (Itori and Papalanto)) in Ogun state in a forest transitional ecological zone. The soils were air-dried to constant weight at room temperature and sieved with a 2 mm mesh sieve. The cattle, goat, and poultry manures were collected from the Federal University of Agriculture, Alabata (FUNAAB) farm, and were air-dried to produce dried manures. Part of the dried manures were burnt in an open space at a temperature range of $320^0$C - $450^0$C to produce manure ash. Olowoboko et al. (2018) have reported the properties of the soils, dried manures and manure ashes used. Mineral N was calculated as the sum of nitrate nitrogen and ammonium nitrogen analyzed with (UV-3200 PCS spectrophotometer) according to Cataldo et al. (1975).

### *2.2 Treatments*

The experiments were replicated three times with eight treatments which included no amendment (control), amendments with dry cattle manure (CMD), dry goat manure (GMD), dry poultry manure (PMD), cattle manure ash (CMA), goat manure ash (GMA), poultry manure ash (PMA), and NPK 15-15-15 applied at 120 kg N $ha^{-1}$.

### *2.3 Incubation Experiment*

This experiment was laid in a completely randomized design, and four soils (Alabata, Osiele, Itori and Papalanto) were used in this experiment. One hundred grams of air-dried soil were dispensed into a 200g capacity plastic. Treatments (CON, CMD, CMA, GMD, GMA, PMD, PMA, NPK) were applied into the plastics accordingly and mixed thoroughly. The soil and amendment mixture were watered to a field capacity and kept in a dark cupboard for fifty-six days (eight weeks). Temperature of the incubation cupboard was determined daily with a thermometer, and an average temperature of $27.5^0$C was recorded. The soil samples taken at 1, 14, 28, 42, and 56 days of incubation were analyzed for mineral N using the aforementioned methodology.

### *2.4 Screen-house Experiment*

This experiment was laid in a completely randomized design and two soils (Alabata and Papalanto) were used for the experiment. The two soils used in this experiment were chosen based on the results of N-release pattern from the incubation experiment. One soil was chosen from each of the two parent materials. Five kilograms of soil were dispensed into 5L capacity buckets with dried-manure treatments (CMD, GMD, PMD) applied before planting, and the soil samples in the pots were watered. Maize seeds (BR-9928-DMR-SR-Y) were sown (three seeds per bucket), and after two weeks, manure ash (CMA, GMA and PMA) and NPK treatments were applied. The plants were thinned to one plant per pot after two weeks. The plants were watered when required and monitored in the screen-house for seventy days (ten weeks). The soil samples taken at 1, 14, 28, 42, 56, and 70 days were analyzed for mineral N using the aforementioned methodology.

### *2.5 Field Experiment*

This experiment was laid in a randomized complete block design, and FUNAAB soil (Alabata) was used for the experiment which was carried out at the Teaching and Research Farms, Federal University of Agriculture, Abeokuta Ogun state Nigeria. Manure manure treatments (CMD, GMD, and PMD) were applied manually two weeks before planting. Manure- ashe treatments (CMA, GMA, and PMA) and NPK treatment were applied two weeks after planting. Maize seeds were sown at a spacing of 25 cm by 75 cm. Soil samples were taken at 1, 14, 28, 42, 56 and 70 days weeks, and were analyzed for mineral N using the aforementioned methodology.

### *2.6 Calculations*

The percentage of total N released from an applied N source at time t was calculated as:

$$(\%N\ rel)\ N\ source = [(N\ (rel)Nsource / N_0(Nsource)]* 100.$$

where N(rel)Nsource is the amount of mineral N released from N source, $N_0$ is the total N in applied N sources.

The Mineral N release kinetics was estimated with first order, second order, and power function equations that were described by Dang et al. (1994) and reported by Azeez and Van Averbeke (2010).

First order:

$$\ln Qt = \ln Qe - k_1 t \quad \text{.....eqn 1}$$

Second order:

$$1/Qt = 1/Qe + k_2 t \quad \text{.....eqn 2}$$

Power function:

$Qt = at^b$ ……..eqn 3

$k_1$, first-order rate constant ($day^{-1}$)

$k_2$, second-order rate constant ($(mg\ N\ kg^{-1})^{-1}$)

a, initial N release rate constant ($mg\ N\ kg^{-1}\ day^{-1}$)

b, release rate coefficient ($(mg\ N\ kg^{-1})^{-1}$)

Qt (mg N kg_1) is the amount of mineral N released after t days; Qe (mg N $kg^{-1}$) is the

amount of mineral N released at equilibrium. N in the equations refers to mineral N ($NH^+_4$–N + $NO^-_3$–N).

### *2.7 Statistical Analysis*

Data collected were analyzed for their variance with the software package SAS (1999). Treatment effect and timing effects were determined using LSD at 5% level of probability.

## 3. Results and Discussion

### *3.1 Soil and Amendment (Dried manures and Manure ash) Characteristics*

Soil and manure characteristics have been discussed in Olowoboko et al., (2018) who reported that the pH of soils used for the experiment ranged from 7.63 in Itori to 6.07 in FUNAAB. Total N in the FUNAAB soil was 0.25%; followed by 0.23% in Itori, 0.21% in Alabata, 0.19% in Osiele, and 0.18% Papalanto. The value of total organic carbon was highest in Osiele (55.9 g $kg^{-1}$), and lowest in Itori (43.7 g $kg^{-1}$). All the experimental soils are loamy sandy except the soil from Papalanto which is sandy in texture. The pH values of the dried manures and manure ashes ranged from 10.90 in GMA to 8.20 in DPM. pH values of the manure ashes were in the order of GMA > PMA > CMA while the pH of the dried manures were in the order of DGM > DCM > DPM. There was no significant difference in the values of total organic carbon (TOC) for the dried manures and manure ashes except for poultry manure ash which had 33% lower TOC as compared with its dried manure. No significant reduction in total organic carbon and nitrogen of the manures was noticed after burning at 320–450 °C. The total nitrogen of the manures did not significantly differ from that of the manure ashes; this shows that the incineration of the manure at this temperature did not lead to a significant loss of nitrogen. Dried poultry manure had the highest total nitrogen value followed by dried goat manure and dried cattle manure. Total organic carbon was in the order of GMA > DGM > CMA > DPM > DCM > PMA.

### *3.2 Mineral N Changes with Applied Amendment*

The incorporation of manure ashes increased mineral N (mineral N) in comparison with dried manures during the incubation, screen-house, and field experiments. This could be attributed to the fact that a proportion of the organic N content has been converted to the inorganic form through the incineration of manures, and hence the mineral N content of the manure ashes were higher at incorporation. Additionally, this could be attributed to differences in the particle size of the dried manures and manure ashes. Particle size plays a major role in N mineralization as it affects the surface area of the N source and contact with microorganisms (Abbasi et al., 2007). Nitrogen mineralization and immobilization vary as a function of the availability of organic carbon (Van kessel et al., 2000). Table 1 shows the effect of amendment on the soil mineral N in the incubation experiment. At incorporation, a significant increase in mineral N was observed at the first day of incubation with PMA, a 164% increase in mineral N was recorded compared to its dried manure. Not all other amendments, except the NPK and PMA, differed from the control soil. On the 14th day of incubation, the highest and lowest mineral N values were observed with CMA and GMD respectively. CMA was able to increase the soil mineral N more than all other amendments; only a significant increase of 109% was found when compared to GMD.

**Table 1.** Effect of amendments on mineral N with incubation time

| Amendments | ……. Mineral N ($mgkg^{-1}$) ……. | | | | |
|---|---|---|---|---|---|
| | 1day | 14days | 28days | 42days | 56days |
| Soil only (CON) | 166.71b | 249.82a | 163.6abc | 151.2ab | 217.77d |
| Dried cattle manure (CMD) | 146.48b | 225.63ab | 199.24ab | 223.51ab | 420.49abc |
| Cattle manure ash (CMA) | 166.99b | 262.94a | 203.93ab | 117.39ab | 486.23ab |
| Dried goat manure (GMD) | 180.83b | 125.51b | 87.84c | 151.26ab | 252.83d |
| Goat manure ash (GMA) | 157.18b | 173.98ab | 241.18ab | 232.64ab | 469.99ab |
| Dried poultry manure (PMD) | 176.82b | 203.11ab | 157.06bc | 172.84b | 322.89bcd |
| Poultry manure ash (PMA) | 465.96a | 237.89a | 249.05ab | 248.21ab | 385.88abcd |
| NPK | 372.91a | 167.50ab | 279.19a | 323.11a | 506.21a |

*Means with the same letters are not significantly different at p≤0.05*

Manure ashes and NPK were similar in terms of effect on mineral N at 28 days of incubation. Although the control soil did not differ from all the amendments except GMD, mineral N in the control soil was lower than that observed for all manure ashes and NPK-amended soils. This is expected since organic manures contain a higher concentration of total N compared to the control soil. This could be attributed to the more labile organic N compounds and the higher level of microbial activity in the soils amended with the manure ashes. The single application of goat and poultry manure ashes allowed mineral N to significantly increase by 175% and 59% compared to the dried manures. On day 42, there was no significant difference in the mineral N of manure ash-amended soil and the soil amended with dried manures even though an increase was observed following the application of manure ashes. The highest mineral N was observed with NPK at 114%, and the lowest value was observed with GMD. The control soil did not differ from the soil amended with GMD on the 56th day of incubation. Abbasi et al. (2007) observed a significant difference among different manures and soils on days 10, 20, 55, 90, and 120, whereas a non-significant difference was observed on days 0, 30, 40, and 70 in a 120-day incubation experiment using three organic manures. However, significant increases were observed for mineral N in soils amended with manure ashes in comparison to the soils amended with their dried manures, a

16%, 86%, and 20% increases in mineral N were observed for CMA, GMA and PMA. Mineral N was similar for NPK, CMA, GMA and PMA at the end of the incubation experiment. The similarities observed in the mineral N release of NPK, CMA, GMA and PMA at the mid, and at the end of the experiment could be attributed to similar nutrient characteristics of these amendment i.e. they contained some proportions of mineral N before being incorporated into the soils.

The effect of amendment on the mineral N in the screen house experiment is shown in Table 2. The highest mineral N was recorded after the application of PMD on day one of the experiment. This is expected since dried manures were incorporated into the soil before day one (before planting), while the manure ashes were incorporated into the soil on day one (at planting). Mineralization of N from the applied organic source had commenced in the soils amended with dried manures compared to the manure ash-amended soil. Poultry manure showed a greater potential for N mineralization, according to the results obtained by Cordovil et al. (2005) in an incubation experiment. Mineral N in the manure ash-amended soil was lower than that in the dried manure-amended soil. All amendments except PMD and CMD did not differ significantly from the control soil, while significant increases of 56% and 79% in mineral N were observed with CMD and PMD respectively compared to their manure ashes. On day 14, mineral N increased with the application of manure ashes in comparison to the dried manures. Manure ashes are thermal products of the dried manure subjected to heat. They are expected to contain more mineral N, so their ability to increase the mineral N of the soil even at incorporation is normal since they were incorporated on the 14$^{th}$ day. The incorporation of CMA increased mineral N significantly by 52% compared to the control; however, mineral N for the dried manure did not differ. There was no significant difference in the control soil and the amended soil on day 28, and the amendment effect was not significant even though increases in mineral N were observed with the cattle and poultry manure ashes. The non-significance of the amendment effect could be a result of the temporary loss of mineral N from the soil or by the plant uptake of mineral N for physiological growth. On day 42, the amendment effect was only significant with NPK, and manure ashes and dried manures did not significantly differ from each other and the control soil. The single application of the cattle manure ash allowed a significant increase of 184% and 245% compared to the control and the dried manure on day 56. Dried poultry manure increased mineral N by 85% compared to the poultry manure ash. The PMA, NPK, CMD did not show any difference from the control. At the end of the experiment, mineral N did not differ following all amendments and even the control.

**Table 2.** Effect of amendments on mineral N in the screen-house experiment

| Amendments | …… Mineral N (mgkg$^{-1}$) …… | | | | | |
|---|---|---|---|---|---|---|
| | 1day | 14days | 28days | 42days | 56days | 70days |
| Soil only (CON) | 470.8c | 1178.3bc | 627.2a | 424.6b | 614.1b | 1290.1a |
| Dried cattle manure (CMD) | 1065.56b | 2495.5abc | 665.0a | 250.6b | 506.4b | 1932.2a |
| Cattle manure ash (CMA) | 468.1c | 3803.6a | 1048.8a | 262.1b | 1746.0a | 1281.4a |
| Dried goat manure (GMD) | 418.5c | 1952.9abc | 556.2a | 293.5b | 1480.4a | 965.3a |
| Goat manure ash (GMA) | 448.5c | 547.6c | 471.6a | 528.4b | 1782.9a | 1035.8a |
| Dried poultry manure (PMD) | 2092.8a | 2331.6abc | 1000.4a | 297.6b | 1519.0a | 2302.8a |
| Poultry manure ash (PMA) | 430.6c | 3084.0ab | 1351.5a | 732.3b | 818.8b | 1091.2a |
| NPK | 501.8bc | 3698.2a | 599.3a | 1357.9a | 325.7b | 821.5a |

*Means with the same letters are not significantly different at p≤0.05*

The highest and lowest mineral N values were observed with PMA and control respectively on day one of the field experiment (Table 3). PMA increased mineral N by 142% and 267% compared to its dried manure and control respectively. The faster mineralization of N from PMA as a result of the lower carbon nitrogen ratio could have been the rationale for its significant effect at the onset of the field experiment. However, other manure ashes were similar to their dried manures. The GMD-amended soil did not differ from the control soil. Mineral N increased drastically in the NPK-amended soil on the 14$^{th}$ day in comparison to other amendments and the control; a significant increase of 1077% above the control was recorded. The majority of the N contained in NPK is in the mineral form, since it is an inorganic fertilizer, and has the capacity to supply N immediately for plant use. In addition, the fact that it was incorporated on the 14$^{th}$ day is the justification for the drastic effect.

**Table 3.** Effect of amendment on mineralized N in field experiment

| Amendments | ……Mineral N (mgkg$^{-1}$) …… | | | | | |
|---|---|---|---|---|---|---|
| | 1day | 14days | 28days | 42days | 56days | 70days |
| Soil only (CON) | 79.57b | 231.02b | 70.37b | 142.34ab | 44.87a | 154.17bc |
| Dried cattle manure (CMD) | 190.81ab | 251.22b | 92.56b | 107.74b | 110.2b | 142.91bc |
| Cattle manure ash (CMA) | 143.76ab | 73.08b | 174.96ab | 227.20a | 292.8ab | 235.19a |
| Dried goat manure (GMD) | 117.75b | 198.38b | 120.76ab | 190.51ab | 195.7ab | 150.61bc |
| Goat manure ash (GMA) | 159.58ab | 75.20b | 275.45a | 167.94ab | 125.3ab | 173.59abc |
| Dried poultry manure (PMD) | 120.52b | 208.52b | 181.49ab | 141.50ab | 440.1ab | 109.95c |
| Poultry manure ash (PMA) | 292.04a | 190.20b | 161.93ab | 150.47ab | 291.8ab | 139.83bc |
| NPK | 184.30ab | 2720.57a | 279.86a | 104.99b | 199.2ab | 189.16ab |

*Means with the same letters are not significantly different at p≤0.05*

A similar response was observed on the 28th day, and the highest mineral N observed with NPK did not differ from that observed with GMA. On day 42, the lowest mineral N was observed in NPK-amended soil. The leaching and immobilization of mineral N is the rationale for the lowest N observed in NPK-amended soil on day 42, since all N is in the inorganic form. Adeniyan et al. (2011) reported that the nutrients released from the NPK fertilizer were only for a short period of time because the leaching of nutrients may be higher in the soil treated with NPK fertilizer than the soil treated with organic manures. GMA and PMA did not differ from their dried manure while CMA differed in mineral N from its dried manure by 111%. On day 56, no amendment difference was observed in terms of mineral N, and the values of mineral N in the amended soil were similar to those observed in the control soil. However, at the end of the experiment, CMA encouraged the highest mineral N compared to the control and other amendments except NPK and GMA. Manure ashes increased mineral N when compared to their dried manures. The incorporation of CMA into the soil increased mineral N by 53% and 65% compared to the control and CMD respectively. CMD, GMD, and PMD did not differ, while CMA and GMA showed similar results.

### *3.3 Amendment Effect on Mineral N across Time and Mineral N Dynamics across Amendments*

Table 4 shows the concentration of mineral N across time in the incubation, screen-house, and field experiments. Mineral N release was similar with NPK, PMA, and CMA amendments during the incubation experiment. This is observable since the incubation experiment was a controlled experiment and changes in the pattern of N release were solely due to the soil environment and amendment characteristics. Lower values of mineral N were recorded for the dried manures compared with the manure ashes, while the control did not significantly differ from the GMD amendment. Dried goat manure contained more carbon than any of the amendments, which may have caused the observed immobilization of mineral N in its amended soil. Azeez and Van Averbeke (2010) also confirmed the lowest value of mineralized N for goat manure, and reported a marginal increase in mineral N for the cattle and poultry manures. Higher ratios of 10%, 60%, and 54% of mineral N were recorded for CMA, GMA and PMA in comparison with CMD, GMD and PMD. The values reported here are higher compared to N mineralization reported by Abbasi et al. (2007). The reason for this disparity in values may be attributed to the lower N rate of 200mg/kg used by the author. However, in the screen-house experiment, there was no significant difference in the amendments. Also, the amendment effect was not significant compared to the control. NPK was able to release the highest mineral N, which was significantly different from other amendments and even the control although the release of mineral N was higher with CMA and PMA compared to their dried manures. The similarities observed in the screen-house and field experiments can be attributed to plant factors, and the non-significance of the amendment effect may be attributed to several factors in addition to the soil and amendment characteristics.

**Table 4.** Amendment effect on mineral N across time

| Amendments | Incubation | Screen-house Mineral N | Field ($mgkg^{-1}$) |
|---|---|---|---|
| Soil only (CON) | 189.85de | 1114.4a | 187.7b |
| Dried cattle manure (CMD) | 243.07cd | 1281.6a | 149.2b |
| Cattle manure ash (CMA) | 267.50abc | 1393.3a | 191.2b |
| Dried goat manure (GMD) | 159.65e | 1039.5a | 162.3b |
| Goat manure ash (GMA) | 254.98bcd | 977.8a | 162.3b |
| Dried poultry manure (PMD) | 206.55cde | 1515.0a | 200.4b |
| Poultry manure ash (PMA) | 317.40ab | 1186.2a | 204.4b |
| NPK | 329.78a | 1366.4a | 6130a |

The dynamics of mineral N release across amendment for the three experiments is presented in Table 5. In the incubation experiment, after the incorporation of the amendments into the soils, mineral N decreased with the increasing of time up to day 28, after which it increased again till the end of the experiment. The initial proliferation of microbes, as a result of the increased reproductive rates which led to a high competition for nutrients and the subsequent trapping of nutrients in the soil, could have led to the immobilization of mineral N observed at the onset of the experiment.

**Table 5.** Timing effect on mineral N across amendments

| Time | Incubation | Screen-house Mineral N | Field ($mgkg^{-1}$) |
|---|---|---|---|
| 1day | 229.23b | 950.1cde | 161.0b |
| 14days | 205.80b | 2387.2a | 493.5a |
| 28days | 197.65b | 790.0de | 169.7b |
| 42days | 215.03b | 518.4e | 154.1b |
| 56days | 382.78a | 1099.1bcd | 263.0b |
| 70days | -------- | 1340.0bc | 161.9b |

*Means with the same letters are not significantly different at $p \leq 0.05$*

Azeez and Van Averbeke (2010) observed that the immobilization of mineral N occurred on day 10 in the incubation experiment. Significantly, a higher mineral N release was observed on the 56th day i.e., the end of the experiment. This is attributed to the decomposition of microbial mass and release of the initially-immobilized nutrients on the days earlier than the 56th day. This is consistent with the findings of Azeez and Van Averbeke (2010) who reported that the highest uptake of N by crops should be expected around day 55 following the manure application.

Using three organic manures in a mineralization experiment, Abbasi et al. (2007) reported that the release of mineral N from organic pools increased over time, and that a significant difference was noticed in the later stages of the incubation experiment. The value of 382.78mgkg$^{-1}$ mineral N recorded the highest increase at 67% compared to the lowest value of 197.65mgkg$^{-1}$ on the 28th day of the experiment. Mineralization reached a maximum value at the end of the incubation experiment. This could have happened because mineralization in the manures was gradual, and it reached a maximum when the conditions were favorable in the soils.

However, in the screen house experiment, mineral N was low immediately after the incorporation of the amendments into the soils, after which a drastic increase of 151% was observed on the 14th day of the experiment. After day 14 of the experiment, mineral N dropped by a significant decrease of 66% on the 28th day up to day 42 after which it increased again by 112% on the 56th day up until the end of the experiment. However, after the incorporation of the amendments into the soils in the field experiment, mineral N increased significantly by 206% on the 14th day, after which it decreased again by 65% on the 28th day up to the 42nd day. On day 56, mineral N increased, though this was not significant and at the end of the experiment, mineral N value was low and similar to that observed at the incorporation stage. The highest mineral N was recorded on day 14, and the values observed on other days were significantly lower. It can be concluded that the mineralization pattern could be affected by the type of environment i.e being controlled or uncontrolled. Utmost N release was observed on the 14th day for the screen-house and field experiments. This means that the application of manure, weeks before planting, as is recommended in some agronomy manuals, may cause a substantial loss of mineralized N, and hence, encourage ground water pollution. The erratic pattern, observed in N release across time, may be attributed to the proliferation and death of microbes leading to a distortion in the N release. Additionally, the data provided were according to the soils and amendment types, which is the reason for the patterns observed.

### *3.4 Nitrogen Mineralization Kinetics*

Tables 6, 7, and 8 show the parameters estimates of the equations used to describe mineral N kinetics in the control soil, soils amended with dried manures or manure ashes, and NPK-amended soils. The $R^2$ was used as the criteria to determine the best fit. Table 6 shows that the first order, second order, and power function were only able to capture the release of N from CMD and GMA, while for the other amendments, the $R^2$ was very low. The first order constant $K_1$ was positive for all amendments and the second order was negative for all the amendments with the highest found in GMA and CMD. The wide variation in mineralization rate constant (k) of the dried manures and manure ashes may be attributed to the differences in amendment characteristics. The ability of the first order model and the second order model to capture the release of N in the control soil was zero. For the power function, GMA and CMD also had the highest $R^2$ and release rate coefficient (b), although the initial N release per day was highest in PMA. This could be due to the lower C:N ratio of PMA which mineralized faster than other amendments, the reason behind the highest N release per day.

**Table 6.** Estimated kinetic model parameters for mineral N in the incubation experiment

| | First order | | Second order | | Power function | | |
|---|---|---|---|---|---|---|---|
| | $K^1$ ($\times 10^{-1}$) | $R^2$ | $K^2$ ($\times 10^{-4}$) | $R^2$ | a | b ($\times 10^{-1}$) | $R^2$ |
| Soil only (CON) | 0 | 0 | -0.01 | 0 | 176.6 | 0.19 | 0.021 |
| Dried cattle manure (CMD) | 0.15 | 0.748 | -0.6 | 0.775 | 138.8 | 1.79 | 0.579 |
| Cattle manure ash (CMA) | 0.09 | 0.155 | -0.2 | 0.042 | 165 | 1.02 | 0.099 |
| Dried goat manure (GMD) | 0.06 | 0.117 | -0.3 | 0.064 | 156.2 | 0.1 | 0.003 |
| Goat manure ash (GMA) | 0.17 | 0.839 | -0.7 | 0.909 | 138.8 | 1.9 | 0.523 |
| Dried poultry manure (PMD) | 0.07 | 0.335 | -0.3 | 0.282 | 167.7 | 0.62 | 0.126 |
| Poultry manure ash (PMA) | 0.02 | 0.029 | -0.5 | 0.014 | 415.6 | 1.1 | 0.346 |
| NPK | 0.09 | 0.241 | -0.3 | 0.198 | 299.5 | 0.12 | 0.002 |

However, in the screen-house experiment (Table 7), the first-order model captured a bit of the N release from GMA and PMD, and the second-order model captured N release from GMA, while the power-function model was unable to capture N release from any of the amendments. The first-order rate constant was highest in GMA, while in other amendments and control soil, $K_1$was very low. The second-order rate constant K was very low in all of the amendments with negative values recorded for CMA, GMD and GMA. For the power-function model, the initial release rate constant was highest in PMD, while negative values of release rate coefficient were observed for the control, CMD, PMD, and NPK. The second-order model and the power-function model were unable to capture any N release in all of

the amendments in the field experiment (Table 8). Moreover, amongst all the amendments and control, only the first-order model captured the release of N from CMA. The first-order model was positive and low for all amendments except NPK which showed the highest value. The second-order constant $K_2$ was very low for all amendments with negative values recorded for GMD, GMA, and PMD. The first-order, second-order and power-function models were unable to capture a release of N from all amendments since the $R^2$, which was used as the criterion of fit, was very low. This is consistent with the findings of Azeez and Van Averbeke (2010) who used the same model and observed that the non-conformity of the data to the models may be ascribed to the inconsistent N release patterns, net mineralization, immobilization, and fixation. They also reported that the models have been developed for abiotic systems rather than microbial induced systems in soil conditions, which is reason behind the inadequacy of the models. This means that the release of N from NPK, dried manures, and manure ashes, except for GMA, was not linear. However, mineral N released from GMA in the incubation experiment follows a linear trend, which is observable from the $R^2$.

**Table 7.** Estimated mineral N kinetics model in the screen-house experiment

| | First order | | Second order | | Power function | | |
|---|---|---|---|---|---|---|---|
| | $K^1$ ($\times 10^{-2}$) | $R^2$ | $K^2$ ($\times 10^{-4}$) | $R^2$ | a | b | $R^2$ |
| Soil only (CON) | 0.7 | 0.133 | 0.08 | 0.099 | 1613 | -0.2 | 0.376 |
| Dried cattle manure (CMD) | 0.5 | 0.029 | 0.1 | 0.041 | 1257 | -0.12 | 0.049 |
| Cattle manure ash (CMA) | 0.2 | 0.005 | -0.06 | 0.014 | 659.9 | 0.142 | 0.055 |
| Dried goat manure (GMD) | 0.5 | 0.038 | -0.1 | 0.049 | 505.7 | 0.134 | 0.081 |
| Goat manure ash (GMA) | 1.6 | 0.577 | -0.2 | 0.668 | 377.6 | 0.201 | 0.334 |
| Dried poultry manure (PMD) | 0.4 | 0.618 | 0.06 | 0.017 | 2095 | -0.15 | 0.094 |
| Poultry manure ash (PMA) | 0 | 2E-05 | 0.08 | 0.084 | 637.2 | 0.157 | 0.14 |
| NPK | 1.5 | 0.238 | 0.2 | 0.221 | 1481 | -0.14 | 0.074 |

**Table 8.** Parameters estimates for mineral N kinetics in the field experiment

| | First order | | Second order | | Power function | | |
|---|---|---|---|---|---|---|---|
| | $K^1$ ($\times 10^{-2}$) | $R^2$ | $K^2$ ($\times 10^{-4}$) | $R^2$ | a | b | $R^2$ |
| Soil only (CON) | 0.1 | 0.006 | 0.3 | 0.017 | 97.14 | 0.022 | 0.003 |
| Dried cattle manure (CMD) | 0.7 | 0.275 | 0.5 | 0.21 | 210 | -0.13 | 0.305 |
| Cattle manure ash (CMA) | 1.4 | 0.554 | 0.9 | 0.417 | 109 | 0.156 | 0.25 |
| Dried goat manure (GMD) | 0.3 | 0.131 | -0.2 | 0.163 | 123.1 | 0.081 | 0.284 |
| Goat manure ash (GMA) | 0.3 | 0.033 | -0.3 | 0.067 | 140.1 | 0.025 | 0.009 |
| Dried poultry manure (PMD) | 0.3 | 0.026 | -0.4 | 0.001 | 129.7 | 0.103 | 0.104 |
| Poultry manure ash (PMA) | 0.5 | 0.162 | -0.3 | 0.203 | 278.6 | -0.11 | 0.321 |
| NPK | 1.7 | 0.164 | 0.4 | 0.119 | 366.1 | -0.88 | 0.012 |

Attempts which have been made to predict the nutrient value of manures, using their mineral N concentration at the time of application, are good approaches for preparing simple-nutrient budgets (Chambers et al., 1999). However, such approaches do not take account of mineralization and immobilization which follow the manure application to the field and ignore any potential changes in the rates of mineralization of the background organic matter (Abbasi et al., 2007). Mineral N release kinetics is shown in Figures 1, 2, and 3 for the incubation, screen-house, and field experiments, respectively. It can be concluded that the relationship between the N release kinetics and the number of days in the three experiments was not linear, and best was described by a polynomial raised to the power of three.

In Figure 1, it is observed that the kinetics of N release per time for GMA was not described by the polynomial raised to the power of three (Figure 1). The $R^2$ shows that about a 50%, 63%, 96%, 69%, 33%, 68% and 52% variation in the amount of N release per unit time was captured by the model for the control soil, CMD, CMA, GMD, PMD, PMA and NPK, respectively. Among the dried manures and manure ashes, only CMA had a polynomial relationship existing between the amount of N released and time. Figure 1 also shows that the pattern of N release was not the same for the dried manures, manure ashes and control. This may be ascribed to differences in the characteristics of the manures and manure ashes used for the experiments. Additionally, the variation in the mineralization pattern observed could be attributed to mineralization-immobilization turnover in the experiment. For CMA, CMD, PMD, and the control soil, there was an initial N release between day 0 and day 14 as a result of the initial wetting and drying of the soil. This was followed by a phase of constant release from day 14 to day 24 due to immobilization, and a slow decline between days 25 and 40, after which a final sharp increase in N release was observed from day 42 to day 56. The similarities in the pattern of N release per time for the dried manures may be attributed to the same carbon nitrogen ratio. This implies that

for CMA, CMD, and PMD, the application of these manures should be synchronized with the N uptake i.e., they should be applied at planting so that the final sharp phase of N increase will correspond with the time of plants' utmost need for N (at taselling) to avoid a substantial loss of mineralized N. Gale and Gilmour (1986) reported that three phases of decomposition and mineralization occurred when broiler manure was incorporated into the soil. However, For GMD, a phase of rapid decline from day 0 to day 28, and a rapid increase from day 32 to day 56 was observed. For PMA, an increase-decrease pattern of N release was observed and for GMA, and a phase of steady increase in N on day 0 to day 28 followed by a decline, after which a sharp increase was observed on days 42 to 56.

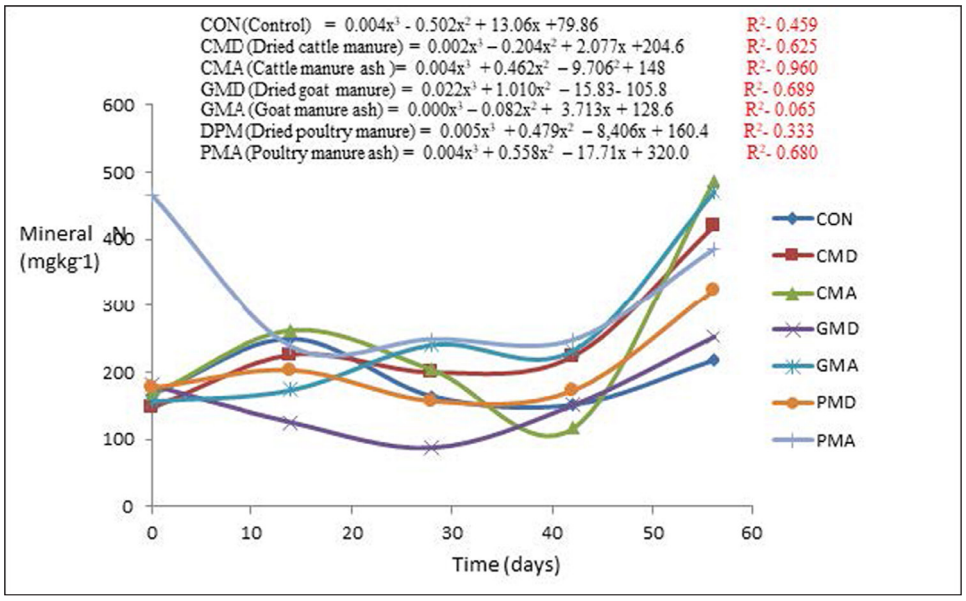


**Figure 1.** Nitrogen release kinetics in incubation experiment

However, in the screen house experiment (Figure 2), the relationship between N release kinetics and time was totally captured by the model for the control soil, since it was 100% fit for the data. This is because mineral N release from the control soil was solely curvilinear not linear. For CMD, CMA, GMD, GMA, PMD and PMA, the variation in the captured data were 79%, 34%, 14%, 61%, 77%, and 68% respectively. The phases of N release kinetics were similar for CMD, PMD and PMA. The reason for the similarities in CMD and PMD has been explained above. These amendments had a sharp increase in N release from day 0 to day 14 followed by an abrupt decrease in N on day 15 to day 42, and a final phase of rapid N release. The immobilization of mineral N occurring on day 15 to day 42 in CMD, PMD, and PMA could be attributed to the temporary loss of the released N by microbes, especially when the carbon in the amended soils increased at this point. This also means that on days 15 to 42, the plant N uptake will be very low, since most of the released N had been immobilized. The increased mineralization of N from these amendment at the final phase is advantageous for the plant, since these phases correspond to the phase of utmost N need for physiological processes such as tasselling.

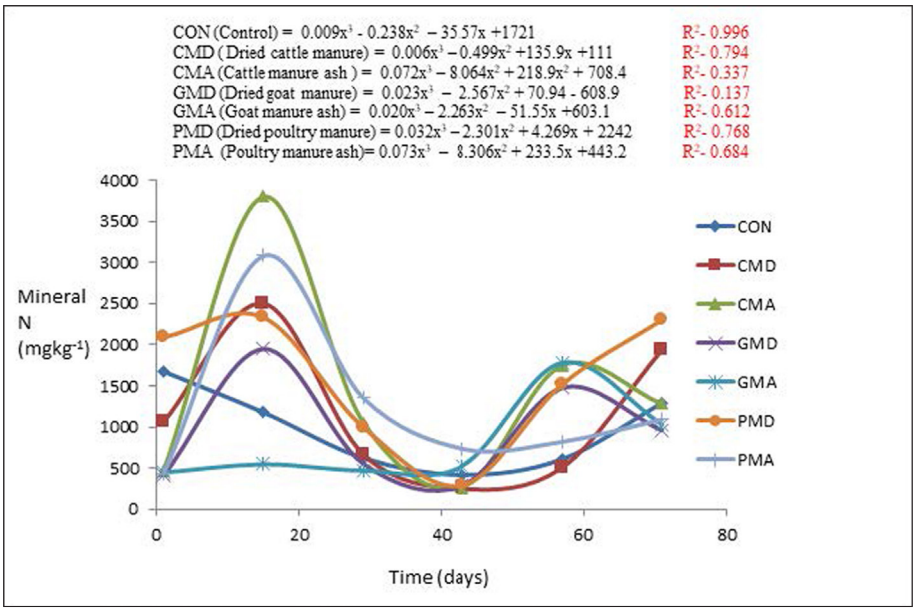


**Figure 2.** Nitrogen release kinetics in the screen-house experiment

The findings presented above is inconsistent with the findings of greenhouse studies by Mugwira and Mukurumbira (1984) who observed a depression in the yields in the first two weeks followed by a significant increase of plant growth after two weeks of being planted in manured pot. The non-conformity could be attributed to the differences in manure characteristics. Conversely, for the control soil, only two phases were observed in the N release per time which are: a phase of steady decrease from day 0 to day 42, and a steady increase from day 43 to day 70. For CMA and GMD, four phases were recorded as follows: an initial phase of sharp increase from day 0 to the 14th day, followed by a sharp decrease from the 15th day to the 42nd day, a steady increase from day 43 to day 56, and a final phase of constant decline in N. A similar pattern was observed for GMA only that the first and second phases were steady. The erratic pattern of N release observed with CMA and GMD could be due to death and growth of N mineralizing microbes, thereby causing the inconsistencies in the observed data.

The goodness of fit measured by the $R^2$ showed that a 86%, 99%, 98%, 98%, 95%, 100%, 95% variation in the data for the control, CMD, CMA, GMD, GMA, PMD and PMA respectively were captured by the model for the field experiment (Figure 3). This means that release of N across time from the amendments was curvilinear, but not linear, and could be attributed to the impacts of soil and environmental factors which could not be controlled on the field experiment. The phases of N release kinetics were similar for the control, and all the dried manures, and an erratic pattern of N release was observed during which N increased at one week, but decreased the succeeding week. The rationale for the erratic pattern of mineral N may be attributed to the proliferation and death of microbes thereby causing inconsistencies in the data. This is in agreement with the findings of Abbasi et al., 2007 who observed an inconsistency (an increase or decrease with time) in the pattern of total mineral N of three organic manures in an incubation experiment. However, three phases were observed for the manure ashes. For PMA, a steady decline from day 0 to day 42, followed by a phase of increase in N up to day 56, and a final phase in which N declined steadily. For CMA, a steady decline from day 0 to day 14 was followed by a steady increase till day 56, and a constant decrease from day 57 to day 70. For GMA, a steady decrease from day 0 to day 14 was followed by a steady increase from day 15 to day 28, and a final steady decline in N was observed.

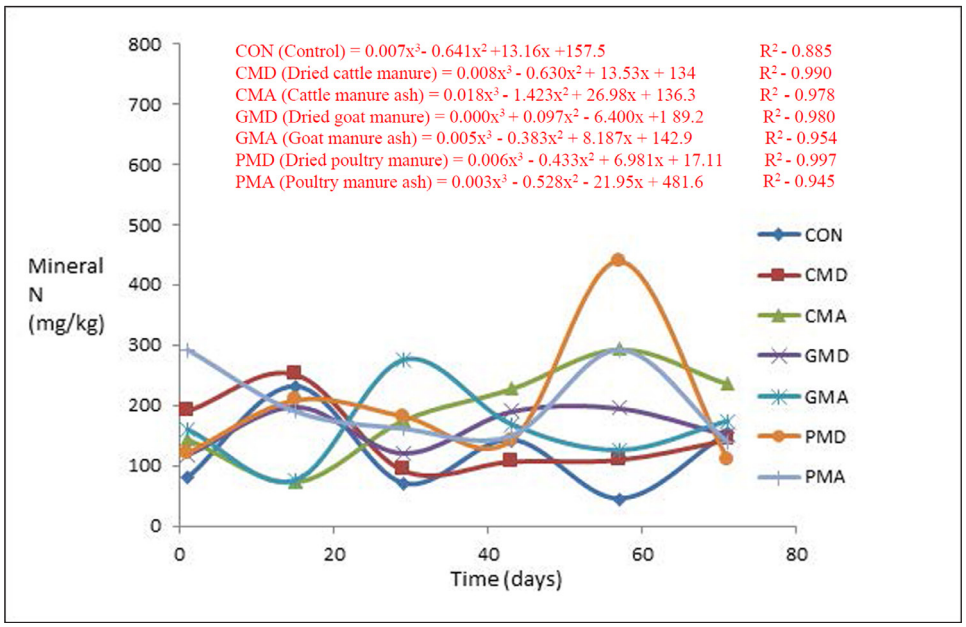


**Figure 3.** Nitrogen release kinetics in the field experiment

The percentage proportions of mineral N released from the applied organic amendments (dried manures and manure ashes) are presented on Figure 4. The release of mineral N was not the same for the three amendments in the three experiments. Mineral N released from the dried manures and manure ashes was in the order of: screen-house experiment > incubation experiment > field experiment. The highest amount of mineral N released from the applied organic sources in the screen-house experiment, compared to the incubation experiment, could be due to the temperature and the increased action of microorganisms in the rhizosphere favoring N release, and also because the pathway of N loss was not as wide as that in the field experiment. The rationale for this is that the mineral N released was subjected to losses that could be through plant uptake of N, immobilization, leaching, and volatilization in the field experiment. Plant uptake of N in the screen-house experiment is expected to be low compared to the field experiment, since it was a controlled experiment, and several factors responsible for the N loss could be controlled. The relatively low mineralization capacity of the manures and manure ashes in the incubation experiment could be attributed to changes in the soil which may have developed during incubation (Abbasi et al., 2007). In the incubation experiment, the mineral N release followed the order PMA > CMA > GMA > CMD > PMD > GMD. However, in the screen house experiment, the order was CMA > PMA > CMD > CMD > GMA > GMD. Moreover, a different order was observed in the field experiment as follows: PMA > CMA > GMA = PMD > CMD = GMD.

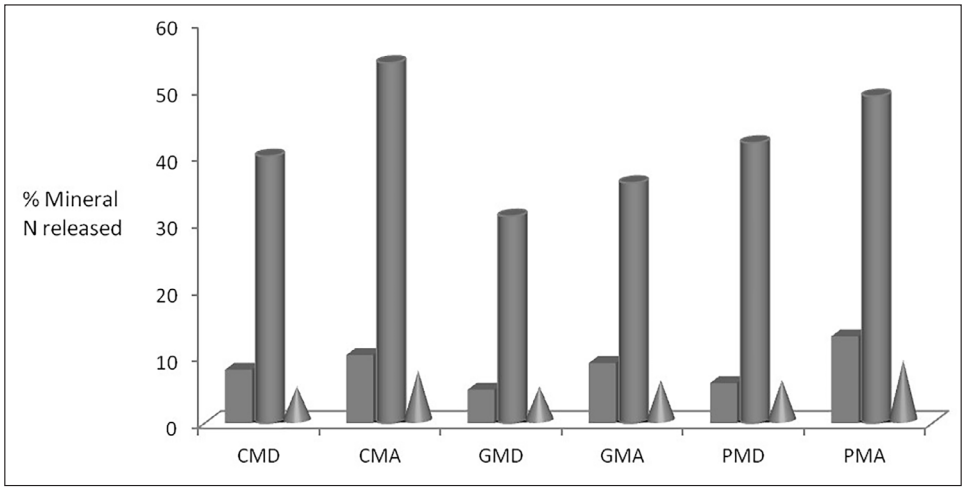


**Figure 4.** Percentage of mineral N released in the incubation, screen-house and field experiments.

## 4. Conclusions

The incorporation of manure ashes increased mineral N in comparison with dried manures in the experiments. Soil environment and amendment characteristics are important factors affecting mineral N release in incubation experiments, while plant factors coupled with the above factors are determinants of the amount of N released from screen-house and field experiments.

Mineralization reached a maximum on day 56 of the incubation experiment (end of the incubation experiment). Utmost N release was on day 14 for the screen-house and field-patterns. The application of manure to the soil, some weeks before planting, as recommended by some manuals, could cause a substantial loss of mineralized N, and hence encourage ground water pollution.

The first-order and second-order models were able to capture the release of N from only GMA amongst other amendments, while the power-function model was unfit for the data. Relationship between the N release kinetics and number of days in the experiments were not linear, and were best described by a cubic polynomial function. In the incubation experiment, the N release kinetics was not the same for the dried manures, manure ashes and the control, while similar phases of N release kinetics were observed for CMD, PMD, and PMA in the screen-house experiment, and an erratic pattern of N kinetics was observed with similar pattern for the control and the dried manures in the field experiment.

Mineral N released from dried manures and manure ashes was in the order of: screen-house experiment > incubation experiment > field experiment. However, PMA > CMA > GMA > CMD > PMD > GMD, CMA > PMA> CMD > CMD > GMA >GMD and PMA > CMA > GMA = PMD > CMD = GMD was observed in the incubation, screen-house and field experiments respectively.

**Acknowledgement**

The authors wish to acknowledge the Soils of Forest Islands in Africa (SOFIIA-FUNAAB) for their support in the laboratory analyses. SOFIIA is a collaborative research project funded through by the UK Government's Royal Society-DFID Africa Capacity Building Initiative. Opinions expressed and conclusions arrived at are those of the authors and are not necessarily to be attributed to the project.

## References

Abbasi, M.K., Hina, M., Khalique, A., Khan, S.R. (2007). Mineralization of three organic manures used as nitrogen source in a soil incubated under laboratory conditions. Communication in Soil Science and Plant Analysis 38:1691-1711. https://doi.org/10.1080/00103620701435464.

Abbasi, M.K., Shah, Z., Adams, W.A. (2003). Effects of nitrification inhibitor nitrapyrin on the fate of nitrogen applied to a soil incubated under laboratory conditions. Journal of Plant nutrition and Soil Science 166: 513-518.

Adeniyan O.N., Ojo A. O., Akinbode, O. A., Adediran J.A. (2011) Comparative study of different organic manures and NPK fertilizer for improvement of soil chemical properties and dry matter yield of maize in two different soils. Journal of Soil Science and Environmental Management Vol. 2 (1), pp. 9-13.

Azeez, J.O., and Van Averbeke, W. (2010). Nitrogen mineralization potential of three animal manures applied on a sandy clay loam soil. Bioresource Technology 101: 5645–5651. doi:10.1016/j.biortech. 2010.01.119.

Calderon, F.J., MeCarty, G.W., Reeves, J.B. (2005). Analysis of manure and nitrogen mineralization during incubation. Biology Fertility and soils 41: 328-336.

Camargo, F.A.O., Gianello, C., Tedesco, M.J. (2004). Soil nitrogen availability evaluated by kinetic mineralization parameters. Communication in Soil Science and Plant Analysis 35: 1293-1307.

Cataldo, D.A., Haroon, M, Schrander, L.E.,Youngs, V.L. (1975). Rapid colorimeteric determination of nitrate in plant tissue by nitration of salicylic acid. Communication in Soil Science and Plant Analysis 6: 71-80 https://doi.org/10.1080/00103627509366547

Chambers, B.J., Lord, E.I., Nicholson, F.A., Smith, K.A. (1999). Predicting nitrogen availability and losses following application of organic manures to arable land. MANNER. Soil Use Management 15:137-143.

Chadwick, D.R., John, F, Pain, B.F., Chambers, B.J., Williams J.C. (2000). Plant uptake of nitrogen from the organic nitrogen fraction of animal manures. A laboratory experiment. Cambridge Journal Agriculture Science 134:159-168 https://doi.org/10.1017/s0021859699007510

Codling, E.E., Rufus, L.C., Sherwell, J. (2002). Poultry litter ash as a potential phosphorus source for agricultural crops. Journal of Environmental Quality 3: 954-961. doi: 10.2134/jeq2002.0954

Cordovil, C.M.D.S., Coutinho, J., Goss, M., Cabral, F. (2005). Potentially mineralisable nitrogen from organic materials applied to a sandy soil: fitting the one-pool exponential model. Soil Use Management 21: 65–72.

Dang, Y.P., Dalal, R.C., Edwards, D.G., Tiller, K.G. (1994). Kinetics of zinc desorption from Vertisols. American Journal of Soil Science Society 58:1392–1399.

Demeyer, A., Voundi Nkama, J.C., Verloo M.G. (2001). Characteristics of wood ash and influenceon soil properties and nutrient uptake: An overview. Bioresource Technology 77: 287–295.

Domburg, P., Edwards, A.C., Sinclair, A.H. (2000). A comparison of N and Pinputs to the soil from fertilizers and manures summarized at farm and catchment scale. Cambridge Journal of Agriculture Science 134:147-158.

Gale, P.M., and Gilmour, J.T. (1986). Carbon and nitrogen mineralization kinetics for poultry litter. Journal of Environmental Quality 15:423-426.

Gilley, J.E., and Risse, M. (2000). Runoff and soil loss as affected by the application of manure. Transaction ASAE, 43:1583- 1588.

Hadas, A., Kautsky, L., Mustafa, G., Kara, E.E. (2004). Rates of decomposition of plant residues and available nitrogen in soil, related to residue composition through simulation of carbon and nitrogen turnover. Soil Biology and Biochemistry 36:255–266.

Mugwira, L.M. and Mukurumbira, L.M. (1984). Comparative effectiveness of manure from communal areas and commercial feedlot as plant nutrient sources. Zimbabwe Journal of Agriculture 81: 241-250.

Olowoboko T.B., Azeez J.O., Olujimi O.O., Babalola, O.A. (2018). Availability and dynamics of organic carbon and nitrogen indices in some soils amended with animal manures and ashes. International Journal of Recycling of Organic Waste in Agriculture 7(4):287-304.

Paulo, P., Carl, R., Jeff, S., Michael, R. (2010). Phosphorus Availability and Early Corn Growth Response in Soil Amended with Turkey Manure Ash. Communication in Soil Science and Plant Analysis 41(11): 1369-1382.

Pereira, J., Muniz, J., Silva, C. (2005). Nonlinear models to predict nitrogenmineralization in an Oxisol. Science and Agriculture (Piracicaba, Braz.) 62: 395-400.

SAS Institute Inc. (1999). SAS/STAT® 9.1 user's guide. Cary, N.C.: SAS Institute Inc.

Smith, J.L., Schnabel, R.B., McNeal, B.L., Campbell, G.S. (1980). Potential errors in the first order model for estimating soil nitrogen mineralization potentials. American Society of Soil Science 44: 996-1000.

Stanford, G., and Smith, S.J. (1972). Nitrogen mineralization potential of soils. Proceeding of American Society of Soil Science 109: 190–196.

Teppei, K., Arata, K., Manabu, Y. (2012). The chemical characteristics of ashes from cattle, swine and poultry manure. Journal of Material Recycling and Waste Management https://doi.org/10.1007/s10163-012-0089-2

Tisdale, S.L., Nelson, W.L., Beaton, J.D., Havlin, J.L. (1993). Soil fertility and Fertilizers, 5th Edn.; Prentice Hall: Upper Saddle River, N.J.

Van Kessel, J.S., Reeves III, J.B., Meisinger, J.J., (2000). Nitrogen and carbon mineralization of potential manure components. J. Environ. Qual. 29, 1669–1677.

Wang, W.J., Smith, C.J., Chen, D. (2003).Towards a standardised procedure fordetermining the potentially mineralizable nitrogen of soil. Biology Fertility and Soils 37:362-374.

Yang, J., He, Z., Yang, Y., Stoffella, P., Yang, X.,Banks, D., Mishra, S. (2007). Use of amendments to reduce leaching loss of phosphorus and other nutrients from a sandy soil in Florida. Environmental Science and Pollution Research 14:266 269. doi:10.1065/espr2007.01.378

Yusiharni, B.E., Ziadi, H.,Gilkes, R.J. (2007). A laboratory and glasshouse evaluation of chicken litter ash, wood ash and iron smelting slag as liming agents and P fertilizers. Australian Journal of Soil Research 45:374–389. https://doi.org/10.1071/sr06136.

JJEES

JJEES (2019) 10 (4): 215-226
ISSN 1995-6681

Jordan Journal of Earth and Environmental Sciences

# Analysis and Modeling of the Hydro-Mechanical Behavior of Ain El Hammam Landslide, Algeria

Fazia Boudjemia* and Bachir Melbouci

*Laboratory of Geomaterials, Environment and Installation (LGEA), University of Mouloud Mammeri - Tizi-Ouzou, Algeria*

*Received 27 April 2019; Accepted 29 July 2019*

**Abstract**

A detailed analysis of the slope of Ain El Hammam, located at 50 km south of Tizi-Ouzou, revealed a complex landslide mechanism. The complexity of this hydrogravity process lies in its heterogeneous operating mode over time and its location in an urbanized environment. The study of the triggering factors and parameters that control the evolution of this instability is a very important stake in understanding the process of this landslide. The analysis made it possible to evaluate the relative influence of the geological, hydrogeological and geomorphological parameters behind the triggering of this landslide.

The current work included a numerical analysis of the behavior of the slope under various geotechnical and hydro-mechanical conditions. A numerical modeling of the slope was thus carried out using the FLAC 2D and OptumG2 softwares. The stability calculation provides safety factors indicating the existence of a superficial slip, a deep slip, and a very deep potential rupture. This allows for the association of the failure mechanisms with the observations made in situ. In addition, the results highlighted the important role of fluid overpressures in the triggering and amplification of the landslide, as well as the aggravation of the phenomenon by the overload due to the urbanization of the site.



**Keywords:** landslide, stability, modeling, water level, mechanical characteristics.

## 1. Introduction

Among the land movements suffered by several regions of the wilaya of Tizi-Ouzou (Guirous et al., 2014; Bouaziz and Melbouci, 2019), the landslide of Ain El Hammam has attracted a maximum attention since its appearance, given its complexity and the important disorders that have generated it. Marked by exceptional climatic events, the landslide is a steep slope composed of metamorphic soil, and is characterized by slow yet extended movements with episodes of acceleration.

Several studies and investigations have been carried out in order to better understand this phenomenon, and seek a comfortable solution. This work (LNTPB, 1973; GEOMICA, 2006; 2009 and ANTEA, 2010) includes essential knowledge which deals with the recognition of this site. A number of assumptions emerged in relation to the origin of the landslides, the mechanisms of failure, and the composition of the grounds which moved. All these ideas make it possible to set up a full description of this phenomenon, and to define the physical and geometrical parameters and the mechanical factors to be taken into account during a modeling.

Numerical calculations of the slope stability (Talren 4) carried out by the ANTEA laboratory (2010), assume the existence of surfaces of discontinuity at several depths of the slope, with a rotational fracture geometry.

Moreover, the modeling of landslides is based on a multidisciplinary approach that derives from distinct conceptions. These include on one hand, the visual analysis of the natural sites, which includes the classification of the types of slip and designation of volumes of the soil masses, affected by the movements, and on the other hand, the deterministic analysis which defines the properties of these moving massifs and their introduction into mathematical models.

In the first part of this work, an overall description of the phenomenon and its probable origins has been presented. In the second part, a numerical modeling has been used to reproduce the hydro-mechanical conditions, inducing the instability of the slope, and analyze the relevance of the different fracture scenarios.

## 2. Description of Landslide

The detection and auscultation of land instabilities and the potentially unstable zones in Ain El Hammam region require a methodology based on a few tools including existing documents, mapping techniques, and direct observation of the study sites (Pisani et al., 2010; Wu et al., 2019).

With a heavy past in terms of ground movements (since 1969), the slope presents a chaotic and a bloated aspect reflecting the fragility of the site and its sensitivity to the evolution of the forms of the relief, by conjugate sets of erosion and deformation due to both subsidence and landslides as well as to earthy flows. Indeed, one can observe several scars of former superficial or semi profound slides which would have led to displacements of voluminous rocky panels. This activity marked the morphological modification and the fragile equilibrium of the entire slope which went through a long period of relaxation.

This situation has led to the concept of several reactivations caused across time (1973, 1984 and 1986), by climate change and inappropriate human intervention. The first estimates of the magnitude of the movement describe an

* Corresponding author e-mail: b_fazia78@yahoo.fr

extent of a 90 m width with a vertical drop reaching 20 m, for an unstable layer with a small thickness which concerns only embankments and materials resulting from the alteration of schist (LNTPB, 1973). These first signs of instability that appeared in the high side of the slope during the process of urbanization have been studied in order to develop a POS (ground occupation plan) which will prohibit high-rise constructions on the affected part by slippage.

Towards the nineties 1990 , after the removal of long and thick thrusts, instabilities were reported, at the bottom of a primary school. This school experienced major disorders then even on its structural frames.

The stability of the site became then fragile until 2002 and 2004 when new disorders reappeared and the movement kept evolving until 2006.

Stretching over 150 m in length between the summit and the frontal part of the slope, the slip began to describe a more complex form until it reached some of the slope on the south-east side beside the road leading to Ait Sidi Said (Figure 1).

The major part of the landslide affects the urbanized area, and many infrastructures are consequently affected. It also affects roads that lead to various localities. Boulevard colonel Amirouche, which constitutes the main axis of regional communication, shoemaker's street, and Bounouard Street, are constantly threatened and degraded.


**Figure 1.** Propagation and evolution of the slide downstream of the slope.

During winters with heavy rains, the movement of the land continued to spread in a strong and steady manner. In the winters of 2008-2009, some particular and marked disorders appeared, such as a distortion of buildings and retaining walls (Figure 2), and also crevasses on the roadways (Figure 3).

During winter of 2009-2010 the activity of the sol was closely monitored, following the propagation of the movement towards the median and lower zones of the slope (Figure 4). Prospecting work has been initiated since October 2009 by setting up a network of points subject to topometric measurements in order to define the kinematics of the movement (displacement reaching 50 cm over a few zones during a period of six months).

**Figure 2.** Obstructions observed in buildings.


**Figure 3.** Dislocation of a retaining wall, subsidence of sidewalks, and cracks in pavements affecting pipeline networks.

Given the great influence of water on these movements, it has been decided since 2012, to set down a diversion system for runoff water and waste water towards the downstream slope of the area. The slippage, then, slowed down to leave behind very slow movements which characterized a calm period. This, without neglecting the new local instabilities, appeared in particular, on the Shoemaker street (Figure 5), as well as during the renewal of numerous cracks in the retaining walls and ways, which are filled in by public services each time.

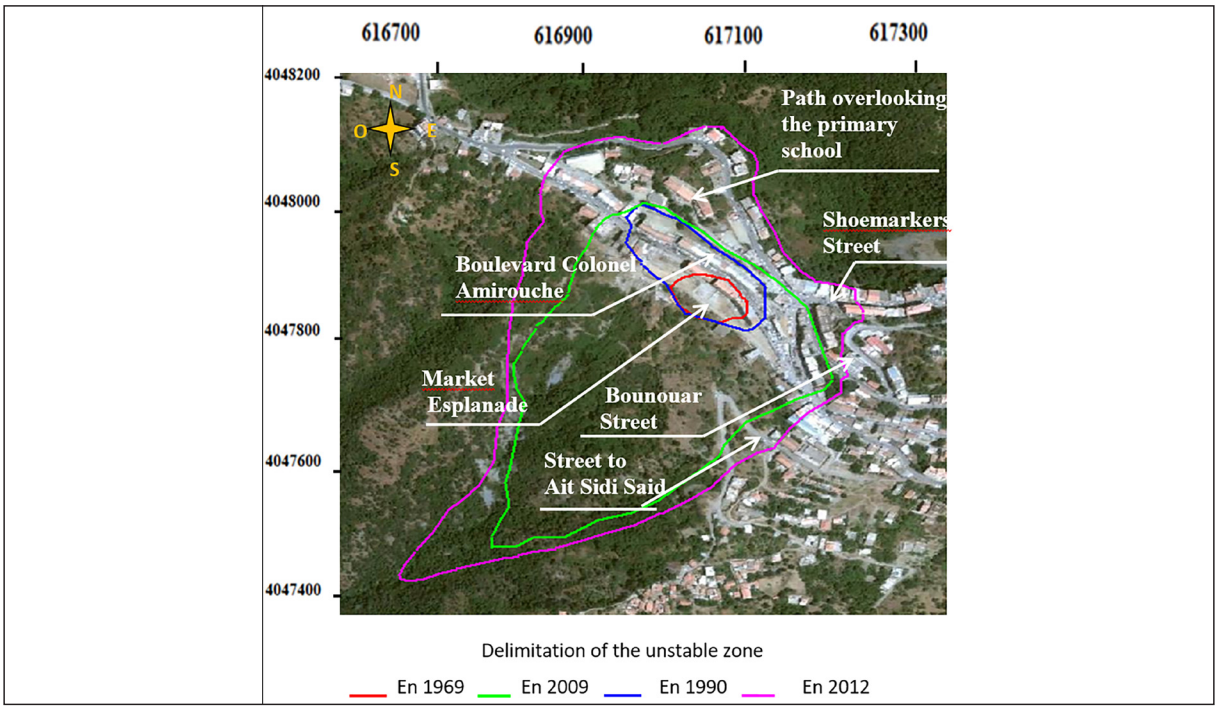


**Figure 4.** Evolution of the area of landslide (Djerbal and Melbouci, 2013), and locating the principal places affected by the movement.


**Figure 5.** New instabilities registered in 2016.

The current monitoring marks a reactivation of the movement under the influence of bad weather recorded in January, 2019. This was observed, in particular, on two buildings in R + 4 which lean towards the market, below, increasingly each day, especially following showers. The adjoining building shows a gap of more than one meter, at the fourth floor, which continues to cause concern to the local population who fear that the impact of this movement may cause the collapse of these buildings at any time.

## 3. Origins of Landslide

The origins of the landslide of Ain El Hammam are probably multiple and remain polemic. Indeed, it is a convergence and conjugation of several factors that can be categorized into three groups of factors: predisposing factors, triggering factors, and aggravating factors (Tullen, 2002; Ietto et al., 2018).

### *3.1 Predisposition Factors*

These factors act through multiple intrinsic conditions of the slope. The topography of the site is characterized by a steep slope, with varying inclines over the entire slope, giving rise to high instability potentials.

The geological nature of the schist formations defines the altered layers at depth, giving rise to underground water circulation which contributes to the reduction of the mechanical strength of materials. These formations are overcome by deposits resulting from the continuous erosion of the slope and a succession of embankments. These deposits form a superficial cover which, by its permeability, contributes greatly to the setting up of preferential channels linked to the infiltration of water, thus promoting the phenomenon of the regressive alteration of the schist.

The geotechnical characteristics define the high clay mineral contents (Kechidi, 2010) and materials that are less resistant, but sensitive to the phenomena of ground movements.

The hydrogeology of the site, is sustained by the presence of several water sources and streams of torrential and permanent flows, which through their erosive action, lead to a decrease in mechanical parameters and a modification of the morphology.

The effect of deforestation also plays a significant role. Landscape areas are characterized not only by a poor vegetation cover, but are also shaved over the urbanized area. In general, vegetation contributes to the stabilization of the slopes by fixing the soil and modifying the water balance (Dapples, 2002; Ismail et al., 2018).

### *3.2 Aggravating Factors*

Land use is the main aggravating factor in Ain El Hammam's landslide, it is basically linked to the development and increasing urbanization of the region. This action of anthropic origin, participates strongly in the degradation of the stability conditions. In this context, the appearance of new disorders around 1990 during the construction of the BDL building can be mentioned. This was noticed as a lowdown period of the landslide process, notably on the upstream side since the demolition of some buildings in 2009. Anthropogenic action is also manifested by the modification of the morphology of the slope induced by the significant earthworks leading to the suppression of natural abutments as well as by the inappropriate jets of embankments contributing to the design steeper slopes.

### *3.3 Triggering Factors*

This part is linked to the climate side which is favorable to landslides. The mean annual rainfall value for this area is 1058 mm between 1968 and 1994, and 1009 mm between 1997 and 2006. This value corresponds to the values of a very rainy region. However, it was found that the most significant trigger and acceleration of the movement are largely conditioned by extreme weather events; for example, the first signs of movements were observed in December, 1969 after a heavy rainfall. The new disorders during 2004-2005, their spread along the crown and on the slope, and also the paroxysm of the displacements in winter of 2008-2009 have also appeared following a heavy rainfall.

As far as snow, that characterizes the region, is concerned, it appears to be important, in particular, in the winters of 2005 and 2012. Its spread over long periods causes the disintegration of the underlying layers by frost, but when melting, it causes saturation of the soft layers and then setting in motion in the short term.

## 4. Geological Overview

The district of Ain El Hammam belongs to the internal zones of the chain of Maghrebides. In this area, the Kabyle crystallophyllian base was found to be mainly composed of metamorphic massifs, namely, gneisses, marbles, micachists, and schists (Figure 6). This base is, in some places, unconformably covered by detrital deposits of the upper Oligocene-lower Miocene age, named Oglio-Miocene kabyle (Durand-Delga, 1969).

In the region of Ain El Hammam, the crystallophyllian basement consists of micaceous schists which were seen on 78.91% of the territory of the commune. The rest is occupied by granite schist (10.66%), gneissic granulites (6.98%), fossiliferous schist, and phyllades (3.16%), to which can be added the quaternary formations corresponding to the filling by alluvium deposits representing 0.29% of the total area.

The geological formations, therefore, include a series of essentially schistose rocks with micaschists dominated by a satin schist feature of a dark gray color. The latter are sometimes in contact with gneisses, and have a mean directional schistosity ENE-WSW. The axial dipping of this formation is oriented towards the south-east with a maximum dip of 60 °. The micaschists are dark cream to light brown; their schistosity takes the same direction as that of the schists, which varies from 30 ° to 80 ° towards the south.

On the slip zone, a detrital sequence of grayish satin schists, containing fine quartzite-rich levels and a predominantly clayey-silty cover, constituting the upper unit (Figure 7).

The nature of the surface structure and the basic formations which are perceptible to the fracturing in the upper part constitutes a geological context very favorable to the movements of ground.

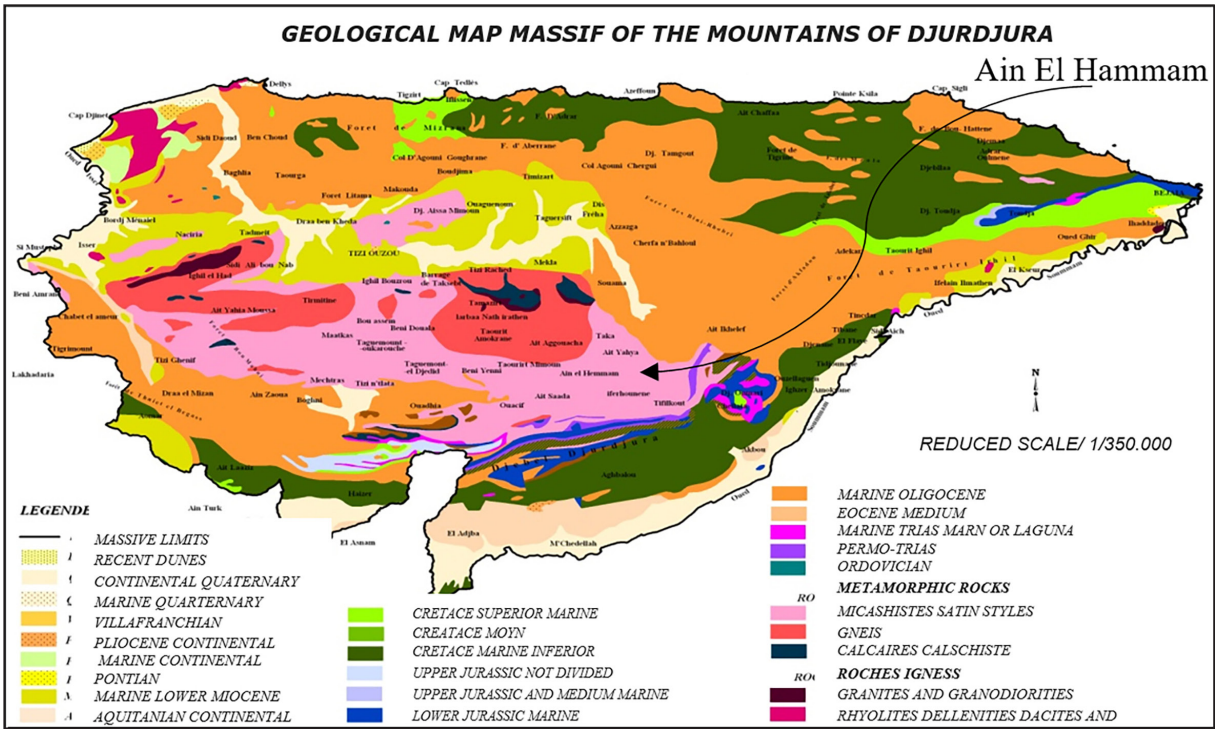


**Figure 6.** Geological map showing solid masses of the mounts of Djurdjura (CENEAP-MATET, 2010).

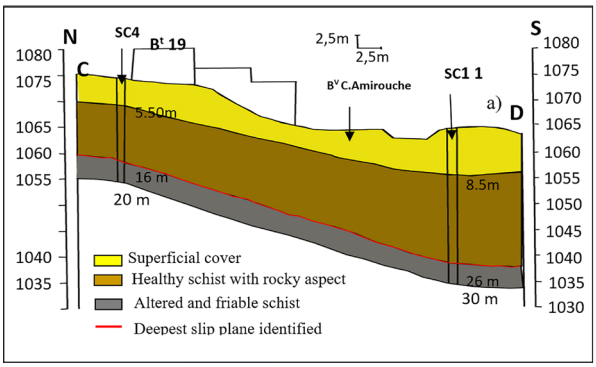


**Figure 7.** Geological section made by GEOMICA laboratory (2009)

## 5. Modeling of the Landslide

Numerical simulations were conducted by two soft wares; Optum G2 enables the use of the two methods of limit analysis: the outer side approach (Upper) (Michalowski, 1995) and the internal side approach (Lower), and Flac (2D) 6.0 using the finite difference method, and is based on the continuous medium approach. The choice of this approach is explained by the presence of layers of loose materials and highly fractured materials, surmounting a rock mass that does not contain significant fractures justifying the use of discontinuous models. It is noted in this context, that the rock behaves as a continuous medium in the case of a massive rock without any family discontinuities; or as a continuous equivalent, in the case of fractured rock with several families of discontinuities (Bemani Yazdi, 2009; Billaux and Dedecker, 2018).

### *5.1 Justification of the Two-dimensional Model*

In the absence of complex or particular topographic shapes (convex or concave forms) along the slope subject to numerical modeling, the two-dimensional simulations can be representative of his real behavior. The visual observations of the site's morphology, the direction of movement, and the examination of topographic surveys suggest that the three-dimensional effects of the model will not be very significant, a two-dimensional profile (Figure 8) was, therefore, chosen.

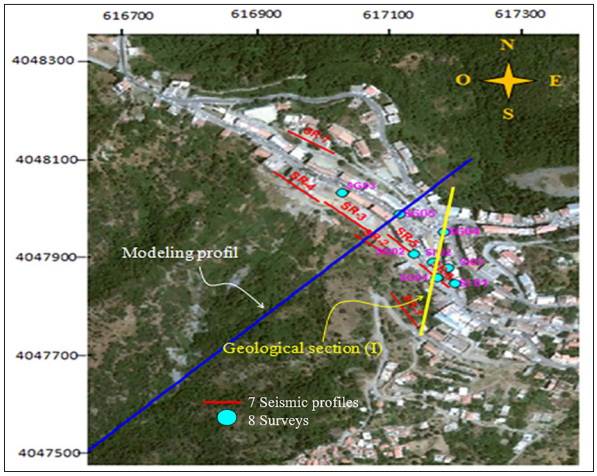


**Figure 8.** Locating the profile used in the modeling and the geological section defined by figure 7.

### *5.2 Calculation Assumptions*

- The superficial formations are considered to be homogeneous over the width of the profile.
- All materials behave on the scale of the slope as a continuous medium.
- The flow of interstitial waters is assumed to be parallel to the slope.

### *5.3. Lithology and Geotechnical Characteristics*

The section of the slope is represented from top to bottom by the tratigraphic formations below (Figure 9) using the geotechnical characteristics defined by the Mohr Coulomb rupture criterion (Table1).

- A clay-silty cover with a thickness of 3.5 to 10 m.
- A layer of altered schist with a thickness of 20 m.
- The compact satiny schist that constitutes the rock substratum.

These geotechnical and lithological characteristics were determined through various soundings carried out by the GEOMICA laboratory (2009).

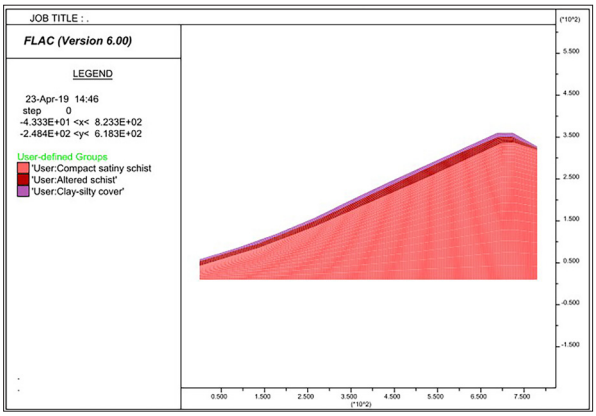


**Figure 9.** Calculation model.

**Table 1.** Principal physical and mechanical parameters of materials.

| Geotechnical parameters | Surface layer | Intermediate layer | Rock substrate |
|---|---|---|---|
| Unit weightγ [kN/ m3] | 19.60 | 19,90 | 22,00 |
| Modulus of volume deformation K [kN/m²] | 410735 | 539824 | 2451000 |
| Shear modulus G [kN/ m²] | 157500 | 207000 | 939850 |
| Cohesion C [kN/m²] | 18 | 40 | 2000 |
| Friction angle φ [°] | 36 | 34,06 | 14,3 |
| Angle of dilatation Ψ [°] | 0 | 0 | 0 |

## 6. Stability Analysis and Amplitude of Displacements.

Similar to all methods of preventing landslides, stability analysis remains an essential tool for assessing the danger of these phenomena. However, the estimation of the safety with respect to the risk of rupture is encountered by a major difficulty (Dadouche et al., 2008; Gravanis et al., 2014), since it requires careful recognition of the geometric and mechanical quantities as well as the geological structure. However, it should be noted that the effectiveness of the results is also assessed by choosing the method which defines the safety factor, through which one seeks to quantify the stability state of a natural slope by a single number. This results in several definitions, the choice of which is generally included in the selection of the calculation method (Faure, 2000).

### *6.1. Recommended Methodology*

Numerical simulations were conducted by sensitivity tests to variations of the mechanical properties of materials, loading ways and hydraulic boundary conditions. The purpose is to know the role of each of these parameters in the triggering of instabilities and on the amplitude of the displacements undergone by the ground set in movement, as well as to define the modes of rupture.

This work, therefore, proposes to vary these different parameters over a wide range of configurations combining the different situations, while seeking a level corresponding to the limit equilibrium (critical level that marks the start of instability).

The study must, therefore, firstly provide decisive results of the main factors leading to the triggering of the instability of the slope and those leading to the aggravation of the sliding process. Secondly, the various mechanisms of rupture that are likely to take place at the level of the slope must be determined.

Several configurations of the parameters have been developed. Flac defines a single value of the safety factor, which corresponds to a breaking or potential breaking surface defined by the fields of shear deformation rate. Optum develops a rupture defined by the fields of energy dissipation by shear. The three calculation methods are all based on the reduction of the mechanical parameters. The safety factor is in this case defined by

$$Fs = \frac{C}{C_{critique}} \text{ or } \frac{tang\varphi}{tang\varphi_{critique}}.$$

Furthermore, during the calculations using the Flac software, the maximum amplitude of vertical and horizontal displacement was recorded for some of the proposed configurations.

### *6.2. Comparative Study of Calculation Methods*

Before analyzing the stability results, it is necessary first to examine the results of the comparison of the safety factor values (Figures 10 and 11) obtained by the three calculation methods.

As preliminary remarks on this subject, the three curves retain the same pace over all the ranges of the chosen parameters and sometimes nearly touch them. Although the Flac software underestimates the stability of the slope compared to the limit analysis methods, the three methods give very close safety factors, and estimate, in the same way, the stability of the slope. For example, using the three methods, the limit equilibrium (Fs = 1) is reached practically with the same parameters.

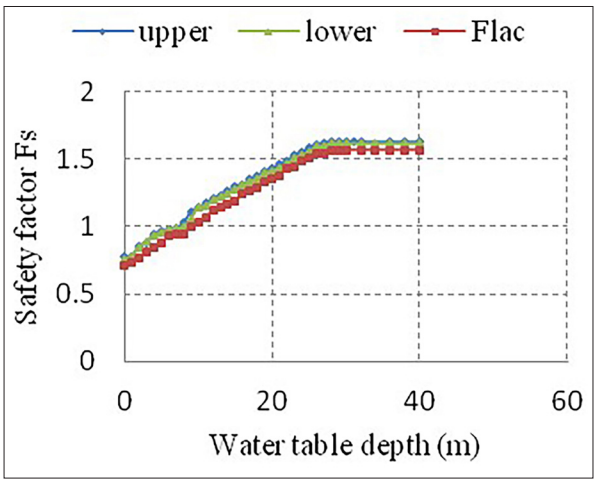


**Figure 10.** Comparison of the curves of variation of the safety factor as a function of the water table depth obtained with the three calculation methods.

Moreover, it is evident that the static method gives values of the safety factor lower than those obtained by the kinematical method. In fact, the first seeks a lower bound value of the safety factor using a field of stresses, whereas the second determines an upper bound value using a field of displacements or velocities. In result, the search for the lower and upper boundaries makes it possible for each

configuration to bound the safety factor that defines the real state of stability (Cubas, 2009; Li et al., 2016).

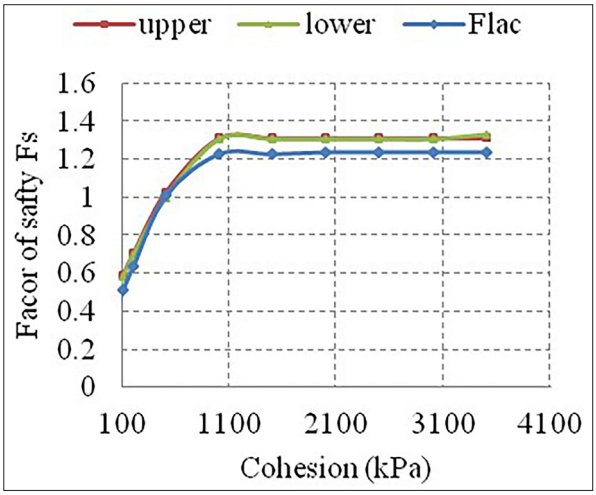


**Figure 11.** Comparison of the curves of variation of the safety factor as a function of cohesion with the three calculation methods.

### *6.3. The Role of Water*

Calculations of the safety factor Fs and the corresponding displacements are carried out through a wide range of configurations which represent more or less effective precipitation; the results have clearly illustrated the significant role of the hydraulic parameter. In fact, it is quickly noted that with the fall down of the water table, the safety factor Fs increases progressively along the first part of the curve (Figure 12), on which a linear increasing of Fs is mostly seen with the increase of the depth of the water table until 28m.

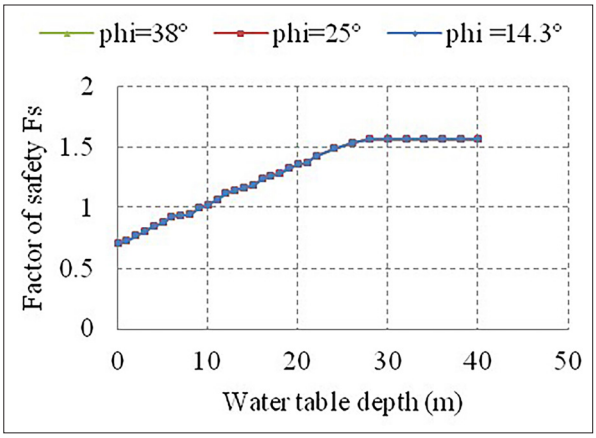


**Figure 12.** Curves of variation of the safety factor as a function of the water table depth.

Over 28 m, Fs remains constant (horizontal curve) and equals 1.57 (Fs = 1.57), This value corresponds to the same state of stability as that found in the absence of the water table, which means that after this depth, water has no effect on the stability of the slope. It must be noted that this level corresponds to the interface delimiting the bedrock and that this is considered as a continuous medium.

For variations, of maximum horizontal and vertical displacement values with the increment of the depth, the curve (Figure 13) marks a quick and intense fall down of displacement with the depth of water table between the ground surface until 4m depth. Underneath this level, there is a second stage throughout displacements which is diminished slowly to be cancelled out at a 9 m depth where the slope has experienced the limit state of stability.

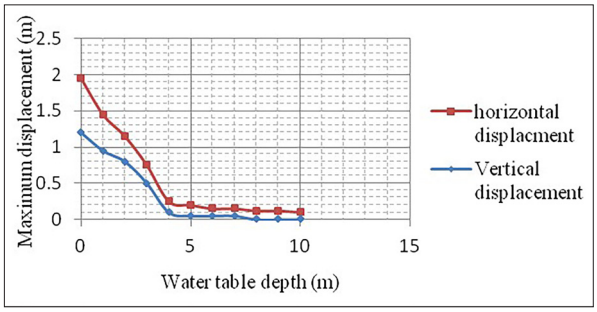


**Figure 13.** Curves of variation of horizontal displacements and vertical displacements as a function of the water table depth.

It should be pointed out that over the whole range of the water table depths, the horizontal displacements are greater than the vertical displacements; the maximum amplitude for the horizontal displacements has occurred at the frontal part of the ridge.

Several piezometric heights are, therefore, considered at the slope: important ($0 \leq h \leq 3$ m), moderate ($3 < h \leq 8$ m), medium to low ($8 < h < 16$ m), very low ($h > 16$ m). This choice can be explained by fluctuations in the water supply during seasonal variations.

The first level corresponds to a complete or partial saturation during periods of intense and long-lasting rainfall and also of massive and slow snowmelt. This represents the worst hydraulic conditions, resulting in superficial instability with very low safety factors, which vary from 0.75 to 0.8, and a large maximum displacement varying from 0.75 to 2 m in the horizontal direction and from 0.5 to 1.2 m in the vertical direction.

The moderate height represents a water table located between 4 and 7 m deep; however, at this level, the calculations always give a low safety factor, not exceeding 0.98, in spite of the strong cohesion of the materials. On this range, the slope remains unstable, but presents displacements less sensitive to the variation of the piezometric height.

With a water table situated at a 9 m depth, the FLAC software shows that a slope in a state of limit equilibrium (Fs = 1), whereas with the OptumG2 software, this state is already reached at 8 m, and instability, thus, begins beyond this depth. Between this level (the limit equilibrium) and a depth of 16 m, stability is always considered precarious ($Fs < 1.25$), so the movements can, thus, appear at this level, with the effect of other mechanical parameters.

The low level defines a piezometric height over 16m beyond which the slope is perfectly stable with safety factors exceeding 1.25.

In general, these results show the important role of water in the stability of Ain El Hammam slope, within large and moderate piezometric heights, which tend to reduce the safety factor by 55% and 40%, and to amplify the displacements in a significant way, in comparison with the results obtained in a dry state.

These conditions can be considered very realistic and representative of the instabilities recorded during periods of heavy rainfall, which led to the rise of the water table that

can reach the ground surface of the soil. It is noted that these situations lead generally to modifications of the mechanical characteristics tending to reduce their internal resistance forces.

Moreover, these results limit the depth of groundwater from which the instability begins (8 to 9 m) and the piezometric level over which water has no effect on stability (28 m).

However, these spacing distances must be analyzed in the presence of other unfavorable conditions, in particular, the modification of the mechanical characteristics and loading at the peak.

### *6.4. The Role of Mechanical Characteristics*

As mentioned above, the characteristics determined in the laboratory for the superficial and intermediate layers have been assigned. The pure schist has not been characterized in the preliminary investigations. For this purpose, the variability of schist parameters over sufficiently broad areas have been taken into account in this study for a better understanding of the role of the mechanical strength of the fall of rock masses in triggering the instabilities.

It must be pointed out that compact schist is often characterized by a friction angle φ= 14.3° and a cohesion value varying between 2000 and 3600 kPa (Chalhoub, 2010). These values should be guaranteed by all means to check out any modification of geological structure within the substrate that can lead to the degradation of the geotechnical characteristics, at least on the upper part.

In the study of the influence of the variation of the piezometric level, three calculations were carried out for each level of the water table, and for three values of the friction angle of the schist: φ= 14.3 °, 25 ° and 48 °, while keeping the other parameters as shown in table 1. These angle values are chosen with respect to the tilt angle of the slope with an average of 25 °.

In this context, it should be noted that any increase in the friction angle alone does not offer any margin of safety even at fairly high values, thus, the safety factor is the same for the three values of φ in each piezometric level. This is clearly seen in Figure 12 where the three curves are merged.

At this stage of the study, it can be concluded that the variation of the friction angle of the rock masses alone does not influence the stability of the slope.

As far as cohesion C is concerned, calculations of Fs have been carried out for a wide range of values (C = 100, 200, 500, 1000, 1500, 2000, 2500 and 3500 kPa) which can define several types of shale, altered, compact and healthy one). For these C values, the analysis is made for three piezometric levels: high, medium, and low (h = 0, h = 9 and h = 26 m) (Figure 14) noting that in this variation of cohesion, the other characteristics are those defined in table 1.

For the low cohesion (C = 100 and C = 200kPa) corresponding to highly fractured schist, the safety factor remains low even at a sufficiently stabilizing piezometric level. These conditions correspond to circles of sliding so deep to the point that they can't be considered very realistic.

Although a small increase of C value (C = 500 kPa) leads to an improvement of the stability, this improvement, however, is very limited and is mainly dependent on the level of the water table. In fact, when the soil is completely saturated with water, the safety factor is less than 1 within the entire cohesion range. From C = 1000 kPa upwards, Fs = 0.75, and it remains constant.

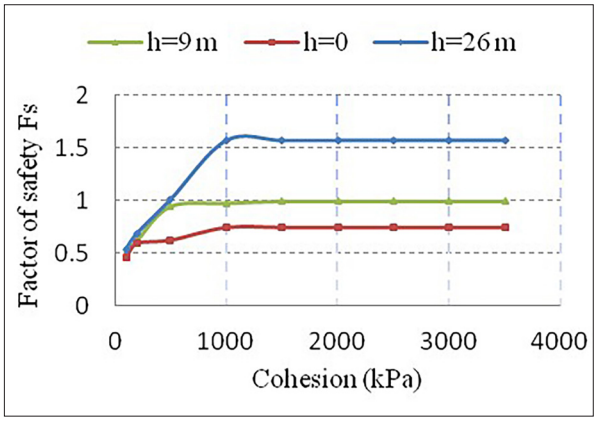


**Figure 14.** Curves of the coefficient of safety as a function of cohesion.

At a moderate piezometric height h = 9 m with a high C value (C≥1500 kPa), the state of stability is very critical. Consequently, the improvement of the cohesion alone does not give any satisfactory evolution of the state of stability.

This has led to study the variation of Fs with the variation of C for a lower piezometric height (water depth h = 26m).

In summary, the variation in cohesion at the rock level significantly affects stability regardless of the level of the aquifer considered, and the coefficient Fs increases constantly with the improvement of the cohesion. For example, a variation of the latter by 50% results in an approximate increase of 20% of the safety factor. However, the progression of cohesion from C = 1500 kPa upwards does not affect Fs which then depends only on the level of the water table.

### *6.5. The Influence of Upstream Loading*

The action of overloading at the top of a natural slope by urbanization can harm its stability. Indeed, the additional weight of the constructions modifies the state of equilibrium of the slope, and can act as an aggravating factor, or a destabilizing factor.

However, the ridge of the slope of Ain El Hammam is a plate that continues to receive projects of more or less vital importance, which is undoubtedly a factor contributing to its instability.

This point has been taken into account in the calculations by considering a uniformly-distributed load on the peak of 100 kN/m² representing the approximate weight brought by buildings of the (R+5) type. This load application did not lead to any change in the safety factor (Table 2).

The amplitude of the displacements varies by 21% in the vertical direction at the slope points of height altitude = 1085 m to 1070 m, while no variation of this magnitude has been recorded in the horizontal direction. However, the effect of this load is remarkable not only by the excessive variation of the maximum displacement intensity, but also by the modification of the distribution of the displacement isovalue fields and of the areas going in plastic behavior by tension by shear and by volume deformations.

**Table 2.** Comparison of the results of the calculation of the safety coefficient and the maximum displacements with or without upstream loading.

| Loads (kPa) | Calculation software | Water table depth [m] | Without loads | With load of 100 kPa |
|---|---|---|---|---|
| Safety factor Fs | Flac | 9 | 1 | 1 |
| | OptumG2 | 9 | 1 | 1 |
| Maximum vertical displacement [m] | Flac | 0 | -1.2 | -1.7 |
| Maximum horizontal displacement[m] | Flac | 0 | -2 | -2 |

The results of this study investigate the spread off of the displacements and their progression downstream and upstream of the slope (Figure 15) as well as the appearance of a new sliding plane defined by the propagation of the areas that have over crossed the plasticity state (Figure 16). It should be noted that these zones had an elastic behavior before the application of the load.

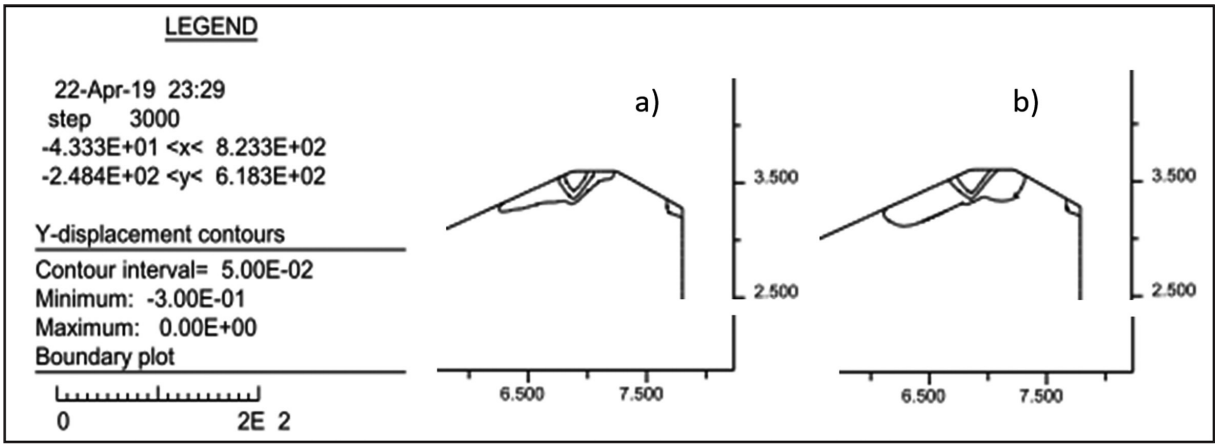


**Figure 15.** Isovalue lines of vertical displacements. (a) Before loading. (b) After loading.

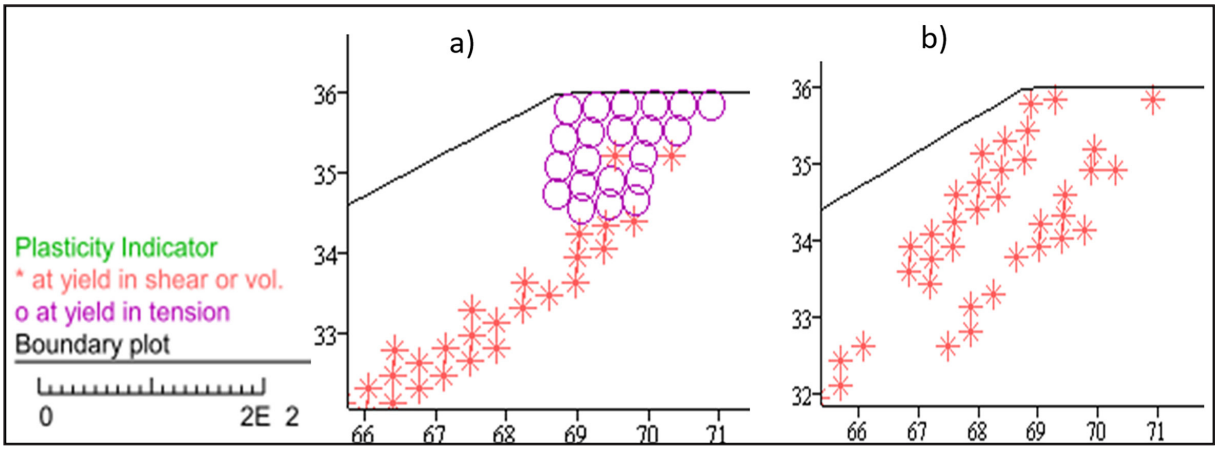


**Figure 16.** Areas of plasticity (a) Before loading. (b) After loading.

Finally, with the simulation of the loading due to urbanization, there is no change in the stability state of the slope. This can be explained by the weight of the overload being low compared with the massif one; therefore, this does not substantially affect the motive force. There is, then, no subsequent change in the ratio: motive force to stabilizing force.

If the overload alone does not lead to the instability of the whole slope, it can, however, influence the behavior of the massifs, the evolution of displacements and the modification of behavior significantly at the level of certain parts.

## 7. Analysis of the Failure Mechanisms

The large diversity in the behavior of the massifs and consequently in the failure mechanisms, results from the mechanical composition and the modification of the hydraulic conditions under the superficial effect of the concentrated runoff of the surface waters and by the internal erosion caused by groundwater in addition to the great variety of the geological structure describing the lithological nature of the rock matrix, the fracturing density, and the intensity of the alteration (Fleurisson, 2001; Wu et al., 2016).

An examination of the main results of calculations indicates that the distribution of the deformations shows a zone of concentration which corresponds to an instability of the slope undergoing a generalized movement towards the south of the region, accompanied by a slight collapse of part of the peak of the hill where the upper sliding limit is located. The downstream limit is linked to the mode of rupture obtained by the calculations and the extent of the sliding as well as the volume and the depth of the lands affected by the movement.

Different failure mechanisms have been highlighted during the calculation of the stability. For several situations, considered according to the mechanical parameters and the hydrogeological conditions, four main rupture configurations were detected (Figures 17-22), and their differences depend mainly on the drainage conditions and the cohesion of the rock mass.

### *7.1. Failure Mechanism 1*

The short-term calculations carried out using the OptumG2 software, considering the water table level with the free face of the slope, show an instantaneous slip marking a plane rupture line along the superficial overlay-altered schist interface (Figure 17), along a 150 m length at a depth not exceeding 10 m. This configuration represents, on one hand, the hypothesis of the superficial slip envisaged by the ANTEA laboratory (2010), and on the other hand, the hypothesis of rupture 1 defined by Djerbal and Melbouci (2012). This type of slip can occur during winter seasons with heavy rains causing mobilization of the soft and completely saturated cover.

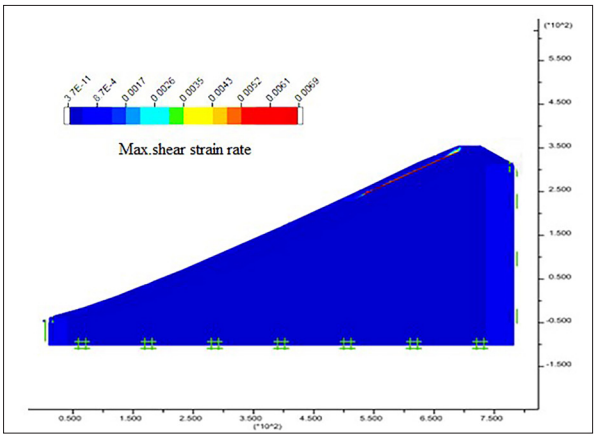


**Figure 17.** Failure mechanism 1 (Short term limit analysis).

### *7.2. Failure Mechanism 2*

Regardless of the mechanical properties considered for the bedrock, using the Flac program combined with a significant piezometric height, many instabilities are registered along several sub-rotational rupture lines indicated by the concentration of the deformations and the direction of the displacement vectors (Figure 18). These results are consistent with the results of in-situ observations which show an encroachment of several landslides.

This configuration in an overall mean reflects a large-scale phenomenon that affects the entire slope along a 450 m length at a depth that can reach the limit of a non-altered schist.

For the mass set in motion, this study highlights the importance of the shear strain rate set on the upper part of the slope; a shear strain which decreases towards the foot of the slip, marked by the strain fields, with a reset downstream of each crack.

The direction of the displacement vectors, however, shows that there is a tension at the level of the urbanized part of the slope at the altitude of 1075m, which is well confirmed by the fairly deep-tension cracks observed on road RN 15 at the market place, and also below the constructions at the top of the slope (Figure 19).

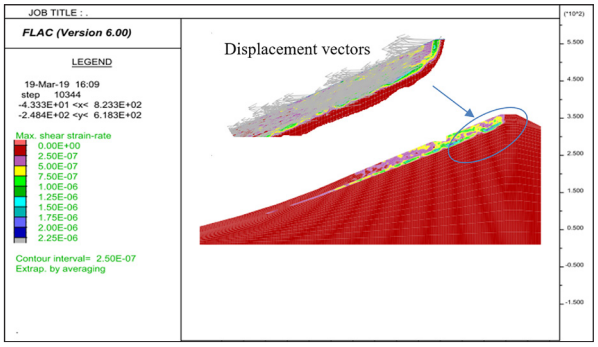


**Figure 18.** Tensile crack observed near a single structure at the top of the slope.

**Figure 19.** Failure mechanism 2 (finite difference analysis with a high piezometric height).

In general, the displacement vectors with regards to their direction show at least three lines of rupture initiated at the summit part of the slope. The first one spreads over a length of about 150 m, the second over 250 m, encroaching another plane sliding on the remaining part of the slope, with deformations decreasing without a net slip mark, but are delimited by the upward vector displacements at the 855m coastline.

### *7.3. Failure Mechanism 3*

For the volume delimited by failure mechanism 2 (Figure 20), the drainage conditions surely modify the nature of the failure surface. In fact, with the drawdown of the water table to a 4m depth (h = 4m), and combined with relatively high cohesions (C = 1000 to 3500 kPa), the failure is located at the altered schist-healthy schist interface, and sets the superficial layer in motion as well as the whole slice of the altered shale within a large drop level (about 200m) and a length of 450 m. The displacement vectors show an overall downward movement in the direction of the slope, marking the foot of the slide at the altitude line of 900 m. This movement may be sustained by the smooth and plastic nature of the formation in contact with the healthy masses (Djerbal and Melbouci 2012), causing a considerable drop in the resistance of the overlying layers. Inside the body of the slip, the strains decrease by nearly 50% in comparison with failure mechanism 2.

In addition, the results of long-term calculations carried out by the OptumG2 software (Figure 21.a) represent the failure mode obtained for all probable hydraulic boundary conditions in association with the high mechanical strength of the existing schist. They make it possible to demonstrate a quasi-plane failure affecting an extended length of the slope. This failure starts on the front part of the slope contrary

to the result of calculation obtained by the software Flac, whose failure has covered a significant part of the urbanized area (Figure 18, 20 and 21b). In any case, the results of both calculations are consistent with regards to the volume, the thickness, and the nature of the lands set in motion.

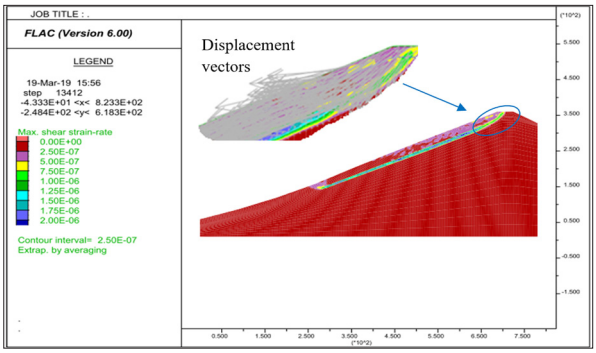


**Figure 20.** Failure mechanism 3 (Moderate piezometric height).

### *7.4. Failure Mechanism 4*

The sliding spreads over a larger part of the slope which shows a mobilization of a thick slice of the substratum (Figure 22). It appears that the lower is the cohesion of the substratum, and the greater is the depth of failure. It is worth noting that this configuration represents the presence of a thick layer of a crushed schist or the presence of poor mechanical characteristics where discontinuities appear. Current knowledge tends to show that this deformation mode seems to be very unrealistic. It shows, however, that the mode of failure depends explicitly on the current mechanical strength of the rock. Therefore, precise knowledge of the current geological structure of the rock massifs should provide answers to this question regarding the possibility of failure or a very deep potential failure.

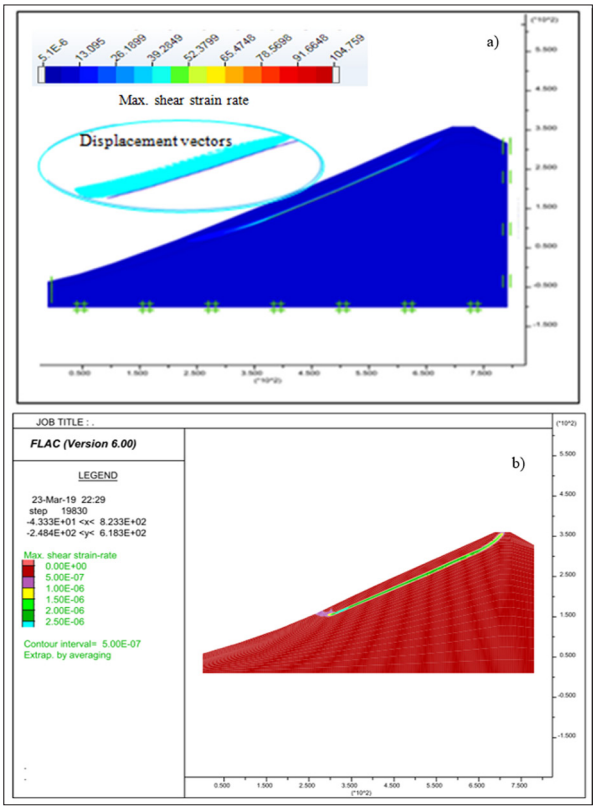


**Figure 21.** Comparison between the results of the two softwares a) limit analysis. b) finite difference analysis (low piezometric height).

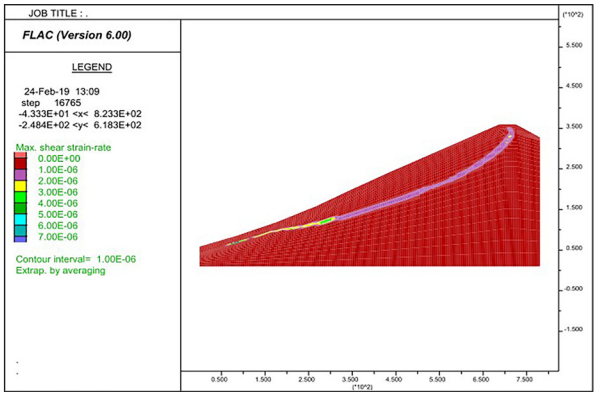


**Figure 22.** Failure mechanism 4 (Average drainage level and low cohesion)

## 8. Conclusions

The stability analysis carried out on the slope of Ain El Hammam shows that the failure occurred in the layer of the altered schist. This was confirmed by the in-situ observations and also by the analysis of the surveys carried out on site. Several conclusions, remarks, and parameters are issued from this study, the most important of which include:

- The main motor generating this movement is water. High interstitial pressures at the sliding surface combined with high inclination and an overload upon the slope caused movements of the slope. The critical phases are closely related to the increase in hydraulic potentials within the slope.
- The evolution of the displacements obtained by the simulations with hydraulic conditions which reflect "real ones" gives orders of magnitude that are very coherent with the real ones. In addition, the spatial distribution of active areas is very similar to that observed in the site.
- The variation of the angle of friction at the level of the rocky massifs has no influence on the stability of the slope.
- The substantial increment of the cohesion factor C leads to an improvement of stability, but this improvement remains very limited and essentially dependant on the level of the water table.
- The effect of the urbanization load is remarkable not only by the excessive variation of the intensity of the maximum displacement, but also by the modification of the distribution of the isovalue fields of displacements.
- The variation of the four main rupture configurations depends mainly on the drainage conditions and the cohesion allocated for the rock mass.

## References

ANTEA-HYDROENVIRONNEMENT-TTI. (2010). Étude du glissement de terrain d'Ain El Hammam – Rapport n°1, Mission A, mars 2010, N° 57665/A.

Bemani Yazdi, P. (2009). Modélisation de la stabilité des massifs rocheux avec prise en compte de l'endommagement des joints et des effets hydromécaniques. Mécanique des matériaux [physics.classph]. Ecole des Ponts ParisTech, 2009. Français. ffNNT : 2009ENPC0921ff. ffpastel-00662311f

Billaux, D., and Dedecker, F. (2018). Modélisation numérique des roches et fracturation : du continu au discontinu, Revue Française de Géotechnique, 155, 2.

Bouaziz, N., and Melbouci, B. (2019). Characterization of Illilten earth flow (Algeria). Bulletin of Engineering Geology and environment, 18(1): 669-689.

CENEAP-MATET. (2010). Étude relative a la délimitation et a la caractérisation des zones de montagne et des massifs montagneux du Djurdjura, phase n°2 : analyse prospective de l'état des lieux du massif, version corrigée n°3.

Chalhoub, M. (2010). Massifs rocheux : Homogénéisation et classification numériques, Mines Paris ParisTech Les presses.

Cubas, N. (2009). Séquences de chevauchement, prédictions mécaniques, validation analogique et application `à la chaîne de l'Agrio, Argentine, Thèse de doctorat Université Paris XI.

Dadouche, F., Belabed, L., Zennir, A. (2008). Analyse probabiliste de la stabilité des talus vis-à-vis du glissement, International Conférence on Computation in Geotechnical Engineering NUCGE'08, pp. 130-135.

Dapples, F. (2002). Instabilités de terrain dans les Préalpes fribourgeoises (Suisse) au cours du Tardiglaciaire et de l'Holocène: influence des changements climatiques, des fluctuations de la végétation et de l'activité humaine, Thèse de doctorat, Université de Fribourg (Suisse).

Djerbal, L., and Melbouci, B. (2013). Contribution to the mapping of the landslide of Ain El Hammam (Algérie), Advanced Materials Research, 601: 332-336.

Djerbal, L., and Melbouci, B. (2012). Le glissement de terrain d'Ain El Hammam (Algérie) : causes et évolution, Bulletin of Engineering Geology and the Environment, 71: 587-597.

Durand-Delga, M. (1969). Mise au point sur la structure du nord est de la Berbérie, Publ. Serv. Geol. Algérie n° 3, pp. 89-131.

Faure, R.M. (2000). L'évolution des méthodes de calcul en stabilité des pentes, Partie I : Méthodes à la rupture, Revue française de géotechnique N° 92 3ème trimestre, pp. 3-6.

Fleurisson, A. (2001). Structures géologiques et stabilité des pentes dans les massifs rocheux: description, analyse et modélisation, Revue française de géotechnique N° 95/96 2ème et 3ème trimestre 2001, pp. 103-116.

GEOMICA. (2006). Rapport Interne- Étude géotechnique de la zone de glissement et de tassement d'Ain El Hammam, Travaux de la phase I.

GEOMICA. (2009). Rapport Interne -Étude géotechnique de la zone de glissement et de tassement d'Ain El Hammam, Travaux de la phase II.

Gravanis, E., Pantelidis, L. Griffiths, D.V. (2014). An analytical solution in probabilistic rock slope stability assessment based on random fields, Int. J. Rock Mech. Min. Sci., 71: 19-24.

Guirous, L., Dubois, L., Melbouci, B. (2014). Contribution à l'étude du mouvement de terrain de la ville de Tigzirt (Algérie), Bulletin of Engineering Geology and environment, 73(4): 971-986.

Ietto, F., Perri, F., Cella, F. (2018). Weathering characterization for landslides modeling in granitoid rock masses of the capo Vaticano promontory (Calabria, Italy), Landslides, 15: 43-62.

Ismail, E.H., Rogers, J.D., Ahmed, M.F., Usery, E.L., Abdelsalam, M.G. (2017). Landslide susceptibility mapping of Blue Nile and Tekeze River Basins using oblique rainfall-aspect rasters. Bull. Eng. Geol. Environ. 2017, 1–19.

Kechidi, Z. (2010). Application des études minéralogiques et géotechniques du schiste au glissement de terrain d'Ain El Hammam, Mémoire Master, université de Tizi-Ouzou (Algérie).

Li, D.Q, Zheng, D., Cao, Z.J., Tang, X.S., Phoon, K.K. (2016). Response surface methods for slope reliability analysis: review and comparison, Eng. Geol., 203: 3-14.

LNTPB. (1973). Rapport Interne -Marché de Ain El Hammam, étude géologique et géotechnique du glissement.

Michalowski, R.L. (1995). Slope stability analysis: a kinematical approach. Geotechnique, 45(2): 283-293.

Pisani, G., Castelli M., Scavia C. (2010) Hydrogeological model and hydraulic behavior of a large landslide in the Italian Western Alps. Nat Hazards Earth Syst Sci 10:2391–2406

Tullen, P. (2002). Méthodes d'analyse du fonctionnement hydrogéologique des versants instables, Thèse de doctorat, École Polytechnique Fédérale de Lausanne.

Wu, L.Z., Liu, G.G., Wang, L.C., Zhang, L.Min., Li, B.E., Li, B. (2016). Numerical analysis of 1D coupled infiltration and deformation in layered unsaturated porous medium, Environ Earth Sci., 75 (9).

Wu, Q., Tang, H., Ma, X., Wu, Y., Hu, X., Wang, L., Criss, R., Yuan, Y., Xu Y. (2019). Identification of movement characteristics and causal factors of the Shuping landslide based on monitored displacements. Bulletin of Engineering Geology and the Environment, 78: 2093-2106.

JJEES

JJEES (2019) 10 (4): 227-233
ISSN 1995-6681

Jordan Journal of Earth and Environmental Sciences

# Multicolored Mosaic Tesserae Used in the Girmil Church, East Gerasa, Jordan: A Microfacial Analysis and Provenance Determination

Khaled Al-Bashaireh[1], Wasif Hwari[2], Mahmoud Al-Tamimi[3]

*1Yarmouk University, Department of Archaeology, Jordan.*
*2Yarmouk University, Department of Conservation and Management of Cultural Resources, Jordan*
*3Yarmouk University, Department of Earth and Environmental Sciences, Jordan*

*Received 29 April, 2019; Accepted 29 July 2019*

**Abstract**

The present research aims at investigating the provenance of the tesserae of the Girmil Church located to the southeast of Gerasa, north Jordan. Six colored tesserae representing the five colors forming the mosaic floor images were collected and investigated both macroscopically by lenses, and microscopically by a polarized-light microscope to determine their lithology and microfacies. The six samples are two tesserae of a very pale brown (white) color of two sizes and four tesserae of yellow, strong brown, bluish black and dusky red colors. Because of the absence of geochemical databases on the rocks of the region, the collected data was compared to the published data on the limestone lithology and microfacies of the Gerasa area. The results show that the mosaic tesserae were most likely of local limestone sources, and they agree well with previous research results that examined the source of mosaic tesserae of ancient churches. They might also indicate the appropriateness of the local stones to design the mosaic floors irrespective of whether the churches were built inside or outside the city center. It is likely that Gerasa mosaics at that time were designed by the same mosaicists, or by mosaic products of the same workshop.



**Keywords:** Mosaic Tesserae, Girmil Church, Gerasa, Provenance, Miocrofacies.

## 1. Introduction

Provenance studies of archaeological materials are among the major fields of archaeological science, conservation, and art history. Mosaic floors and other building stones represent some of the widespread archaeological materials that have remained well-preserved since antiquity. Although considerable provenance studies were mainly focused, during the past decades, on archaeological white and colored marbles used in the archaeological sites of Jordan, little attention was paid to the provenance of mosaic and other building stones. Al-Bashaireh (2011), Al-Bashaireh and A-Housan (2015), Al-Bashaireh and Bedal (2017), and Al-Bashaireh (2018) analyzed white and colored marbles from different archaeological sites in Jordan aiming to determine their provenance. The results indicated that all the high quality marbles used for building or carving sculptures were imported mainly from Asia Minor or Greece. Al-Bashaireh and Lazzarini (2016) study of the basalt and granite columns used in the Cruciform church of Abila (north Jordan) concluded that the basalt was local, while the granite was imported from Asia Minor. In Jordan, studies of mosaics have only focused on their artistic, archaeological and conservation aspects (Nassar and Al-Muheisen, 2010; Turshan, 2010; Nassar, 2013; Arinat, 2014 and 2016). Haddad (1999) investigated mosaic production technologies and the sources of the raw materials used in their construction at both Madaba and Yajouz (Jordan) during the Byzantine period. She used petrographic analyses to compare mosaic tesserae with limestone samples collected from the limestone outcrops' surroundings of the two cities. She concluded that the most common stone used for the mosaic floors was the local limestone because of its suitable hardness, solidity, and multiple colors.

Khrisat et al. (2011) proposed a comprehensive approach for the conservation of the mosaic floor of the saints Cosmas and Damian Church built in 533AD. Petrographic analyses of the tesserae, which were performed to characterize and conserve them properly, indicated their local geologic source. Hamarneh (2015) investigated the provenance of mosaic tesserae scattered at different parts of the Qasr Mushatta (built around 743-744 AD), by petrographic and scanning electron microscopic analyses. Her results indicated that the tesserae were made of local limestone.

The most common and efficient method that was performed to match mosaic tesserae to their quarries is the microfacies characterization (Flügel and Flügel, 1997; Flügel, 1999, 2004; Tasker et al., 2011; Šmuc et al., 2017). Moreover, combined petrographic and geochemical analyses were performed (Capedri et al., 2001; Allen and Fulford, 2004).

This research examines the provenance of tesserae samples collected from the mosaic floor of Girmil Church located about 2.5km to the east of Gerasa, Jordan (Figures 1 - 2). The analysis of the provenance of the tesserae samples sheds light on the production technology of the mosaic floor, contributes much to the understanding of the use and trade patterns of raw materials in mosaic manufacture, and helps select appropriate stones to repair and conserve the mosaic floor. In addition, it will enhance the knowledge whether the peripheral regions of Gerasa managed the same natural

* Corresponding author e-mail: khaledsm@email.arizona.edu

resources utilized at the city center. The current research represents a collaborative study between the disciplines of archaeology, archaeometry, conservation, and geology that allowed the provenance analyses of the tesserae based on their macro- and micro-facies.

## 2. Mosaics of Girmil Church

The church is located at the Girmil area, which is a local name given to the place, about 3kms to the east of Gerasa and few hundred meters to the north of the small village of Hud (Figure 1).

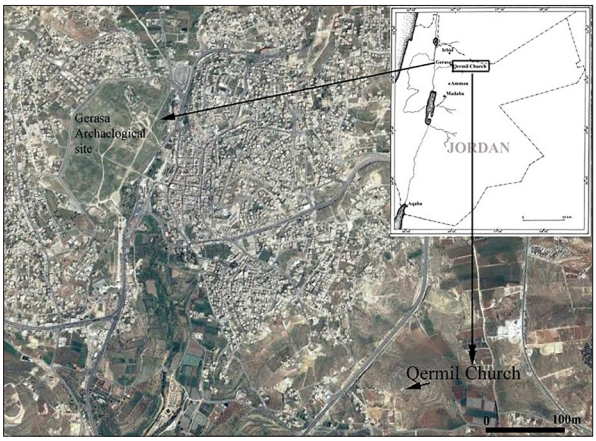


**Figure 1.** Location map of Gerasa and Girmil Church.

**Figure 2.** The mosaic floor of the Girmil Church and below: the plan of the site including the church (Photos courtesy of Dr. Harahsheh).

The church was uncovered by a salvage excavation directed by the Department of Antiquities of Jordan after extensive archaeological thefts (Harahsheh and Abu Azeizeh 2014). The church is surrounded by different archaeological features including walls, water cisterns and wells, graves carved into solid rocks, small quarries, etc. It is most likely that the church was destroyed by the 747AD earthquake, while its stones were reused in agricultural activities such as fencing. The church is composed of one hall and a rectangular apse measuring 15m long and 6m wide, in addition to other adjacent rooms from the west. According to the archaeological artifacts uncovered, the site was used during several periods starting from the Roman till the Islamic periods.

Based on an inscription uncovered in front of the nave, the mosaic floor was added as a donation in 591AD (Figure 2). It occupies an area of 48m$^2$ (8mX6m) and is beautifully decorated with human, floral, faunal, and geometric designs of several colors: very pale brown or yellowish white, yellowish brown (commune) or strong brown, yellow, brick red or dusky red, and dark grey (black) or bluish black (Harahsheh and Abu Azeizeh, 2014).

## 3. Brief Description of the Geology of Gerasa Area

The whole area of Gerasa is covered with sedimentary rocks of the Early to Late Cretaceous age (Figure 3). Most of these rocks are carbonates and belong to Ajlun and Belqa Groups. Outcrops of the Kurnub Group form the basal part of the Cretaceous sequence, and consist mainly of clastic fluvial quartz sandstones with yellowish, shallow, sandy marine carbonates and marly sandstone intercalations at the top of the sequence (Quennell, 1951). The Ajlun Group overlies the Kurnub Group and comprises five shallow marine carbonate formations of marl to limestone lithologies (Masri 1963). These five formations are arranged from the bottom (oldest) to the top (youngest) as follows: Naur nodular Limestone, Fuheis Marl, Hummar cavernous dolomitic recrystallized Limestone, Shuayb Marl, and Wadi As Sir Limestone.

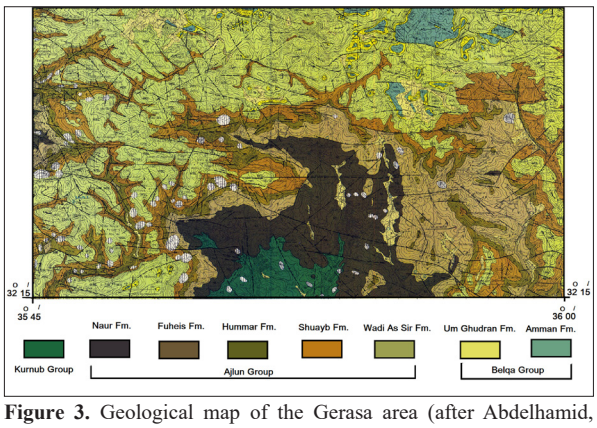


**Figure 3.** Geological map of the Gerasa area (after Abdelhamid, 1995).

Naur Formation is about 180m thick, and forms three limestone units of grey to yellowish grey marly, fossiliferous (Echinoids and Bivalves) medium to a massive micritic bedded limestone. It mainly outcrops at the area of the Gerasa archaeological site and its surroundings. Fuheis Marl, which overlies Naur Limestone is about 70m thick. It

consists of yellowish grey to greenish grey marls intercalated with a nodular fossiliferous limestone, containing Bivalves (Pelecypods), Gastropods, and burrows. Hummar Limestone consists mainly of pink to yellowish grey micritic recrystallized fossiliferous (Bivalves, Gastropods and Forams) dolomitic limestone and ranges in thickness from 40 to 50m. Shuayb Marl overlies the Hummar Formation, and is mainly made of 65m thick yellow to yellowish grey fossiliferous (Bivalves, Gastropods, Forams and Ammonites) marl to marly limestone beds. Wadi As Sir Limestone has a thickness ranging between 70m at the center of the area and 150m at its northwestern parts. The limestone varies from dolomitic at its lower part, to marly at its middle part, and micritic at its upper part. It contains a variety of fossils including Pelecypods, Ammonites, and Gastropods.

The Ajlun Group is overlain by upper Coniacian-Santonian chalks and marls of the Belqa Group (Powell, 1989). It includes mainly deep marine carbonate rocks such as chalk, phosphatic limestone, chert and bituminous marl. The Belqa Group is of the Late Cretaceous to Paleogene age, and is formed of the following formations arranged from the bottom (oldest) to the top (youngest) as follows: Wadi Umm Ghudran Chalk, Amman silicified Limestone, Al-Hisa phosphatic Limestone, Muwaqqar Chalk-Marl, Umm Rijam Chert Limestone. A comprehensive description of the aforementioned formations is given by Powell (1989) and Schulze et al., (2005).

The Wadi Umm Ghudran Chalk is the basal formation of Belqa Group that overlies the older Ajlun Group. It is about 35m thick of yellow to white-grey locally pink grey fossiliferous chalk to chalky limestone with chert concretions near the top of the formation. It contains different types of fossils and fossil fragments including fish fragments, shark teeth, Pelecypods, Ammonites, and Forams. Amman Silicified Limestone and Al Hisa Formation are not differentiated. They consist of 50m to 70m thick of intercalations of chert beds, silicified limestone, limestone, and phosphatic limestone, which contain Ammonites, Forams and Pelecypods. Lenses of Tripoli are found occasionally in the silicified limestone beds.

Both Muwaqqar Chalk and Umm Rijam Limestone are not exposed in the area of the archaeological site, but outcrop poorly in the northeastern corner of the Gerasa geological sheet (Abdelhamid, 1995).

## 4. Material and Methods

Mosaicists used small and large tesserae of different colors to design the Girmil mosaic floor. Sampling was restricted to six tesserae; only one tessera of each color and one large white tessera were used. The samples were taken from a small dig (lacuna) at the southeastern edge of the mosaic floor in order to maintain its aesthetic values and integrity. The large white tessera was collected from the scattered white large tesserae alongside the south wall of the church. The color of the tesserae was determined by naked eyes and Munsell colour charts, and the macroscopic features were observed with lenses.

Thin sections were prepared at the workshop of the department of Earth and Environmental Sciences, at Yarmouk University, and studied by optical microscopy (OM) using a Leica 600 polarized light microscope to observe and describe their microfacies types, and classify them accordingly. The classification of carbonate rocks forming the tesserae followed the nomenclature of Dunham (1962).

Because of the absence of geochemical or/and mineralogical databases of the limestone rocks of Jordan, in particular colored rocks, the results and the collected data of the tesserae are compared to published charts, maps, and literature about the geology and microfacies of the sedimentary rocks of the Gerasa area including Bender (1974), Abdelhamid (1995), Abed (2000), schulze et al. (2005) and Abu-Jaber et al. (2009) in order to identify the provenance of the limestone tesserae of the mosaic floor.

## 5. Results and Discussion

The tessellatum layer does not contain glass or ceramic but limestone tesserae. The tesserae have five colors (given below): very pale brown or yellowish white, yellowish brown (commune) or strong brown, yellow, brick red or dusky red, and dark grey (black) or bluish black. The first and the sixth tesserae are of the same yellowish white limestone, but differ in their sizes which range from small ($1cm^3$) to large (2x2x1.5) $cm^3$. The tesserae examined are formed of limestones, generally micritic and mostly fossiliferous. The major fossils observed are microscopic Foraminifera, Gastropods, and Bivalves (Pelecypods), while the minor fossils observed are Echinoderms. In some cases, fragments of unidentified species (ghosts) were common. The petrographic description of each individual tessera is presented schematically below based on the sample's number.

**Sample 1.** Macroscopically, the tessera is a pale yellowish white (10YR 8/1 (very pale brown) homogeneous limestone. Microscopically, the limestone tessera is a micritic wacketone, where the fine micrite (matrix) constitutes about 80% of the slide, and the grains form the remaining 20%. The grains are heterogeneous, randomly scattered, and mainly formed of Forams and shell fragments with some pellets (pelloids). The most shells noticed are Bivalves (or Pelecypods) which vary in size up to 2mm (Figure 4A-B). Fissures are filled with recrystallized sparitic calcite, and partially with well-developed dolomitic rhombs. The absence or very low amounts of impurities (e.g. iron oxides) which, most probable, caused the sample's white color are remarkable. These microfacies are very compatible with the those of the Late Cenomanian Shuayb Formation characterized by the presence of planktonic Forams of globular forms, and an occasional presence of yellowish patches of an organic material; see Schulze et al. (2003): Figure 5, MFT15. These features indicate that Shuayb Formation (Late Cenomanian) is the most likely source of this tessera.

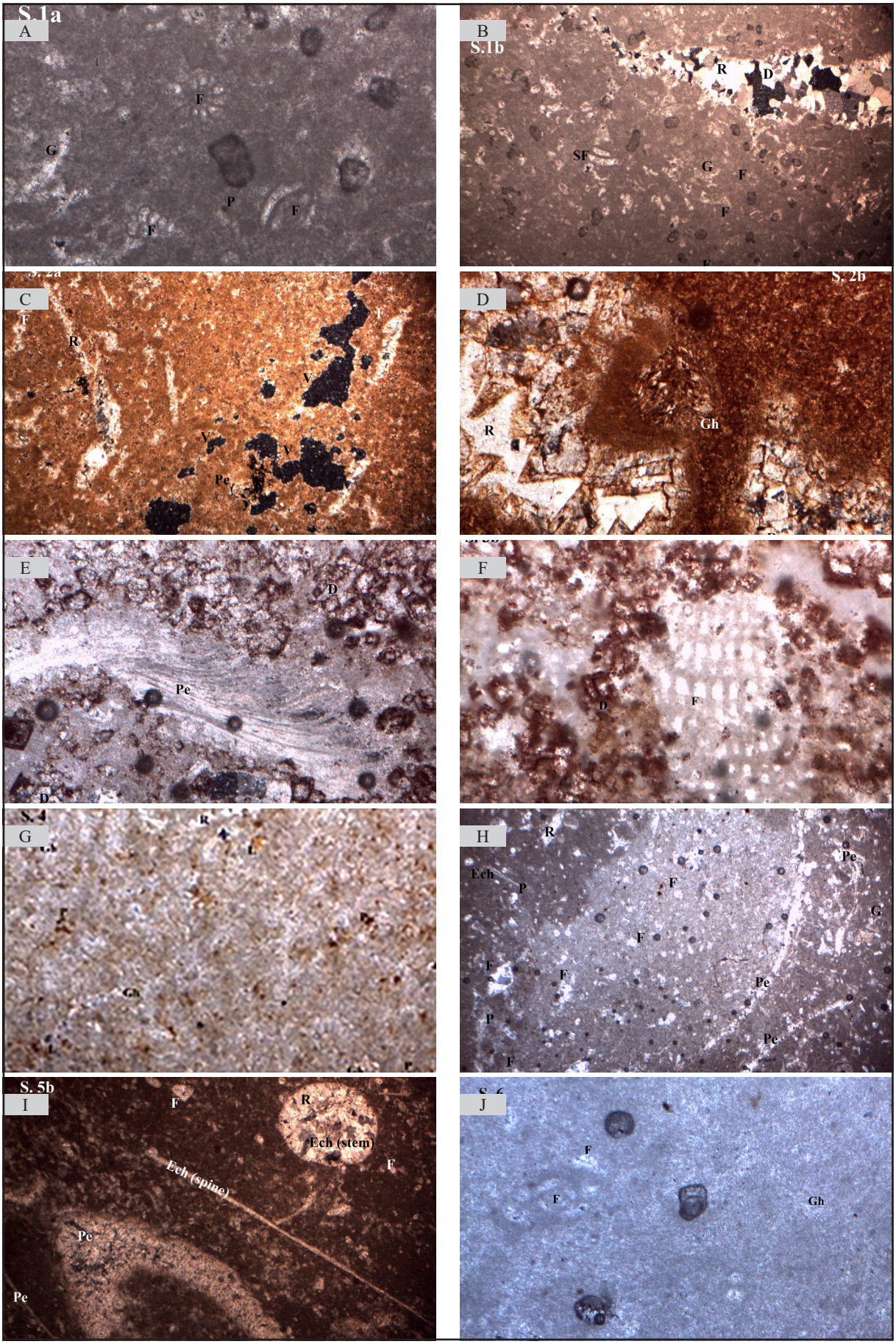


**Figure 4.** Microphotographs of Girmil tesserae showing the micritic limestone of tesserae and their content of fossils and recrystallized calcite and dolomite rhombs. Sample 1 (4A and 4B), sample 2 (4C and 4D), sample 3 (4E and 4F), sample 4 (4G), sample 5 (4H and 4I), and sample 6 (4J).

**Sample 2.** Macroscopically, the tessera is a commune or (7.5R 4/6 strong brown), homogeneous limestone. Microscopically, the sample is a micritic wackestone where about 80% of the sample is made of the fine micrite (matrix), and plenty of voids or vuggs filled with a secondary calcite (Figure 4C - D). The sample shows several voids partially filled with dolomitic rhombs forming a cavernous dolomitic limestone. The recrystallized sparite, in many cases, reflects the shape of Pelecypod shells. The sample has Forams and other obliterated fossils and fossil fragments (Ghosts) due to digenetic processes of the rock's material including dolomitization and dissolution which formed the voids. The sample has a mixture of iron oxides present in the form of limonite and hematite forming the commune (strong brown) color. All of these microfacies are similar to those of the Early Cenomanian Naur Formation characterized by a vuggy texture, recrystallization of the micritic matrix (groundmass), and the abundance of Forams and Pelecypod shell fragments; see Schulze et al. (2005: Fig. 4, MFT1 and MFT2), , and Abu-Jaber et al. (2009: 72-74).

**Sample 3.** Macroscopically, the tessera is a brick red (10R 3/4 dusky red) hard limestone. Microscopically, the sample is a dolomitic limestone of a brick-red color. Dolomitization produced dolomite rhombs randomly-scattered in certain zones of the micritic matrix. The matrix forms about 60% of the sample, while the benthic Forams, Pelecypods of different lengths, up to more than 1mm, and Dasycladacean Algae fossils (Figure 4E-F), form the rest of the sample. The brick-red color of the sample is most likely caused by the fine ferric oxide (Hematite $Fe_3O_4$) particles dispersed in the fine matrix. All of these diagenetical features and microfacies indicate a clear origin of the tessera from the Hummar Formation of Early Turonian which is characterized by a red color wackstone to a packstone, intensive dolomitization, cavernous texture, and the presence of Echinoids, benthic and planktonic Forams, and other fossil fragments; see Schulze et al., 2005: Figure 4, MFT6, and Abu-Jaber et al., 2009: 72-74, and Figure 7.

**Sample 4.** Macroscopically, the sample is a yellow colored (10YR 8/6 yellow) compacted limestone. Microscopically, it is formed of a homogeneous marly micritic wackstone. The fine micrite forms about 60% of the sample, and the rest is filled with fossils and fossil fragments. Diagentic processes caused the recrystallization of the micritic matrix into sparite which obliterated most of the sample's fossils, forming unidentified fossils (ghosts). The presence of fine particles of limonite (hydrated iron oxide), dispersed in the matrix, most likely produced the sample's yellow color. The severe diagenetic changes of the sample's materials and fossil content prohibit tracing it back to its exact source, i.e limestone formation. However, the sample's marly composition, richness in fossils (although altered), and yellowish iron oxide strongly indicate the Shuayb or Fuheis Formation as a source of this tessera since both have similar features (Abed, 2000; Schulze et al., 2005; Al-Tamimi et al., 2001; Abu-Jaber et al., 2009: 72-74).

**Sample 5.** Macroscopically, the tessera is a dark grey to black or grey (2-2.5/5PB bluish black) compacted limestone. Microscopically, the sample is formed of a homogeneous micritic fossiliferous packstone, where the fine matrix makes about 50% of the sample, and the recrystallized sparite fills the voids and replaces the shells' material. In addition to the presence of organic matter and pellets, Forams, Pelecypods, and Echinodal, fragments of stems and spines are the most grains present in the sample. Some Pelecypods and Echinoidal fragments are about 5mm long (Figure 4H -I). It is worth noting that planktonic Forams are more abundant than the benthic ones. The abundance of planktonic Forams indicates a deeper marine depositional environment which preserved the dark colored organic (bituminous) matter, and has, most likely, generated the tessera's black color. These microfacies are consistent with the Late Cenomanian Shuayb Formation formed of a micritic wackstone to Packstone which comprises large Echinoidal fragments, Gastropod, and Ostracod fragments. In addition, it is dominated by Pelecepod (Bivalve) fragments. The sample's microfacies (Figure. 4H -I) are similar to those of Shuayb Formation presented in Schulze et al. (2005: Figure 5, MFT11 and MFT12).

**Sample 6.** Macroscopically, the tessera is a pale yellowish white (10YR 8/1 very pale brown) and homogeneous compacted limestone. Microscopically, the sample is a micritic homogeneous massive wackstone. Micrite forms about 85% of the sample, and is affected by diagenetic processes including dissolution and recrystallization. While the dissolution of the micrite formed micro voids, its recrystallization into sparite of different sizes has obliterated most of the sample's fossils forming unidentified fossils (ghosts) (Figure 4J). However, benthic Miliolids and planktonic Forams were observed. It is most likely that the absence or low amounts of fossils and impurities of iron oxides in the sample produced its yellowish white color. The similarity of these microfacies to those of the Early Cenomanian Naur Formation, most likely, indicates that this formation is the provenance of this tessera; see Schulze et al. (2005: Figure 5, MFT7). Naur Formation is a micritic wackstone characterized by the abundance of Peloids, shallow-water benthic Forams such as Miliolids, and the characteristic Chrysalidina Gradate form (Schulze et al., 2005: 508, Abu-Jaber et al., 2009: 72-74).

The different colors of the limestone tesserae depend on their textures and compositions. The bituminous micrite and content of fossils are the reason behind the dark grey or black color, while the absence of impurities (mainly iron oxides), and low amounts of bituminous materials make the limestone brighter and yellowish white. Besides, the different types of iron minerals dispersed in the fine matrix of the limestone tesserae form a variety of colors from yellowish brown to brick red (or dusky red). In fact, the limonite mineral (hydrous basic iron oxide) produces yellow colors, and the hematite (iron III oxide) produces brick red or dusky red colors, while the presence of both limonite and hematite produces the yellowish brown (commune) colors.

The similarity of the results of the present study to those of the study of Khrisat et al. (2011) perhaps suggest that mosaicists utilized the same local raw stones for the construction of mosaic floors of both churches despite their locations inside the archaeological center or the rural Girmil site. The mosaic tesserae of the Girmil Church are

well-preserved suggesting a high quality for the stones, which are hard and of low porosity. It is most likely that the presence of multi-colored and high quality limestones, which outcrop within the Gerasa area, provided suitable choices of raw materials for the construction of mosaic floors. The limestone formations used for the tesserae have similar characteristics and outcrop in different locations in the Gerasa area such as Suf and Asfour (Abu-Jaber et al., 2009); therefore, it is not possible, with the present data, to determine the exact quarries that produced the studied tesserae. An ongoing project, which is still in its initial stage, suggests a distinction between Gerasa limestone quarries by geochemical characterization. The success of this new project will help determine the exact location of each kind of tessera, by matching their geochemical signatures.

The spread of Christianity during the Byzantine period and the construction of new churches probably increased the demand for, and the production of mosaic tesserae. It is possible that this pattern of mosaic production and this class of artifacts indicate that specialized workshops or craftsmen cut these tesserae, and skilled mosaicists constructed the mosaic floors.

## 5. Conclusions

This research is concerned with the application of microfacies characteristics to the question of mosaic stones provenance. The microfacies of six tesserae representing the stones of the mosaic floor of the Girmil church, in southeast Gerasa, revealed their local source. The limestone formations of the Ajlun Group (Shuayb, Naur, Hummar, and Fuheis), dating from the Cenomanian till Turonian and covering the Gerasa area, are most likely the source of the tesserae samples. Two of the tesserae are distinguished by their dusky (brick) red and the bluish black colors owing to their content of iron oxide (Hematite) and bituminous matter, respectively. They and the yellow and strong brown tesserae are used to design the faunal, floral, and geometric decorations in the white background of the mosaic floor made of the white tesserae.

The results show that the local rock sources were capable of supplying all the necessary colored raw material which the mosaicists of the Girmil Church required to design the mosaic floor. The results of this study concord with those of Khrisat et al. (2011) and Hamarneh (2015); see the introduction. Both studies concluded that local limestone sources were used in the production of the tesserae of the saints Cosmas and Damian Church built in 533AD at the archaeological site of Gerasa and the Qasr Mushatta built around 743-744 AD. The use of local sources to produce the tesserae concords with the abundance criterion which assumes that the majority of a collection of archaeological materials found in an archaeological site are usually made locally of local raw materials. The results reveal that the peripheral region of Girmil managed the same natural stone resources utilized at the city center because of the presence of raw materials in the Gerasa area and the close distance of Girmil to the Gerasa center. The use of similar materials probably indicate that the same mosaicists were involved in the construction of the Gerasa churches inside or outside the city center, or the presence of central mosaic workshops that provided the same products for the construction of mosaic floors. However, recent data do not support these theories, which require a more detailed research.

## Acknowledgement

The authors would like to acknowledge the Department of Antiquities of Jordan for the permission to collect the samples and perform the study. We thank Dr. Rafe Al-Harahsheh for providing necessary information and the photos.

## References

Abed, A.M. (2000). The geology of Jordan and its environment and water (in Arabic). The Jordanian Geologists Association, Amman.

Abdelhamid, Gh. (1995). The geology of Jarash Area. Map Sheet (3154-I), Report of Natural Resources Authority. Natural Resources Authority, Amman.

Abu-Jaber, N., al Saad, Z., Smadi, N. (2009). The quarryscapes of Gerasa (Jarash), Jordan. Geological Survey of Norway, Special Publication, 12: 67-77.

Al-Bashaireh, K. (2011). Provenance of marbles from the octagonal building at Gadara "Umm-Qais", Northern Jordan. Journal of Cultural Heritage, 12(3): 317-322.

Al-Bashaireh, K. (2018). Archaeometric characterization and provenance determination of sculptures and architectural elements from Gerasa, Jordan. Applied Physics A, 124(2), p.135. DOI: 10.1007/s00339-018-1556-y

Al-Bashaireh, K., and Al-Housan, A.Q. (2015). Provenance investigation of white marbles of chancel screens from Rihab Byzantine churches, northeast Jordan. Journal of Cultural Heritage, 16(4): 591-596.

Al-Bashaireh, K., and Dettman D.L. (2015). Geochemical analyses and provenance determination of white marble samples from churches in north Jordan. Bulletin of the American Schools of Oriental Research, 374(1): 49-59.

Al-Bashaireh, K., and Lazzarini, L. (2016). Marbles, granites and basalt used in the cruciform basilica of Abila (Decapolis, Jordan): Archaeometric characterization and provenance. Archaeological and Anthropological Sciences, 8(3): 545-554.

Al-Bashaireh K., and Bedal, L.A. (2017). Provenance of white and colored marbles from the Petra garden and pool complex, Petra, South Jordan. Archaeological and Anthropological Sciences, 9 (5): 817-829.

Allen, J.R.L., and Fulford, M.G. (2004). Early Roman mosaic materials in southern Britain, with particular reference to Silchester (Calleva Atrebatum): a regional geological perspective. Britannia, 35: 9-38.

Al-Tamimi, M., Saqqa, W., Sadeddin W. (2001). Holothurian sclerites from the Early Late Cretaceous, south of Al-Mastabah Area (North Jordan). Neues Jahrbuch fur Geologie und Palaontologie-Monatshefte, 8: 463-482.

Arinat, M. (2014). In situ mosaic conservation: a case study from Khirbet Yajuz, Jordan. Mediterranean Archaeology and Archaeometry, 14(2): 67-76.

Arinat, M. (2016). An evaluation of the conservation state of the mosaic floor of the Virgin Church, Madaba, Jordan. Dirasat: Human & Social Sciences, 48(111):1-5.

Bender, F. (1974). Geology of Jordan. Contribution to the regional geology of the world. Gebrueder Borntraeger, Berlin.

Capedri, S. Venturelli, G. De Maria, S. Uguzzoni, M.P.M., Pancotti, G. (2001). Characterisation and provenance of stones used in the mosaics of the domus dei Coiedii at Roman Suasa (Ancona, Italy). Journal of Cultural Heritage, 2(1): 7-22.

Dunham, R.J. (1962). Classification of carbonate rocks according to depositional texture. American Association of Petroleum Geologists 1: 108-121.

Flügel, E. (1999). Microfacies-based provenance analysis of Roman imperial mosaic and sculpture materials from Bavaria (southern Germany). Facies, 41: 197–208.

Flügel, E. (2004). Microfacies of carbonate rocks: analysis, interpretation and application. Springer-Verlag, Berlin.

Flügel, E., and Flügel C. (1997). Applied microfacies analysis: Provenance studies of Roman mosaic stones. Facies, 37(1): 1-48.

Haddad, R. (1999). Methods of mosaic production in Madaba and Yajouz during the Byzantine Period and its restoration. Unpulished Msc. Thesis, The University of Jordan, Amman.

Hamarneh, C. (2015). Understanding early Islamic mosaic production: Archaeometric study of material from Qasr Mushatta. Mediterranean Archaeology and Archaeometry, 15(3): 249-58.

Harahsheh, R., and Abu Azeizeh L. (2014). Girmil Church. ADAJ 58: 59-77.

Khrisat, B., Hamarneh, C., Mjalli A.M. (2011). Comprehensive approach for the conservation of the mosaic floor of the Saints Cosmas and Damian church of Jerash Greco-Roman city. Mediterranean Archaeology and Archaeometry, 12(1): 43-61.

Masri, M. (1963). Report on the geology of the Amman-Zerqa area, Central Water Authority, Unpublished, Amman, Jordan, 74 pp.

Nassar, M. (2013). The art of decorative mosaics (hunting scenes) from Madaba area during Byzantine period (5th-6th c. Ad). Mediterranean Archaeology & Archaeometry, 13(1): 67-76.

Nassar, M., and Al-Muheisen, Z. (2010). Geometric Mosaic Pavements of Yasileh in Jordan. Palestine Exploration Quarterly, 142(3): 182-198.

Powell, J.H. (1989). Stratigraphy and sedimentation of the Phanerozoic rocks in Central and South Jordan. Part B: Kurnub, Ajlun and Belqa Groups. Bulletin 11. Geological Mapping Division, Natural Resources Authority, Amman, 130 p.

Quennell, A.M. (1951). The geology and mineral resources of (former) Transjordan. Colonial Geology and Mineral Resources, 2: 85–115.

Schulze, F., Lewy, Z., Kuss, J., Gharaibeh, A. (2003). Cenomanian–Turonian carbonate platform deposits in west-central Jordan. International Journal of Earth Sciences, 92(4): 641–660.

Schulze, F., Kuss, J., Marzouk, A. (2005). Platform configuration, microfacies and cyclicities of the upper Albian to Turonian of west-central Jordan. Facies 50:505–527.

Šmuc, A., Dolenec, M., Lesar-Kikelj, M., Lux, J., Pflaum, M., Šeme, B., Županek, B., Gale. L., Kramar, S. (2017). Variety of black and white limestone tesserae used in ancient mosaics in Slovenia. Archaeometry, 59(2): 205-221.

Tasker, A., Wilkinson, I.P., Fulford, M.G., Williams, M. (2011). Provenance of chalk tesserae from Brading Roman Villa, Isle of Wight, UK. Proceedings of the Geologists' Association, 122: 933–7.

Turshan, N. (2010). The Magi: A rare mosaic floor in the Ya'amun Church (Jordan). Greek, Roman, and Byzantine Studies, 50: 616–624.

JJEES

JJEES (2019) 10 (4): 234-246
ISSN 1995-6681

Jordan Journal of Earth and Environmental Sciences

# A Provenance Study of the Paleogene Lithostratigraphic Units of the Niger Delta: An Insight into the Plate-Tectonic Setting

Wilfred Mode, Tochukwu Anidobu, Ogechi Ekwenye*, Ikenna Okwara

*University of Nigeria, Department of Geology, Nsukka, Enugu State, Nigeria*

*Received 13 June 2019; Accepted 4 August 2019*

**Abstract**

Integrated heavy-mineral analysis and paleocurrent characteristics of the outcropping Paleogene strata of the Niger Delta Basin, southeastern Nigeria were studied in order to reconstruct the provenance, with an emphasis on the sandstone maturity and tectonic setting. The depositional environment of the strata in the study area is a shallow marine to shoreline deposit, which records the transgressive and regressive episodes of three outcropping Paleogene strata (Imo, Ameki, and Ogwashi formations). The regional paleocurrent pattern shows predominance of bimodal WNW and ENE paleoflow directions with a high to medium variance. The integration of the heavy minerals and paleocurrent analyses show a mixed provenance of low- to high-grade metamorphic, igneous and reworked older sedimentary sources that lie southwest, southeast and east of the study area. The major source terrains are the Oban Massif and pre-Santonian sedimentary units of the Southern Benue Trough to the southeast and east, as well as the gneisses and schists' belt of the West African Massif to the southwest of the study area. The zircon-tourmaline-rutile (ZTR) index indicates that sandstones are mineralogically immature to mature, while the triangular plot of MF-MT-GM suites shows that the sediments were deposited in a mature passive continental margin on the stable craton of the African plate.



**Keywords:** Heavy minerals, mineralogical maturity, provenance, tectonic setting, Paleogene, Niger Delta

## 1. Introduction

The Paleogene strata consisting of the Imo, Ameki and Ogwashi formations of the Niger Delta Basin have been widely studied and varying interpretations on the environment of the deposition of these formations have been documented (Reyment, 1965; Short and Stauble, 1967; Adegoke, 1969; Arua, 1986; Nwajide and Hoque, 1979; Nwajide 1980; Reijers et al., 1997; Oboh-Ikuenobe, 2005; Odunze and Obi, 2011; Ekwenye et al., 2014; 2017; Ekwenye and Nichols, 2016). The stratigraphic succession in the Niger Delta Basin in the southeastern part of Nigeria begins with the Paleogene Imo Formation of the Late Paleocene to the Early Eocene age (Reyment, 1965; Arua, 1980). The Imo Formation is succeeded conformably by the Ameki Group (Nsugbe, Nanka and Ameki formations) of the Early to the Middle Eocene age (Reyment, 1965; Adekoge, 1969; Oloto, 1984), while the Ameki Group is conformably overlain by the Ogwashi Formation of the Middle Eocene to the Oligocene age (Jan du Che`ne et al., 1978; Reyment, 1965).

The nature and abundance of heavy minerals are widely used in sedimentological studies of sandstone provenance, and when combined with paleocurrent data, can provide useful clues on sediment dispersal patterns (Hussain et al., 2004; Fossum et al., 2019). Heavy minerals are very useful in interpreting source rock geology as some of the minerals have a restricted paragenesis, and are diagnostic of specific source lithologies. Few studies on heavy-mineral and petrographic analyses have been carried out on the Paleogene formations. The provenance of the successions was interpreted to be of a mixed origin, and the paleoclimatic conditions at the time of deposition are suggested to be semi-humid to humid conditions (Nwajide, 1980; Ekwenye et al., 2015). These works, however, did not determine the relationship between heavy-mineral assemblages and the tectonic setting of these formations. This research presents detailed heavy-mineral interpretation for the Paleogene sedimentary strata, and also uses the integrated study of the depositional facies, paleocurrent analysis and heavy-mineral assemblages to improve the understanding and reconstruct the paleoenvironment and provenance of the Paleogene formations of the Niger Delta Basin. This study also documents, for the first time, the mineralogical maturity and the tectonic setting of the Paleogene strata, based on heavy-mineral data.

## 2. Tectonic Setting and Basin Evolution

The Niger Delta Basin was formed along a failed arm of a triple junction system that originally developed during the separation of the South American from the African plates during the Late Jurassic to Early Cretaceous (Burke et al., 1972; Whiteman, 1982). Three major tectonic episodes which occurred during the Aptian-Albian, Santonian and Eocene times controlled the formation of the Southern Nigerian basin complex, as a result of the displacement of the axis of the main basin, giving rise to the formation of three successive basins (Fig. 1). These three tectonic phases formed the three sedimentary phases which include the Abakaliki-Benue phase (Aptian-Santonian), Anambra-Afikpo phase

* Corresponding author e-mail: ogechi.ekwenye@unn.edu.ng

(Campanian-Mid Eocene), and the Niger Delta phase (Late Eocene-Pliocene) (Short and Stauble, 1967; Murat, 1972; Obi et al., 2001).

The first tectonic phase of the Aptian–Santonian times resulted in the movement along the NE-SW trending fault that forms the rift-like Abakaliki-Benue Trough (Short and Stauble, 1967), while on the southeastern margin, the movement along the NW-SE trending faults or hinge line formed the Calabar Flank, within which sedimentation was similar to that in the Southern Benue Trough. The second tectonic phase coincided with the structural deformation of the Abakaliki-Benue Trough and the formation of the Anambra Basin and the Afikpo Syncline during the Santonian-Maastrichtian time. The down-faulting of the Anambra Platform to the west of the Abakaliki Trough formed the Anambra Basin, whereas, on the eastern margin of the trough, a down-warping rather than faulting occurred, and led to the formation of the Afikpo Syncline. The third tectonic phase occurred towards the end of the Eocene as a result of a major earth movement which caused another structural inversion that raised the Anambra Basin and shifted the depocentre down dip (southwards) to form the petroliferous Niger Delta Basin (Obi et al., 2001; Nwajide, 2013).

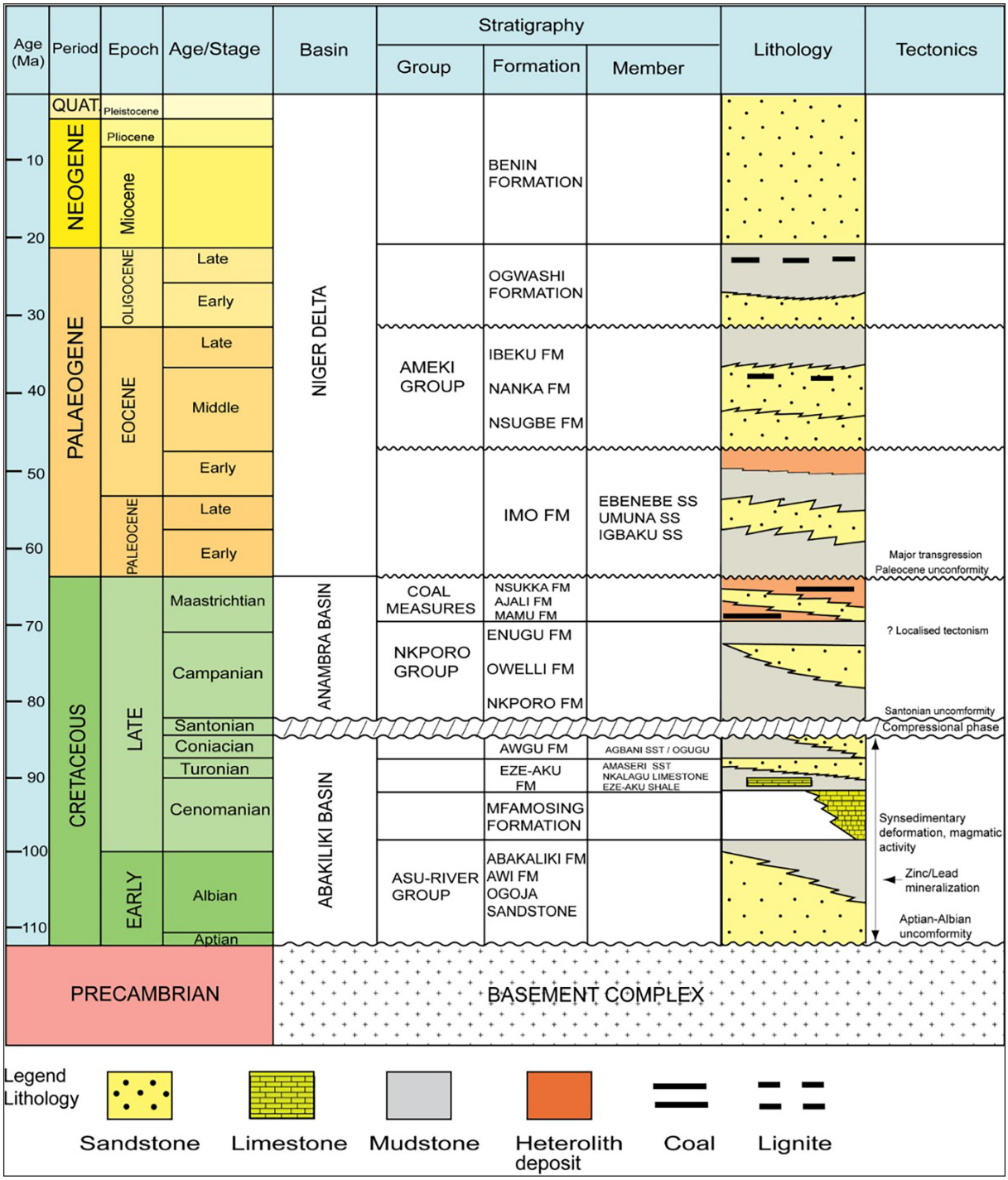


**Figure 1.** Stratigraphy of the Early Cretaceous-Cenozoic outcropping strata in the Southern Benue Trough, Anambra Basin and Niger Delta Basin (after Ekwenye et al., 2016).

## 3. Stratigraphic Setting

The detailed study of the stratigraphic units of the southern Nigerian sedimentary basin was first carried out by Reyment (1965). These Paleogene sediments (Fig. 1) were initiated when the Anambra Basin sedimentation was terminated by an extensive Paleocene transgression (Kogbe, 1989).

The Imo Formation consists of blue-grey mudstones and shales and black shales with bands of calcareous sandstone, marl, and limestone (Reyment, 1965). Ostracods and foraminifera biostratigraphy (Reyment, 1965), and microfauna recovered from the basal limestone unit (Adegoke et al., 1980; Arua, 1980) indicate a Paleocene age for the formation. Whiteman (1982) stated that the Imo Formation is the basal unit of the Niger Delta Complex. The Imo Formation has three Sandstone Members – the Ebenebe, Igbaku and Umuna Sandstones which are interpreted as tidal sand waves (Ekwenye et al., 2014). The lateral equivalent of the outcropping Imo Formation in the subsurface Niger Delta is the Akata Formation (Table 1; Short and Stauble, 1967; Maron, 1969; Avbovbo, 1978).

The Ameki Group consists of a series of a highly fossiliferous grayish-green sandy-clay with calcareous concretions and white clayey sandstones. The Ameki Group consists of the Nsugbe, Nanka, and Ameki formations (Nwajide, 1980), which are lateral equivalents. The age of the formation has been considered to be either Early Eocene (Reyment, 1965) or Early to Middle Eocene (Berggren, 1960; Adegoke, 1969). The thickness of Ameki Group is estimated to be around 1,400 m in some places. The depositional environment of the Ameki Group was observed as a barrier ridge-lagoon complex, open marine and a tide-dominated estuarine environment, based on the lithofacies interpretation and faunal content (Adegoke, 1969; Nwajide, 1979; Arua, 1986; Ekwenye et al., 2017). Fayose and Ola (1990) suggested that the sediments were deposited in marine waters between the depths of 10 m and 100 m.

The Ogwashi Formation consists of white, blue and pink clays, coarse-grained and cross-bedded sandstones, carbonaceous mudstones, shales and seams of lignite (Kogbe, 1976). An Oligocene-Miocene upper flood plain environment of deposition has also been detected (Short and Stauble, 1967). The Ogwashi Formation was re-interpreted as a tidally-influenced coastal plain system (Ekwenye and Nichols, 2016). The Ameki Group and the Ogwashi Formation are correlative lateral equivalent of Agbada Formation in the subsurface Niger Delta (Table 1).

**Table 1.** Outcropping and subsurface units of the Cenozoic Niger Delta Basin (modified from Maron, 1969).

| Age | Present Niger Delta | Outcropping Units - Reyment (1965) | | Subsurface Units - Short and Stauble (1967) | Characteristics |
|---|---|---|---|---|---|
| Miocene - Present | Continental (fluviatile) deposits, mainly sands | Benin Formation | | Benin Formation (Afam Clay Member) | Cross-bedded, coarse pebbly continental sands, with clay lenses and lignites, has marine shale breaks with foraminifera, ostracods and mollusca |
| Oligocene - Miocene | Mixed continental brackish water and marine deposits, sands and clays | Ogwashi Formation | | Agbada Formation | Clays, silts and sands with thin to thick lignite seams |
| Middle Eocene | | Ameki Group | Ameki Fm. | | Mainly sands with some conglomerate bands |
| | | | Nanka Fm. | | Calcareous clays and silts with thin shelly limestone, rich in foraminifera |
| | | | Nsugbe Fm. | | Calcareous clays and silts with thin shelly limestone, rich in foraminifera, mainly sands, minor silt and clay intercalations |
| Late Paleocene - Early Eocene | Marine deposits mainly clays | Imo Formation | Igbaku Sst. | Akata Formation | Blue-grey shales with sand lenses, marls and fossiliferous limestones, sandstone members - Ebenebe, Umuna and Igbaku Sandstones; shales with foraminifera and ostracods |
| | | | Umuna Sst. | | |
| | | | Enenebe Sst. | | |

## 4. Methodology

### *4.1 Field Mapping*

Detailed field description and measurements of fifteen outcrop sections ranging in thicknesses from 5 to 50 metres were carried out based on the essential parameters for studying sedimentary rocks in the field, including textural characteristics, measurements of strikes and dips, vertical and lateral distributions of lithofacies, stratigraphic types, spatial distribution of the physical sedimentary and biogenic structures, and lateral extent of outcrops (Fig. 2). These essential parameters have been used to delineate the different facies successions and associations. Important sedimentological parameters (bed thickness, lithology, physical and biogenic structures, intensity of bioturbation, and type of basal contacts) were inputted in the SedLog 2.1.4™ software to create the sedimentary logs (Fig. 3). Detailed measurements of the azimuth and dip of cross-beds were taken in the field to be used in interpreting the paleocurrent directions of the sediments of the different strata.

### *4.2 Heavy-Mineral Analysis*

Twenty-three disaggregated sandstone samples were taken from five different locations across the three formations within the study area for heavy-mineral analysis. Fourteen samples were obtained from the Imo Formation, while three and six samples were obtained from Ameki and Ogwashi formations, respectively. The sandstone samples were sieved and separated into grain size fractions using sieve mesh of 250, 180, 150, 125, 90, and 63 microns. Ten grams of disaggregated sandstone samples retained in the 125 micron sieve were soaked in a sodium metahexaphosphate (calgon) solution, and were, then, washed thoroughly with distilled water and oven-dried. Krumbien and Pettijohn (1938) gravity method of extracting and separating heavy

minerals has been effectively used to separate and extract these heavy minerals using bromoform ($CHBr_3$) (liquid with density of 2.89). They were rinsed with acetone, oven-dried, and mounted on slides using Canada balsam. About 200 point counting of the non-opaque mineral assemblages was done in the Petrology Laboratory of the University of Nigeria Nsukka, using a petrological microscope. Photomicrographs of salient features of the heavy minerals were taken.

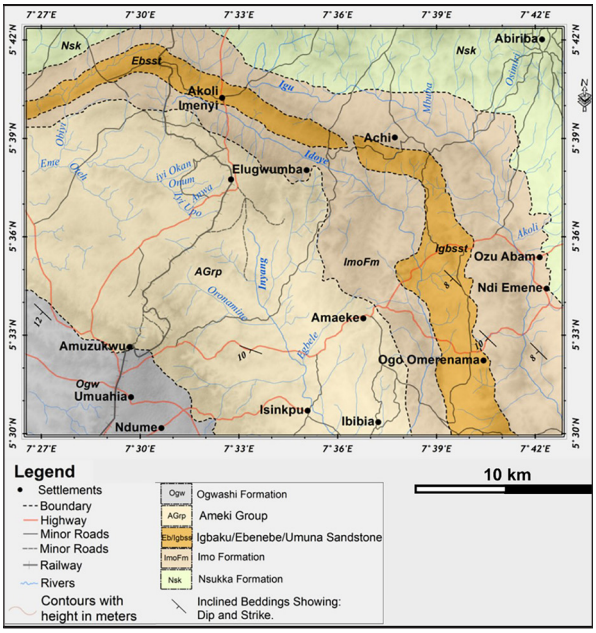


**Figure 2.** Detailed geological map of the study location in the Umuahia-Bende area of the Niger Delta, southeastern Nigeria (modified from Nigerian Geological Survey Agency, 2009).

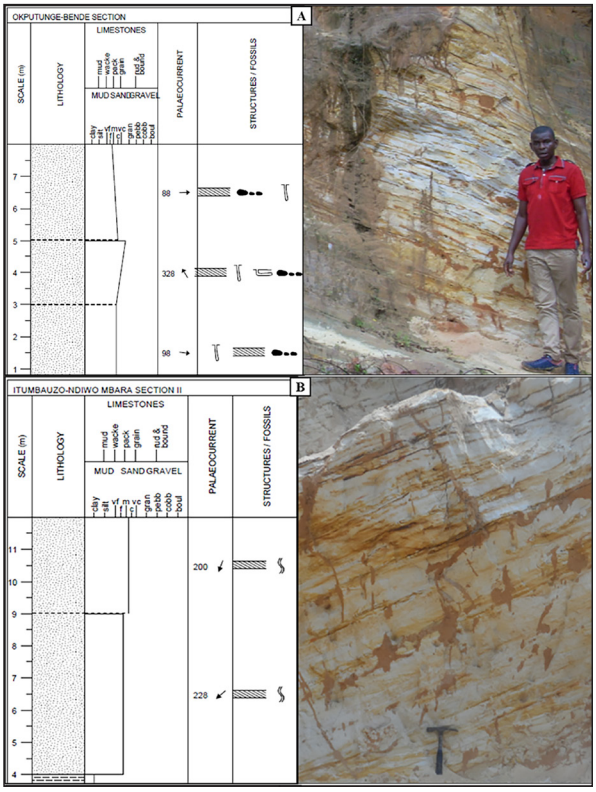


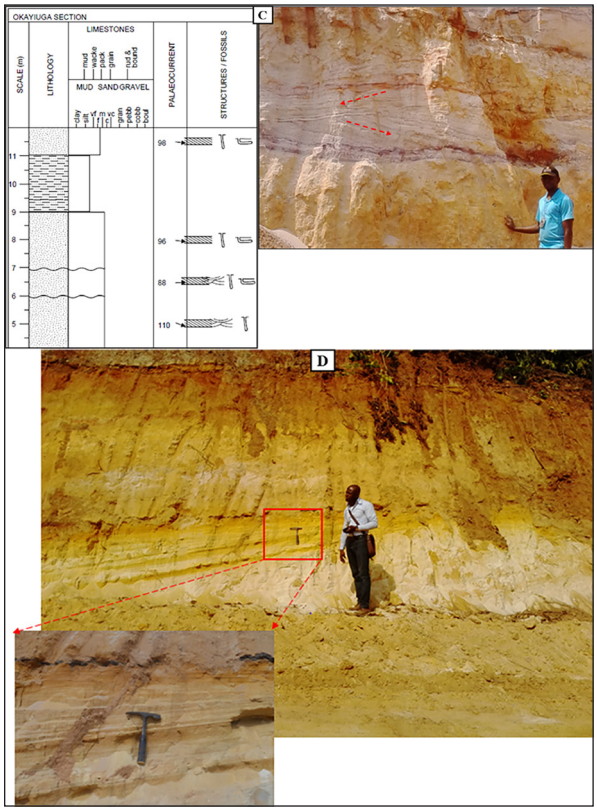


**Figure 3. (A)** Litholog and outcrop photo of the Imo Formation at Okputunge-Bende showing large-scale planar cross-bedded sandstone; **(B)** Litholog and outcrop photo of the Imo Formation at Itumbauzo-Ndiwo showing large-scale planar cross-bedded sandstone; **(C)** Litholog and outcrop photo of the Ogwashi Formation at Okaiuga showing bi-directional, trough cross-bedded sandstone; **(D)** Outcrop photo of the Imo Formation at Idima Abam road cut section showing planar cross-bedded sandstone.

## 5. Results and Interpretations

### *5.1 Paleocurrent Analysis*

The methodology and applications of paleocurrent analysis have been studied and reviewed by several authors (Tanner, 1955; Kuenen, 1957; Selley, 1968; Potter and Pettijohn, 1977; Tucker, 2003). In this study, the paleocurrent data were obtained from planar cross-beds measured from five different locations in the Imo, the Ameki, and the Ogwashi formations. The parameters of the azimuth data of each location from the three formations were grouped and plotted as rose diagrams (Fig. 4). In order to determine the dominant (mean) directions and variability, and the data were treated as vectors. The variance is a measure of the variability of the flow direction. Variance values in the range of 6000 and above suggest shallow marine environments, while variance values ranging between 2000 and 6000 indicate fluvio-deltaic sands (Potter and Pettijohn, 1977). Long and Young (1978) suggested that variance values greater than 4000 indicate a marine shelf environment. Paleocurrent parameters, vector patterns, and interpretations of the cross-bedded sandstones in this study are summarized in (Table 2).

The paleocurrent vector patterns of the Imo Formation (Figs. 4a-c) are characterized by a bimodal-oblique pattern

that is oriented sub-parallel to the ancient shoreline, while that of the Ameki Formation (Fig. 4d) is characterized by a bimodal-bipolar pattern, which indicates a strong tidal current influence with modes perpendicular to the shoreline. The paleocurrent pattern of the Ogwashi Formation (Fig. 4e) is characterized by a unimodal pattern with small dispersion, oriented perpendicularly to the ancient shoreline.

The mean vector azimuth computed from the paleocurrent parameters indicates a southwesterly and easterly directions for the sediments of Imo and Ogwashi formations, while the Ameki Formation exhibits a southeasterly direction. From the rose diagram, the provenance or sediment source of the study area suggests that the sediments were derived from different source directions. The sediment sources of the Imo Formation indicate ESE and SW directions. The sediment source of the Ameki Formation is in the NW direction, whereas that of the sandstones of the Ogwashi Formation is from WSW (Figs. 4a-e).

The variability values fall within the range of 235 to 36000 (Table 2) which suggests a dominantly shallow marine shelf environment with a tidal influence for the Imo Formation (3803–35,600), while that of the Ameki Formation (4321) suggests shallow marine/estuarine environments, and the Ogwashi Formation showed relatively low variability values (235), which are indicative of fluvio-deltaic/estuarine environments (Potter and Pettijohn, 1977; Long and Young, 1978). These results are largely in consonance with the results of the facies analysis and the depositional environments of these three formations, where the paleocurrent data were measured, and they support the interpretations.

**Table 2.** Paleocurrent parameters, vector patterns and interpretations of the cross-bedded sandstones in the study area.

| Formation | Locality | MVA | Variance | Vector Strength | Vector Pattern | Environment of deposition |
|---|---|---|---|---|---|---|
| Imo | Idima-Abam | 243.33° | 3802.91 | 2.35 | Bimodal-oblique pattern showing strong tidal current influence that is parallel to the shoreline | Tide-dominated deltaic environment |
| | Okputunge-Bende | 212.27° | 21,320.73 | 3.49 | Bimodal-oblique pattern showing strong tidal current reversal influence that is oriented or parallel to the shoreline | Shallow marine shelf environment |
| | Itumbauzo-MbaraNdiwo | 97.00° | 35,596.29 | 2.95 | Bimodal-oblique pattern showing strong tidal current reversal influence that is normal to the shoreline | Shallow marine shelf environment |
| Ameki | Ozu-Item | 175.42° | 4321.88 | 3.57 | Bimodal-bipolar and perpendicular pattern which shows strong tidal current influence with modes perpendicular to the shoreline | Tide-dominated estuarine environment or shallow marine environment |
| Ogwashi | Umuahia (Okaiuga sand mining pit) | 90.60° | 235.96 | 4.53 | Unimodal pattern with low variability | Fluvio-deltaic environment |

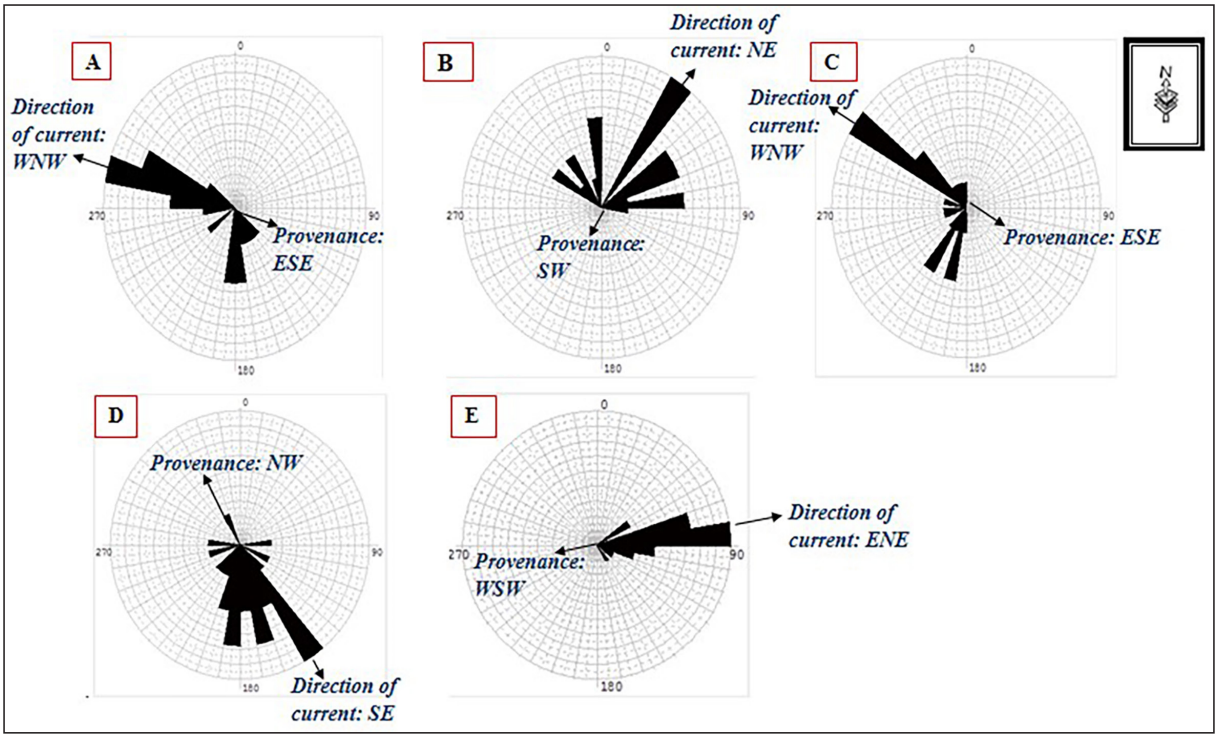


**Figure 4.** Rose diagrams of the study area at different locations for the three formations: **(A)** Idima-Abam (Imo Fm. – n = 20), **(B)** Okputunge-Bende (Imo Fm. – n = 25), **(C)** Itumbauzo-Ndiwo (Imo Fm. – n = 25), **(D)** Ozu-Item (Ameki Fm. – n = 25), and **(E)** Okaiuga Sandstone mining pit (Ogwashi Fm. – n = 22). n = number of grouped azimuth measurements.

*5.2 Heavy-Mineral Analysis*

Most of the sediments from the study area are medium- to coarse-grained and poorly consolidated sediments, except for a few samples from the Ameki Formation which contain a high proportion of fine-grained sediments that are not suitable for heavy-mineral analysis. Thus, only three viable samples were obtained from the Ameki Formation. The zircon-tourmaline-rutile (ZTR) maturity indexes of all the samples were also calculated and classified following the Hubert (1962) scheme (Table 3). Results show that zircon, tourmaline, rutile, apatite, garnet, staurolite, epidote, kyanite, sillimanite, sphene, pyroxene, and andalusite form the major non-opaque heavy-mineral suites, while magnetite, hematite, and limonite form the major opaque mineral suites of the sandstone samples (Figs. 5-6). Tables 4- 6 show the relative percentage of the abundance of the main heavy-mineral suites of the Imo, Ameki, and Ogwashi formations, while Fig. 7 shows the histogram plots of their relative abundance and ZTR indices.

The percentages of opaque minerals relative to non-opaque minerals are lower in the Imo Formation and the Ameki Formation samples, while the samples from the Ogwashi Formation showed a high percentage of opaque minerals compared to the non-opaque minerals. The sandstone samples of the Imo Formation, Ameki Formation, and Ogwashi Formation are rich in ultrastable heavy minerals (zircon, tourmaline and rutile), which consist of 60% of the entire non-opaque heavy minerals identified. The enrichments of zircon, tourmaline and rutile is due to the mechanical and chemical stability of these ultrastable heavy minerals during the periods of transport, deposition and diagenesis compared to the abrasion of unstable minerals such as the kyanite, sillimanite, pyroxene, hornblende, and andalusite during transport, deposition and diagenetic changes. The ultrastable heavy minerals show different colours ranging from colourless, deep-red, to brownish-yellow colours, which suggests different source rocks (Figs. 5-6). Zircon, tourmaline, and rutile grains retain all their depositional characteristics with no signs of modification due to chemical dissolution processes. These features confirm their stability during burial diagenesis.

Rutile is the most fairly abundant of all the transparent heavy-mineral grains. On average, it constitutes 31% of all the heavy minerals in the studied sandstone samples in the study area (Tables 4- 6). Most of the rutile grains are short prismatic, angular to sub-angular, and rounded shapes. Zircon grains form 24% of all the transparent heavy-mineral suites of all the studied sandstone samples (Tables 4-5). The zircon grains from the three formations range from euhedral to subhedral as well as from rounded to well-rounded, and a few prismatic crystals (Figs. 5-6). The Tourmaline grains show the dominance of prismatic, rounded prismatic and sub-rounded to rounded shapes. The Imo Formation has predominantly euhedral and angular to sub-angular heavy-mineral grain shapes, while the Ameki and Ogwashi formations have more sub-rounded to well-rounded grain shapes.

The metastable heavy-mineral suites, which include staurolite, apatite, garnet, sillimanite, kyanite, sphene, epidote, hornblende, andalusite, and pyroxene, consist of 39% of the non-opaque heavy minerals, occurring in varying proportions throughout the three formations. These metastable heavy minerals occur in most sandstone samples from the Imo Formation (Table 4, Fig. 7a). Sphene, hornblende, andalusite, and pyroxene were present in most of the Imo Formation sandstone samples, but were noticeably absent in almost all of the samples from the Ameki Formation (Table 5, Fig.7b) and the Ogwashi Formation (Table 5, Fig.7c).

**Table 3.** Mineralogical maturity based on zircon-tourmaline-rutile (ZTR) indices (modified from Hubert, 1962).

| Maturity | Immature | Sub-mature | Mature | Super mature |
|---|---|---|---|---|
| ZTR index (%) | < 50 | 50 - 70 | 70 - 90 | > 90 |

**Table 4.** Heavy-mineral composition of representative samples of the Imo Formation. Zrn - Zircon; Tur - Tourmaline; Apt - Apatite; Spn - Sphene; Rt - Rutile; St - Staurolite; Sil - Sillimanite; Kyn - Kyanite; Ept - Epidote Group; Grn - Garnet; Hb - Hornblende; And - Andalusite; Px - Pyroxene.

| Sample ID. | Formation | Location | Zrn | Tur | Apt | Spn | Rt | St | Sil | Kyn | Ept | Grn | Hb | And | Px | Total % |
|---|---|---|---|---|---|---|---|---|---|---|---|---|---|---|---|---|
| ID/L2/01 | Imo Fm. | Idima-Abam | 8.6 | 3.8 | 5.6 | 1.8 | 25.3 | 7.8 | 2.7 | 18.3 | 2.7 | 10.2 | 0.4 | 2.3 | 9.8 | 100 |
| ID/L2/02 | Imo Fm. | Idima-Abam | 10.4 | 3.6 | 3.5 | 1.0 | 38.2 | 6.6 | 3.4 | 15.4 | 2.0 | 12.1 | 0 | 0 | 3.8 | 100 |
| ID/L2/03 | Imo Fm. | Idima-Abam | 15.4 | 6.7 | 2.5 | 0 | 32.7 | 3.6 | 4.8 | 17.6 | 3.6 | 6.2 | 0 | 1.3 | 4.2 | 99.9 |
| NW/L4/02 | Imo Fm. | Ndiwo-Itumbauzo | 6.8 | 4.4 | 1.8 | 0.8 | 52.8 | 8.3 | 4.9 | 8.4 | 1.2 | 2.3 | 0 | 1.0 | 4.0 | 100 |
| NW/L4/03 | Imo Fm. | Ndiwo-Itumbauzo | 12.5 | 5.5 | 0.6 | 0 | 40.9 | 7.1 | 8.3 | 10.7 | 4.8 | 4.8 | 0.8 | 2.2 | 0 | 100 |
| NW/L5/01 | Imo Fm. | Ndiwo-Itumbauzo | 9.3 | 2.9 | 3.2 | 0 | 47.3 | 4.8 | 3.8 | 9.5 | 9.8 | 7.3 | 0 | 0 | 0 | 100 |
| NW/L5/02 (B) | Imo Fm. | Ndiwo-Itumbauzo | 14.6 | 8.8 | 5.6 | 0 | 37.8 | 5.0 | 5.3 | 13.1 | 4.3 | 1.6 | 0 | 0 | 2.6 | 100 |
| NW/L5/02 (T) | Imo Fm. | Ndiwo-Itumbauzo | 12.7 | 1.5 | 4.7 | 0 | 48.8 | 3.2 | 2.6 | 11.5 | 7.4 | 2.6 | 1.0 | 0.3 | 3.7 | 100 |
| NW/L6/01 | Imo Fm. | Ndiwo-Itumbauzo | 5.3 | 7.9 | 3.3 | 2.0 | 30.6 | 5.3 | 5.1 | 16.4 | 5.4 | 11.5 | 0 | 0 | 6.8 | 100 |
| NW/L6/02 | Imo Fm. | Ndiwo-Itumbauzo | 8.7 | 2.6 | 2.0 | 1.5 | 32.5 | 8.7 | 3.8 | 18.9 | 6.3 | 2.0 | 1.8 | 0.5 | 8.5 | 99.9 |
| NW/L6/03 | Imo Fm. | Ndiwo-Itumbauzo | 11.8 | 3.2 | 1.7 | 2.8 | 27.4 | 6.2 | 2.6 | 13.2 | 12.8 | 6.1 | 0 | 0 | 9.2 | 100 |
| OKP/L3/01 | Imo Fm. | Okputunge-Bende | 18.2 | 1.9 | 4.9 | 0 | 39.2 | 2.1 | 4.8 | 10.9 | 7.5 | 2.8 | 1.2 | 0 | 6.5 | 100 |
| OKP/L3/02 | Imo Fm. | Okputunge-Bende | 15.3 | 4.6 | 2.3 | 0 | 30.7 | 5.5 | 6.9 | 16.2 | 4.2 | 3.4 | 0 | 0 | 9.1 | 100 |
| OKP/L3/03 | Imo Fm. | Okputunge-Bende | 14.5 | 3.5 | 5.2 | 0 | 34.9 | 8.0 | 3.3 | 9.9 | 9.3 | 5.7 | 1.6 | 0 | 3.7 | 100 |

**Table 5.** Heavy-mineral composition of representative samples of the Ameki and the Ogwashi formations. Zrn - Zircon; Tur - Tourmaline; Apt - Apatite; Spn - Sphene; Rt - Rutile; St - Staurolite; Sil - Sillimanite; Kyn - Kyanite; Ept - Epidote Group; Grn - Garnet; Hb - Hornblende; And - Andalusite; Px - Pyroxene.

| Sample ID. | Formation | Location | Zrn | Tur | Apt | Spn | Rt | St | Sil | Kyn | Ept | Grn | Hb | And | Px | Total % |
|---|---|---|---|---|---|---|---|---|---|---|---|---|---|---|---|---|
| OZI/L9/01 | Ameki Fm. | Ozu-Item | 36.3 | 5.2 | 2.8 | 0 | 31.8 | 0.4 | 4.7 | 14.0 | 3.3 | 0 | 0 | 0 | 1.3 | 99.8 |
| OZ/L10/01 | Ameki Fm. | Ozu-Akoli | 26.5 | 6.7 | 6.3 | 0 | 35.7 | 5.7 | 1.3 | 12.7 | 2.3 | 1.6 | 0 | 0.5 | 0.7 | 100 |
| OZ/L10/02 | Ameki Fm. | Ozu-Akoli | 43.2 | 3.8 | 4.6 | 0 | 29.3 | 3.5 | 2.6 | 9.5 | 0.6 | 0 | 0 | 0 | 1.1 | 100 |
| OK/L15/01 | Ogwashi Fm. | Okaiuga | 45.2 | 10.9 | 6.3 | 0 | 20.3 | 0 | 3.6 | 8.5 | 0 | 4.5 | 0 | 0 | 0 | 100 |
| OK/L15/03 | Ogwashi Fm. | Okaiuga | 32.9 | 6.2 | 0 | 0 | 26.6 | 2.8 | 2.7 | 23.8 | 1.8 | 3.2 | 0 | 0 | 0 | 100 |
| OK/L15/05 | Ogwashi Fm. | Okaiuga | 47.3 | 2.6 | 2.2 | 0 | 19.7 | 1.6 | 1.5 | 17.9 | 4.2 | 2.9 | 0 | 0 | 0 | 99.9 |
| OK/L15/06 | Ogwashi Fm. | Okaiuga | 57.7 | 3.2 | 1.7 | 0 | 18.2 | 1.3 | 2.1 | 10.3 | 1.4 | 1.3 | 0 | 0 | 0 | 100 |
| OK/L15/07 | Ogwashi Fm. | Okaiuga | 64.2 | 1.6 | 0 | 0 | 10.6 | 3.6 | 0.7 | 6.5 | 4.6 | 6.3 | 0 | 0 | 1.8 | 100 |
| OK/L15/08 | Ogwashi Fm. | Okaiuga | 35.5 | 7.8 | 1.6 | 0 | 9.3 | 0.8 | 5.6 | 24.7 | 9.8 | 2.0 | 0 | 0 | 0 | 100 |

**Table 6.** Maximum, minimum, and average percentage of the main non-opaque heavy minerals.

| Non-Opaque Minerals | Imo Formation | | | Ameki Formation | | | Ogwashi Formation | | |
|---|---|---|---|---|---|---|---|---|---|
| | Max. % | Min. % | Ave. % | Max. % | Min. % | Ave. % | Max. % | Min. % | Ave. % |
| Zircon | 18.2 | 5.3 | 11.7 | 43.2 | 26.5 | 35.3 | 64.2 | 32.9 | 47.1 |
| Tourmaline | 8.8 | 1.5 | 4.4 | 6.7 | 3.8 | 5.2 | 10.9 | 1.6 | 5.4 |
| Apatite | 5.6 | 0.6 | 3.4 | 6.3 | 2.8 | 4.6 | 6.3 | 0 | 2.0 |
| Sphene | 2.8 | 0 | 0.7 | 0 | 0 | 0 | 0 | 0 | 0 |
| Rutile | 52.8 | 23.3 | 37.1 | 35.7 | 29.3 | 32.3 | 26.6 | 9.3 | 17.5 |
| Staurolite | 8.7 | 2.1 | 5.9 | 5.7 | 0.4 | 3.2 | 3.6 | 0 | 1.7 |
| Sillimanite | 8.3 | 2.6 | 4.5 | 4.7 | 1.3 | 2.9 | 5.6 | 0.7 | 2.7 |
| Kyanite | 18.9 | 8.4 | 13.6 | 14 | 9.5 | 12.1 | 24.7 | 6.5 | 15.3 |
| Epidote | 12.8 | 1.2 | 5.8 | 3.3 | 0.6 | 2.1 | 9.8 | 0 | 3.6 |
| Garnet | 12.1 | 2.0 | 5.6 | 1.6 | 0 | 0.5 | 6.3 | 1.3 | 3.4 |
| Hornblende | 1.8 | 0.4 | 0.5 | 0 | 0 | 0 | 0 | 0 | 0 |
| Andalusite | 2.3 | 0 | 0.5 | 0.5 | 0 | 0.2 | 0 | 0 | 0 |
| Pyroxene | 9.8 | 0 | 5.1 | 1.3 | 0.7 | 1 | 1.8 | 0 | 0.3 |

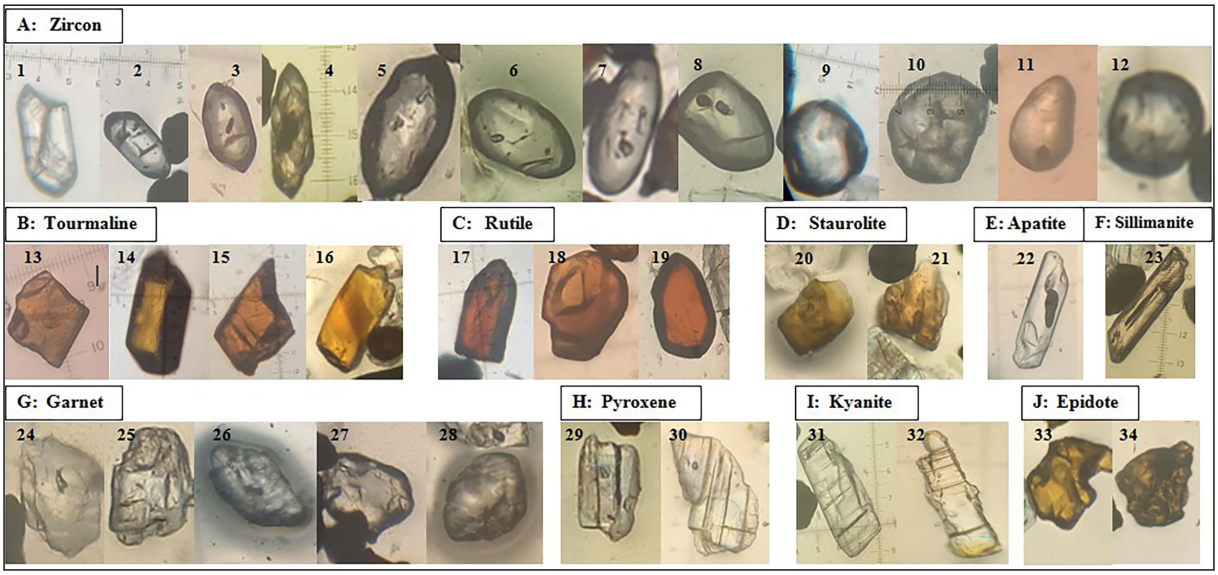


**Figure 5.** Photomicrographs of selected non-opaque heavy-mineral suites from sandstone samples within the study area. **(A)** 1 - 6 show euhedral zircon grains with zoning, while 7 - 12 show well-rounded polycyclic zircon grains; **(B)** 13 – 16 show prismatic tourmaline grains; **(C)** 17 – 19 show euhedral and well-rounded oblong form rutile grains with well-developed pyramidal terminations; **(D)** 20 – 21 show prismatic and angular shape staurolite grains; **(E)** 22 shows long slender prisms of apatite grains; **(F)** 23 shows sillimanite grain with parallel cleavage fragments; **(G)** 24 - 28 show sub-rounded to rounded garnet grains; **(H)** 29 – 30 show pyroxene grains with parallel cleavage fragments; **(I)** 31 – 32 show elongated kyanite grains; and **(J)** 33 – 34 show irregular, angular, and equant grains of epidote group. (Scale bar is 3 mm).

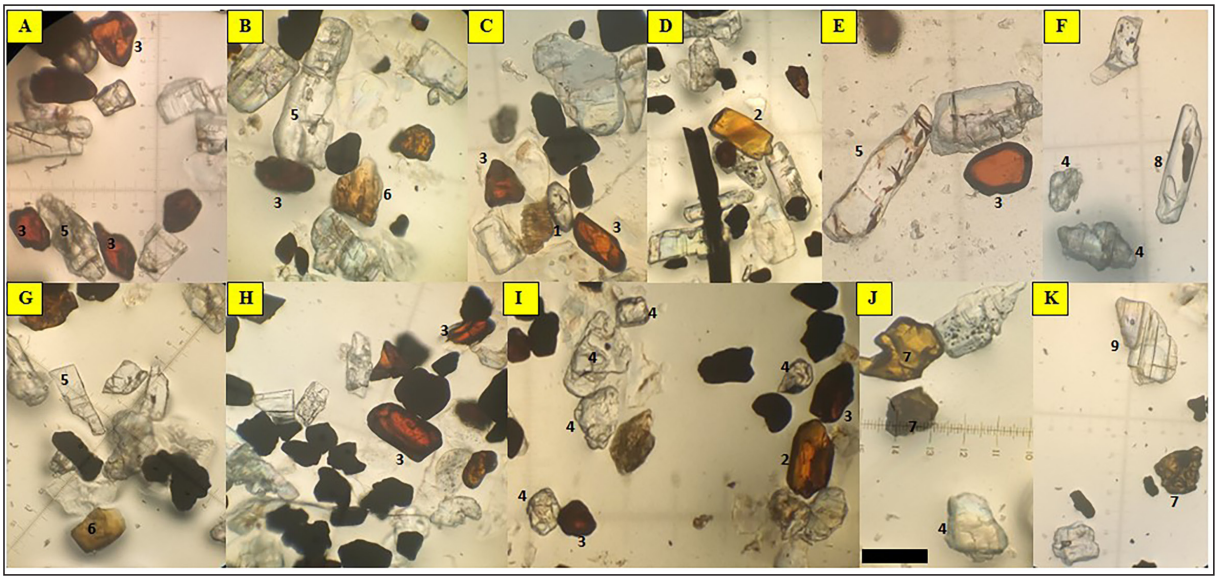


**Figure 6.** Selected photomicrographs of heavy-mineral suites from sandstone samples of the Paleogene sediments (Imo, Ameki and Ogwashi formations). Transparent heavy minerals dominate, but opaque heavy-mineral grains (dark) probably magnetite, hematite and limonite are also present. Numbered labels represent different minerals **(A)** 3 - rutile, 5 - kyanite; **(B)** 3, 5, 6 - staurolite; **(C)** 1 - zircon, 3; **(D)** 2 - tourmaline; **(E)** 3, 5; **(F)** 4 - garnet; 8 - apatite; **(G)** 5, 6; **(H)** 3; **(I)** 2, 3, 4; **(J)** 4, 7 - epidote; **(K)** 7, 9 - pyroxene. (Scale bar is 3mm).

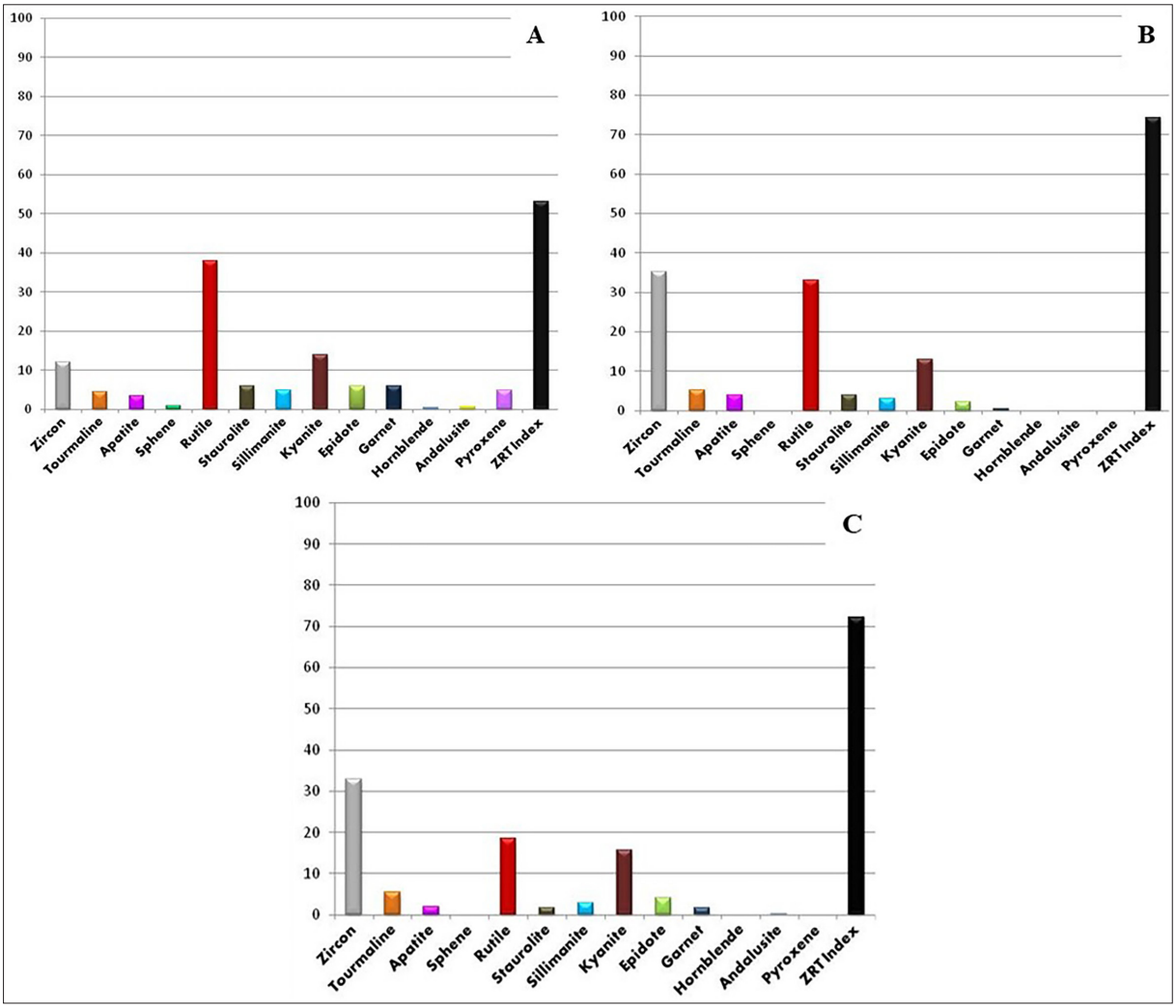


**Figure 7.** Distribution bar charts of the average percentages of the different non-opaque heavy-mineral assemblages and their ZTR indices for the three Paleogene formations sandstone samples. **(A)** Imo Formation; **(B)** Ameki Formation; and **(C)** Ogwashi Formation.

## 6. Discussion

### *6.1 ZTR Heavy-Mineral Index as an Indicator of Sandstone Mineralogical Maturity*

In the process of weathering, transportation, and deposition, unstable minerals are progressively destroyed, concentrating the stable ones. A stable mineral index, commonly used to determine the abundance of stable minerals in sandstones, and referred to as the zircon-tourmaline-rutile (ZTR) index, is employed in this study (Hubert, 1962; Table 7). The ZTR-maturity index analysis of the sandstone samples of the three formations within the study area shows that the Imo Formation sandstone samples vary from 37.7% to 64%, with an average of 53%; the Ameki Formation sandstone samples vary from 68.9% to 76.3%, with an average of 73%, while the Ogwashi Formation sandstone samples vary from 52.6% to 79.1%, with an average of 70% (Tables 6-7). This indicates that the sediments are mineralogically immature to mature. The general concept is that there is an increase in the ZTR index with the increasing geological age of the sediments as a result of the progressive dissolution of the unstable minerals (Hubert, 1962), but this is not the case with the Imo Formation, which has the lowest ZTR index on average, due to a higher percentage of metastable heavy minerals (Table 7).

Based on Folk (1980) and Pettijohn et al. (1987) petrographic classification of sandstones, Ekwenye et al. (2015) classified sandstone samples of the Imo Formation into submature arkosic arenite to sub-arkose, while the Ameki Formation and Ogwashi Formation sandstones were classified into mature sub-litharenite, sub-arkose and quartz arenite. This classification of the Imo Formation is reflected in its average ZTR index of 53% (submature), while the Ameki Formation and the Ogwashi Formation sandstone samples have a higher average ZTR index of 73% and 70%, respectively (i.e. mature). A possible reason why the Imo Formation has a lower ZTR index could be that the Imo Formation sandstones were deposited after a short distance of transportation and rapid deposition. This is characterized by their predominantly euhedral and angular to sub-angular heavy-mineral grain shapes, while Ameki and Ogwashi formations have more sub-rounded to well-rounded grain shapes, which were deposited after a longer distance of transportation, farther away from the source rocks. Therefore, the higher a sandstone sample tends towards quartz arenites, the higher its ZTR-maturity index will be (Hubert, 1962). This is because most of the non-stable mineral grains in the sandstone samples have undergone chemical dissolution, while retaining the stable mineral grains (quartz, zircon, tourmaline and rutile), which dominates the sandstone samples of the Ameki Formation and Ogwashi Formation classified as sub-litharenite, sub-arkose, and quartz arenite (Ekwenye et al., 2015).

### *6.2 Relationship between Heavy-Mineral Assemblage and Tectonic Setting*

The relationship between tectonic setting and sediment composition has been studied by several authors (Dickinson and Suczek, 1979; Pettijohn, et al., 1987; Nechaev and Isphording, 1993). The relationship between heavy-mineral assemblages and tectonic environments was evaluated using the triangular plot of interrelationship of the MF-MT-GM suites in the studied sediments, according to Nechaev and Isphording (1993). "MF" indicates common heavy minerals of mafic magmatic rocks (i.e. the total content of pyroxene, hornblende and olivine), "MT" indicates common heavy minerals of basic metamorphic rocks (total content of epidote, garnet and pale-coloured and blue green amphibole), while "GM" indicates accessory minerals of granitic and silicic metamorphic rocks (zircon, tourmaline, staurolite, kyanite, andalusite, monazite, and sillimanite).

The results show that the Imo Formation has an average MF of 9.5%, MT of 19.8% and GM of 70.7%; and the Ameki Formation has the average MF of 1.6%, MT of 4.2% and GM of 94.1%; while the Ogwashi Formation has the average MF of 0.3%, MT of 8.6% and GM of 91.1% (Table 7). The plotting of the heavy-mineral assemblages of these three formations on the MF-MT-GM triangular plot of Nechaev and Isphording (1993), as shown in Fig. 8, indicates that these sandstone samples fall within the field of mature passive continental margins, characterized by a high percentage of heavy minerals derived from acidic igneous and regional metamorphic rocks, as a result of sediments' reworking, and deep weathering in regions with no active tectonic events (Nechaev and Isphording, 1993). The results of the data plotted are in line with earlier studies of the Niger Delta Basin as a rifted Atlantic-type and a mature passive continental margin basin which resulted from the thermal contraction of the lithosphere (Sleep, 1971; Steckler and Watts, 1978; Ofoegbu and Onuoha 1990).

According to Nechaev and Isphording (1993), heavy-mineral assemblages of the continental margins far from the volcanic areas contain GM values greater than MF values, as clearly seen in Table 7. Also, according to Dickinson and Suczek (1979), Ingersoll and Suczek (1979), and Valloni and Maynard (1981), the provenance of passive continental margin sediments has a wide range of variability – quartz, feldspars, and some lithic fragments, as well as zircon, tourmaline and rutile dominate in the sediments found in passive continental margin sediments. The data plotted in Fig. 8 show that the heavy-mineral suites of the three formations were derived from a passive continental margin of the Niger Delta Basin, and indicate a mixed provenance of acidic igneous and metamorphic sources, which are dominated by a high proportion of GM compared to MF suites.

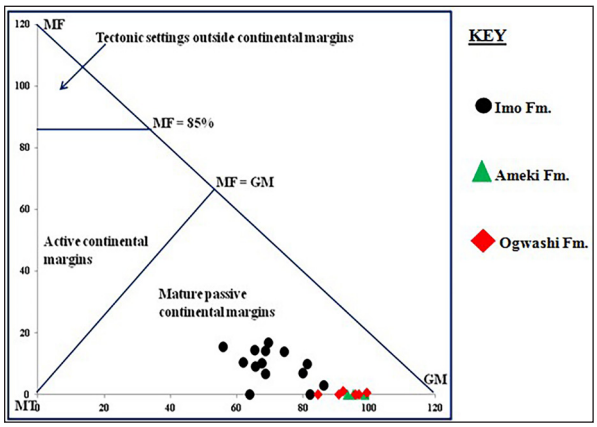


**Figure 8.** Distribution bar charts of the average percentages of the different non-opaque heavy-mineral assemblages and their ZTR indices for the three Paleogene formations sandstone samples.

**Table 7.** ZTR indices and MF, MT, and GM percentages of the studied sandstone samples of the three formations in the study area. MF, MT, GM calculated after Nechaev and Isphording (1993).

| Formation | Sample ID. | ZTR Index % | Ave. ZTR Index % | MF% | MT% | GM% | Ave. MF% | Ave. MT% | Ave. GM% |
|---|---|---|---|---|---|---|---|---|---|
| Imo Fm | ID/L2/01 | 37.7 | 53 | 15.3 | 19.4 | 65.3 | 9.5 | 19.8 | 70.7 |
| | ID/L2/02 | 52.2 | | 6.6 | 24.61 | 68.8 | | | |
| | ID/L2/03 | 54.8 | | 6.6 | 15.5 | 77.9 | | | |
| | NW/L4/02 | 64.0 | | 9.7 | 8.5 | 81.8 | | | |
| | NW/L4/03 | 58.9 | | 1.4 | 16.9 | 81.7 | | | |
| | NW/L5/01 | 59.5 | | 0 | 36.1 | 63.9 | | | |
| | NW/L5/02(B) | 61.2 | | 4.7 | 10.7 | 84.6 | | | |
| | NW/L5/02(T) | 63.0 | | 10.1 | 21.5 | 68.4 | | | |
| | NW/L6/01 | 43.8 | | 10.7 | 26.5 | 62.8 | | | |
| | NW/L6/02 | 43.8 | | 16.7 | 13.4 | 69.9 | | | |
| | NW/L6/03 | 42.4 | | 14.1 | 29 | 56.8 | | | |
| | OKP/L3/01 | 59.3 | | 13.8 | 18.4 | 67.8 | | | |
| | OKP/L3/02 | 50.6 | | 14 | 11.7 | 74.4 | | | |
| | OKP/L3/03 | 52.9 | | 8.9 | 25.2 | 65.9 | | | |
| Ameki Fm | OZI/L9/01 | 73.3 | 73 | 2.0 | 5.1 | 92.9 | 1.6 | 4.2 | 94.1 |
| | OZ/L10/01 | 68.9 | | 1.2 | 6.7 | 92.1 | | | |
| | OZ/L10/02 | 76.3 | | 1.7 | 0.9 | 97.4 | | | |
| Ogwashi Fm | OK/L15/01 | 76.4 | 70 | 0 | 6.2 | 93.8 | 0.3 | 8.6 | 91.1 |
| | OK/L15/03 | 65.7 | | 0 | 6.8 | 93.2 | | | |
| | OK/L15/05 | 69.6 | | 0 | 9.1 | 90.9 | | | |
| | OK/L15/06 | 79.1 | | 0 | 3.5 | 96.5 | | | |
| | OK/L15/07 | 76.4 | | 2 | 12.2 | 85.8 | | | |
| | OK/L15/08 | 52.6 | | 0 | 13.7 | 86.3 | | | |

### *6.3 Provenance Evaluation and Tectonic Setting*

The heavy-mineral suites (Tables 4- 6) identified in the Paleogene sediments of the Niger Delta Basin revealed that the ultrastable heavy-mineral grains are euhedral to subhedral, as well as rounded to well-rounded and a few prismatic crystals, while the metastable heavy minerals have prismatic, angular to subangular and irregular shape (Figs. 5-6). The euhedral and angular to subangular morphology probably indicates short transportation and rapid deposition derived from igneous sources, while the sub-rounded to the well-rounded shape zircon, tourmaline, and rutile indicate a moderate to long transportation from reworked sedimentary sources (Poldervaart, 1955). The presence of brown and pale brown varieties of tourmaline indicates that the sediments were derived from a metamorphic provenance (Blatt et al., 1980), while the prismatic, yellow and brown-colored tourmaline, indicates the derivation of sediments from granitic and pegmatic rocks (Krynine, 1946). The relative abundance of different varieties of zircon, tourmaline, and rutile of different morphology suggests that these heavy minerals came from a mixed provenance of igneous, metamorphic, and reworked older sedimentary rocks, while the occurrence of sillimanite, kyanite, andalusite, staurolite, and hornblende, as accessory minerals in this assemblage (Tables 4-5), clearly suggests a parent rock affiliation to an area of medium- to high- grade metamorphism of aluminum-rich pelitic rocks (Nockolds et al., 1978). The percentages of the contribution of the different associated parent rocks to the three formations were calculated based on their associated heavy-mineral assemblages (Table 8). In the Imo Formation, acidic igneous and/or recycled sedimentary rocks contributed 20.2%, basic igneous rocks contributed 5.1%, with the regional metamorphic rocks being the greatest contributor with 73%, and contact metamorphic rocks with 0.5%. The Ameki Formation is sourced predominantly by regional metamorphic rocks (53.1%), with a significant contribution from acidic igneous and/or sedimentary rocks (45.1%), while the Ogwashi Formation is sourced predominantly from acidic igneous and/or sedimentary rocks (Table 8).

Ekwenye et al. (2015) noted that the orogenic recycling of the sedimentary rocks corresponds to the Santonian tectonic events, which resulted in the folding and uplifting of the Abakaliki area to form Abakaliki anticlinorium and the subsequent formation of Anambra and Afikpo depocentres. The anticlinorium became one of the sediment sources for the Cretaceous Anambra and Afikpo basins. The compositional maturity and dominance of the stable heavy minerals indicate a lack of tectonism during the Paleogene and moderate to high-energy conditions during sedimentation. It can be concluded that the Paleogene sediments in the study area were deposited after a short- to long-distance transportation from the source areas to the deposition sites.

Th plot of the paleocurrent data shows that the Paleogene sediments of the Niger Delta Basin in the study area were transported from southeasterly and southwesterly source terrains (Fig. 4). The paleocurrent modes are mainly a bimodal pattern except for the Ogwashi Formation which shows a unimodal pattern with little dispersion. The northwesterly to

southeasterly and northeasterly to southwesterly distribution of the paleocurrent modes suggests that the source could be the high- to medium- and low-grade metamorphic terrain of the Obudu Plateau (Adamawa Highlands) and Oban Massif, which consists of magmatic-gneiss complex rocks (Ekwueme, 2006), and/or the magmatic-gneiss complex and schist belt of the West African Massif, as well as recycled sedimentary rocks from the Anambra and Afikpo basins (Fig. 9).

**Table 8.** Summary of the associated parent rock percentages of contribution of heavy minerals to the three formations. Each parent rock is the percentage sum of the associated heavy minerals. Acid igneous and/or sedimentary rock (zircon + tourmaline + apatite + sphene); regional metamorphic rock (rutile + staurolite + sillimanite + kyanite + epidote + hornblende + garnet); contact metamorphic (andalusite); Basic igneous (pyroxene).

| Formation | Acid Igneous and/or Sedimentary | Regional Metamorphic | Contact Metamorphic | Basic Igneous |
|---|---|---|---|---|
| Imo Fm | 20.2% | 73% | 0.5% | 5.1% |
| Ameki Fm | 45.1% | 53.1% | 0.2% | 1% |
| Ogwashi Fm | 54.5% | 44.2% | 0% | 0.3% |

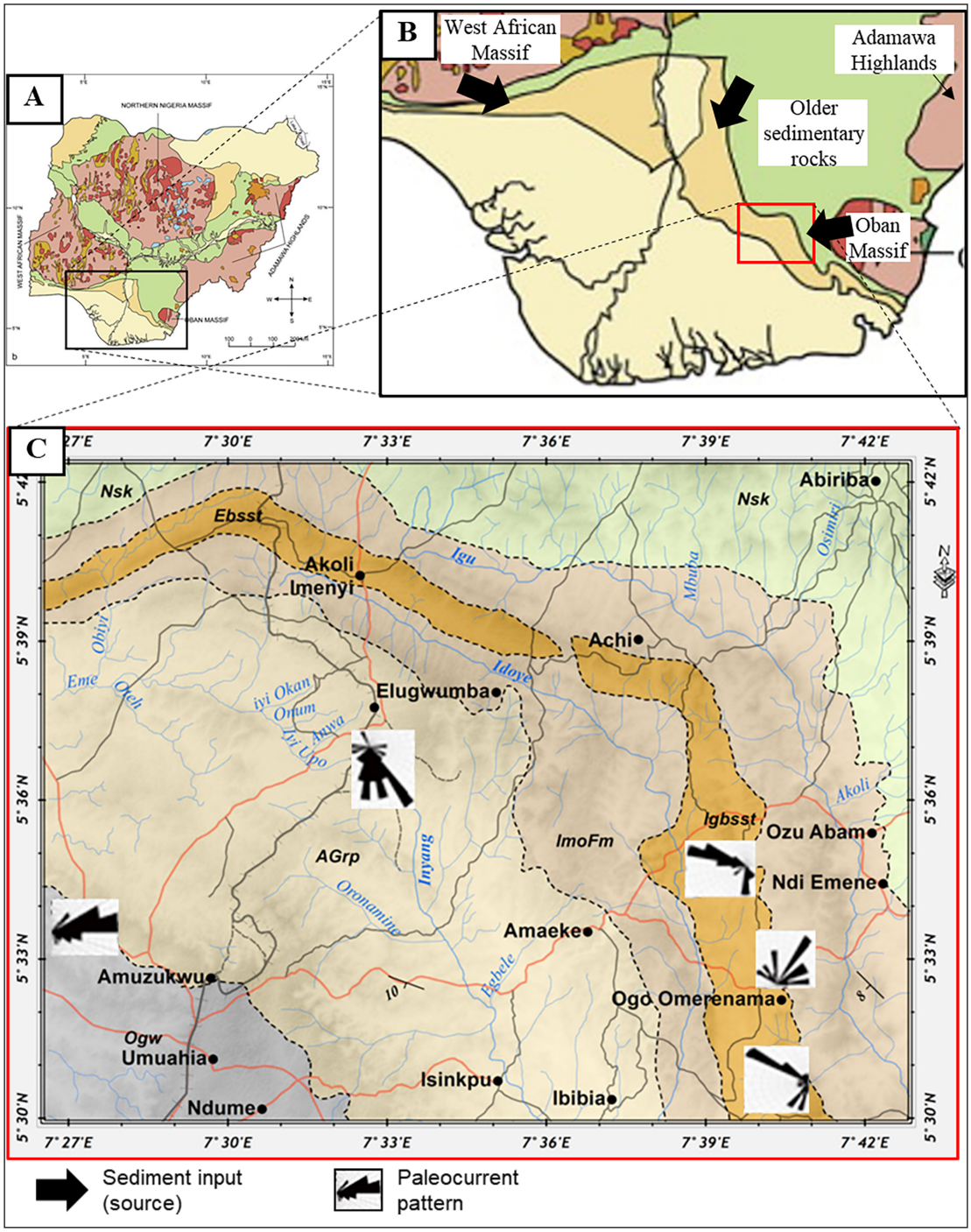


**Figure 9. (A)** Inset geologic map of Nigeria (after Nigerian Geological Survey Agency, 2009); **(B)** Zoom in on the southern part of Nigeria showing the basement complex and older sedimentary rocks distribution **(C)** Detailed geologic map of the study showing paleocurrent patterns.

## 5. Conclusions

This study has examined the provenance and tectonic setting of the Paleogene strata exposed at the southeastern part of the Niger Delta. The petrographic study shows the occurrence of zircon, tourmaline, and rutile of different forms, suggesting a mixed provenance from igneous, metamorphic, and reworked older sedimentary rocks, while the occurrence of sillimanite, kyanite, andalusite, staurolite, and hornblende heavy minerals in this assemblage clearly suggests a parent rock affiliation to an area of medium- to high-grade metamorphic rock sources.

The mineralogical maturity of the sandstones were calculated from the ZTR maturity index, with the ZTR index increasing in the younger sediments of Ameki and Ogwashi formations, which have a high proportion of stable heavy minerals and are submature to mature, while the older sediments of the Imo Formation have an almost equal stable and metastable heavy- mineral species, and a ZTR- maturity index range of immature to submature.

The plot of MF-MT-GM suites indicates that the sandstone units of the Paleogene strata occur within the mature passive continental margin on a stable craton of the African plate in the Niger Delta. This could be attributed to the dominance of stable heavy-mineral species, after a medium to a long distance of transportation from a source area lacking active tectonism, to the site of deposition.

The paleocurrent and provenance analyses indicate that the depositional systems of the Paleogene formations derived their detritus mainly from the metamorphic and granitic basement complex rocks of the Oban Massif and the Obudu Plateau (Adamawa Highlands), east and southeast, as well as the gneisses and schists' belt of the West African Massif from the northwest and west of the study area, whereas the regional paleocurrent analysis shows the predominance of bimodal WNW and ENE paleoflow, with a high to medium variance.

## Acknowledgement

The authors would like to express their gratitude to the Petroleum Technology Development Fund (PTDF) for their financial support for this research. Special thanks are due to Mr. Ikegwuonu Okechukwu for his field assistance, as well as Mr. Itoro Gabriel and Mr. Nduese for their help with the heavy-mineral analysis.

## References

Adegoke, O.S. (1969). Eocene stratigraphy of Southern Nigeria. Colloquesur l' Eocene, 3, Bureau de Recherché Geologiques et Miniers Memoir, 69: 23–48.

Adegoke, O.S., Arua, I., Oyegoke, O. (1980). Two new nautiloids from the Imo Shale, (Paleocene) and Ameki Formation (Middle Eocene), Anambra State, Nigeria. Journal of Mining and Geology, 17: 85–89.

Arua, I. (1980). Paleocene macrofossils from the Imo Shale in Anambra state. Nigeria Journal of Mining and Geology, 17: 81-84.

Arua, I. (1986). Paleoenvironment of Eocene deposits in the Afikpo Syncline, southern Nigeria. Journal of African Earth Sciences, 5(3): 279-284.

Avbovbo, A.A. (1978). Tertiary lithostratigraphy of the Niger Delta. American Association Petroleum Geologist Bullentin, 62: 295–306.

Berggren, W.A. (1960). Paleocene biostratigraphy and planktonic foraminifera of Nigeria (West Africa). Rep. 21 Intern. Geol. Congr., Copenhagen. Section 6.

Blatt, H., Middleton, G., Murray, R. (1980). Origin of Sedimentary Rocks: Prentice-Hall, New Jersey.

Burke, K.G, Dessaugie, T.F.J., Whiteman, A.J. (1972). Geological history of the Benue valley and adjacent areas. In: Dessauvagie, T.F.J and Whiteman, A.J. (ed.), African Geology, Ibadan, Nigeria, University of Ibadan.

Dickinson, W.R., and Suczek, C.A. (1979). Plate tectonics and sandstone compositions. American Assoc. Petroleum Geologists Bull., 63, 2164 - 2182.

Ekwenye, O.C., and Nichols, G.J. (2016). Depositional facies and ichnology of a tidally influenced coastal plain: Oligocene Ogwashi Formation, south-eastern Nigeria. Arabian Journal of Geosciences, 9: 700, doi:10.1007/s12517-016-2713-2.

Ekwenye, O.C., Nichols, G.J., Collinson, M., Nwajide, S.C., Obi, G.C. (2014). A paleogeographic model for the sandstone members of the Imo Shale, southeastern Nigeria. Journal of African Earth Sciences, 96: 190–211.

Ekwenye, O.C., Nichols, G.J., S. C. Nwajide., G. C. Obi., and Onyemesili, O.C. (2017). An insight into the Eocene tide-dominated estuarine system: implications for palaeoenvironmental and sequence stratigraphic interpretations. Arabian Journal of Geosciences, 10: 371, doi:10.1007/s12517-017-3150-6.

Ekwenye, O.C., Nichols, G.J., Mode, A.W. (2015). Sedimentary petrology and provenance interpretation of the sandstone lithofacies of the Paleogene strata, South-eastern Nigeria. Journal of African Earth Sciences, 109: 239–262.

Ekwueme, B.N. (2006). Summary of isotopic ages from Oban – Obudu Massif of Southeastern Nigeria and its implications for the evolution Precambrian basement complex of Nigeria. Global Journal of Geologic Sciences, 4(2): 103–108.

Fayose, E.A., and Ola, P.S. (1990). Radiolarian occurrences in the Ameki type section, eastern Nigeria. Journal of Mining and Geology, 26: 75-80.

Folk, R.L. (1980). Petrology of Sedimentary Rocks. Hemphill Publishing Company, Austin Texas.

Fossum, K., Morton, A.C., Dypvik, H., Hudson, W.E. (2019). Integrated heavy mineral study of Jurassic to Paleogene sandstones in the Mandawa Basin, Tanzania: sediment provenance and source-to-sink relations. Journal of African Earth Sciences, 150: 546-565.

Hubert, J.F. (1962). A zircon-tourmaline-rutile maturity index and interdependence of the composition of heavy minerals assemblages with the gross composition and texture of sandstones. Journal of Sedimentary Petrology, 32: 440–450.

Hussain, M., Babalola, L.O., Hariri, M.M., 2004. Heavy minerals in the Wajid Sandstone from Abha-Khamis Mushayt area, southwestern Saudi Arabia: implications on provenance and regional tectonic setting. GeoArabia, 9(4): 77-102.

Ingersoll, R.V., and Suczek, C.A. (1979). Petrology and provenance of Neogene sand from Nicobar and Bengal fans, DSDP sites 211 and 217. Journal of Sedimentary Petrology, 49: 1217-1228.

Jan du Che`ne, R., Onyike, M.S., Sowumi, M.A. (1978). Some new Eocene pollen of the Ogwashi-Asaba Formation, Southeastern Nigeria. Rev. Espanol Micropaleontology, 10: 285–322.

Kogbe, C.A. (1976). The Cretaceous and Paleogene sediments of Southern Nigeria. In: Kogbe, C.A. (Ed.), Geology of Nigeria. Elizabethan Publishing Company, Lagos, 273–28.

Kogbe, C.A. (1989). Paleogeographic history of Nigeria from Albian Times. In: Kogbe, C. A. (ed.) Geology of Nigeria, Elizabeth Publication Company. Lagos, 257 – 275.

Krumbein, W.C. and Pettijohn, F.J. (1938) Manual of Sedimentary Petrography. Appleton Century Crofts, New York, 549 p.

Krynine, P.D. (1946). The tourmaline group in sediments. Journal of Geology, 54: 65 –87.

Kuenen, P.H. (1957). Longitudinal filling of oblong sedimentary basins. Verhandl. Koninkl. Nederlandse Geol. Mijn. Genootscap. Geol. Ser., 18: 189-195

Long D.G.F., and Young G.M. (1978). Dispersion of cross-stratification as a potential tool in the interpretation of Proterozoic arenites. Journal of Sedimentary Petrology, 48: 857-862

Maron, P. (1969). Stratigraphical aspects of the Niger Delta. Jour. Min. and Geol., 4 (1- 2): 3-12

Murat, R.C. (1972). Stratigraphy and paleogeography of the Cretaceous and Lower Tertiary in southern Nigeria. In: Dessauvagie, T.F.J., Whiteman, A.J. (Eds.), African Geology. University of Ibadan Press, Nigeria, 251–266.

Nechaev, V.P., and Isphording, W.C. (1993). Heavy mineral assemblages of continental margins as indicators of Plate tectonic environments. Journal Sedimentary Petrology, 63(6): 1110-1117.

Nigerian Geological Survey Agency. (2009). Geological Map of Nigeria. Published by the Authority of the Federal Republic of Nigeria.

Nockolds, S.R., Knox, R.W.O'B, Chinner, G.A. (1978). Petrology for Students, Cambridge University Press, London.

Nwajide, C.S. (1980). Eocene tidal sedimentation in the Anambra Basin, Southern Nigeria. Sediment. Geol., 25: 189-207.

Nwajide, C.S. (2013). Geology of Nigeria's sedimentary basins. CSS Bookshops Limited, Lagos.

Nwajide, C.S., and Hoque, M. (1979). Trace fossils from Nanka Formation southeastern Nigeria. Geologie en Mijnbouw, 58: 85-88.

Obi, G.C., Okogbue, C.O., Nwajide, C.S. (2001). Evolution of the Enugu Cuesta: a tectonically driven erosional process. Glob. J. Pure Appl. Sci., 7: 321–330.

Oboh-Ikuenobe, F.E., Obi, C.G., Jaramillo, C.A. (2005). Lithofacies, palynofacies and sequence stratigraphy of Paleogene strata in Southeastern Nigeria. Journal of African Earth Science, 41: 79–102.

Odunze, O.S., and Obi, G.C. (2011). Sequence stratigraphic framework of the Imo Formation in the Southern Benue Trough. Journal of Mining and Geology, 47(2): 135–146.

Ofoegbu, C.O., and Onuoha, K.M. (1990). A review of geophysical investigations in the Benue Trough. The Benue Trough Structure and Evolution. Friedr. Viewegand Sohn, Braunschweig, Germany.

Oloto, I.N. (1984). A palynological study of the Late Cretaceous and Tertiary boreholes from Southern Nigerian sedimentary basin, Doctoral dissertation, University of Sheffield, Department of Geology.

Pettijohn, F.J., Potter, P.E., Siever, R. (1987). Sand and Sandstone. 2nd ed. Springer-Verlag, New York.

Poldervaart, A. (1955). Zircons in rocks. Sedimentary rocks: Am. Jour. Sci., (253): 433-461.

Potter, E.P., and Pettijohn, F.J. (1977). Paleocurrents and Basin analysis. 2nd ed. Springer-Verlag, Berlin.

Reijers, T.J.A., Petters, S.W., Nwajide, C.S. (1997). The Niger Delta Basin. In: Selley, R.C. (ed.), African Basins. Sedimentary basins of the world. Elsevier Science B.V., Amsterdam, 151–172.

Reyment, R.A. (1965). Aspects of the Geology of Nigeria: The Stratigraphy of the Cretaceous and Cenozoic Deposits. Ibadan University Press, Ibadan.

Selley, R.C. (1968). A classification of paleocurrent models. Jour. Geol., 76: 99-110.

Short, K.C., and Stauble, A.J. (1967). Outline of geology of Niger Delta. Am. Assoc. Pet. Geol. Bull., 51: 761–779.

Sleep, E.H. (1971). Thermal effects of the formation of Atlantic continental margins by continental break-up. Geophys. J. Roy. Astron. Soc, 24: 325-350.

Steckler, M.S, and Watts, A.B. (1978). Subsidence of the Atlantic-type continental margin off New York, Earth Planetary Sci. Letters, 41: 1-13.

Tanner, W.F. (1955). Paleogeographic reconstruction from cross-bedding studies. American Association of Petroleum Geologists Bulletin, 39: 2471-2483.

Tucker, M.E. (2003). Sedimentary Rocks in the Field, 3rd ed. The Geological Field Guide Series. ix+234 pp. Chichester: Wiley.

Valloni, R., and Maynard, J.B. (1981). Detrital modes of recent deep-sea sands and their relation to tectonic setting: A first approximation. Sedimentology, 28: 75-83.

Whiteman, A.J. (1982). Nigeria: Its petroleum Geology, Resources and Potentials, Graham and Trotman, London.

JJEES

JJEES (2019) 10 (4): 247-251
ISSN 1995-6681

Jordan Journal of Earth and Environmental Sciences

# Polychlorinated Biphenyls Residue in Citrus and Vegetables in the Jordan Valley, Jordan

Gaid AlRabadi[1], Farh Al-Nasir[2], Anwar Jiries[*3],
Rasha Al-Dmour[3], Osama Madanat[3], Saddam Al-Dalain[2]

*1Mutah University, Faculty of Agriculture, Jordan*
*2Al Balqa Applied University, Al-Shobak University College,-Jordan*
*3Mutah University, Faculty of Science, Jordan*

*Received 6 April 2019; Accepted 4 August 2019*

**Abstract**

In this study, four types of citrus fruits (Lemon, Orange, Mandarin, and Grapefruit) and four types of vegetables (eggplant, zucchini, cucumber, and tomato) irrigated with different types of water at three sites in the Jordan valley were evaluated for their polychlorinated biphenyl (PCBs) content.

The concentrations of six types of PCBs (PCB52, PCB101, PCB138, PCB153, PCB180, and PCB209) in the citrus fruits varied according to the type of the species and within each type.

The concentrations of PCBs in the citrus fruits were in the range of 2-13.8 ppb, 3.6-9.8 ppb, 11.0-138.0 ppb and 5.2-501.5 ppb for the grapefruit, orange, lemon, and mandarin, respectively. Although all citrus trees were irrigated with the same water, a big variation was observed with each fruit species suggesting other PCBs sources than the irrigation water; atmospheric deposition could, most probably, be a contamination pathway.

For the vegetables, the total PCBs concentrations were higher for the plants irrigated with the KTD water than those of the same plant species irrigated with mixed water which indicates that irrigation water and contaminated soils are the main sources of PCBs in the investigated vegetable types. This study has also found that the variation in the PCB levels in the fruits and vegetables irrigated with the same type of water is due to accumulation from other sources present in the environment rather than from the irrigation water.



**Keywords:** polychlorinated biphenyl, irrigation water, soil, citrus, vegetables.

## 1. Introduction

PCBs are a class of persistent organic pollutants (POPs) produced mainly by industry in the production of plasticizers, adhesives, and flame retardants among others (WHO / IPCS, 1993). The occurrence of some organic pollutants including PCBs in an aquatic environment is a major concern as they have been responsible for many health problems when existing above certain limits (Bakogluo et al., 2004, Ulrech, 2005). Therefore, they were banned from being produced or used by the Stockholm convention agreement 2001 (Stockholm convention, 2011). Although their use has been now largely phased out, but due to being highly resistant to breakdown, they still exist in the environment. The highly lipophilicity of these compounds causes their accumulation in the accessible food chains, therefore, many researches were done on their presence in the diets.

Human exposure to PCBs is risky, and that is why PCBs have been the target of many researches worldwide. Once PCBs are produced, they can be transported through the atmosphere and accumulate on other locations (Benanoue, 2009). PCBs can enter the food chains through different routes such as irrigation with polluted water (Al-Nasir and Batarseh, 2008, Shahalam et al., 1998) or when being transferred and deposited on fruits and vegetables.

There are many studies showing the uptake of PCBs by plants through irrigation with polluted water as well as plantation in contaminated soils. The accumulation of POPs in plants can vary due to different factors such as atmospheric pollution, leaf-morphology, and physiology (Franzaring and Van der Eerden, 2000).

In Jordan, many investigations showed that the irrigation water originating from the King Talal dam was within the acceptable international and national limits (Al-Omari et al., 2019 and Yahya et al., 2017). Fandi et al., 2009 maintains that the pollution tendencies of the surface waters of the KTD reservoir were attributed to high levels of organic pollutants. Al-Nasir and Batarseh, 2008 reported a PCBs residue in four types of vegetables (Okra, eggplant, paprika, and tomato). The uptakes of PCBs as well as other organic pollutants such as phenols and polycyclic aromatic hydrocarbons were dependent on the plant variety and plant part, and they showed different uptake concentrations.

The Jordan valley is known for its importance for food production in Jordan, and its products are partially exported to many countries around the world. Therefore, it is important to examine the contamination of the eatable parts of these products in terms of their PCBs content, for the reason that all previous investigations done in the area were on the fruit as a whole. Therefore, the present work is aimed at investigating the concentration of PCBs in irrigation water, soil, and the eatable parts of four types of citrus and vegetables irrigated with water of different sources to estimate its influence on these diets' contamination.

* Corresponding author e-mail: jiries57@hotmail.com.

## 2. Methodology

### *2.1 Study Area*

The investigation area is located in the Jordan valley near Deir-Alla village at the mouth of King Talal Dam (KTD) in the Jordan valley. The area is characterized by its arid hot climatic conditions with intensive agricultural activities where many types of vegetables and fruits are planted.

The water used for irrigation originates from three sources, namely: a) King Talal dam collecting water originating from small springs, surface runoff and effluents from treated wastewater of the Kherbet Alsamra. The water quality of this water source is known to have a high concentration of many pollutants such as heavy metals, PAHs and PCBs (Batarseh,et al., 2003). b) Fresh water with a very low pollutant content from the King Abdullah Canal (KAC) (Jiries et al., 2004). c) a mixture of these two types.

### *2.2 Site Selection*

The criteria of site selection are based on the type of water used for irrigation as mentioned earlier. The three selected sites are:

Site A: The area surrounding the KTD where the dam water is used without any modification for irrigation.

Site B: The area located to the north of Deir-Alla which receives only water from King Abdullah Canal without any impact of the KTD water.

Site C: The area located to the south of Deir-Alla where the irrigation water is a mixture of the KTD and the KAD water.

From site B, four types of eatable citrus plant species were selected (Lemon, grapefruit, orange, and mandarin). For sites A and C, four types of vegetables (eggplant, cucumber, squash, and tomato) from areas already planted, and on soil already irrigated with different types of water by the local farmers.

### *2.3 Sampling*

#### *2.3.1 Sample Collection*

Water: Thirty-six water samples were collected on a monthly basis over a period of one year representing the three types of irrigation water used in this study. Sampling of each site was done in triplicates for quality assurance.

Soil: Sixty soil samples (20 samples from each site) were collected from the investigated area at two depths, from the upper soil (0-15 cm) and from the lower soil (15-30 cm) as most of the roots exist at these depths.

Plant: For plants, only the eatable parts of the plants were collected from each site as these are the parts which may have a direct impact on human health. The samples were collected at the end of the growing period when the fruits and vegetables are ripe and ready to be eaten. Four kinds of pealed citrus fruits from site B and four types of vegetables from sites A and C were selected for this study.

#### *2.3.2. Sample Pre-treatment*

The collected water samples were acidified for pH=2 and filtrated via a vacuum filtration apparatus. A one-litter sample was transferred subsequent to the Solid Phase Extraction (SPE) HLB Qasis column (cartridge) using a varian SPE apparatus equipped with a vacuum pump purchased from (Varian, Australia). For the soil and plants, the samples were homogenized and stored at -20 Co until the time of analysis.

#### *2.3.3 Water Extraction*

After the passage of the water samples through the pre-treatment stage, the SPE column was pre-conditioned prior to use. The samples were first washed with 6ml of ethyl acetate, followed by 6ml of methanol; and finally with 6ml of HPLC water. After that, the samples were loaded to the cartridge, and the cartridge was washed with 6ml 5% methanol in water. The targeted compounds were eluted with 6ml of ethyl acetate, and dried with Na2SO4, and the elute was concentrated to a final volume via a nitrogen stream. Finally, the residue was stored in amber glass vials for analysis.

#### *2.3.4 Soil Extraction*

The wet homogenized samples containing 50g of soil material were placed into a 500ml Erlenmeyer flask. Extraction was carried out with 2:1 acetone/water mixture (after being adjusted to its moisture content) (v:v) overnight using a horizontal shaker at a shaking velocity of 220 cycle/min. The liquid/liquid partitioning was performed by adding 15g of NaCl and 100ml cyclohexane, and the mixture was shaken for one hour. The organic layer was decanted into a 250ml Erlenmeyer flask and dried over 15g sodium sulfate. 100 ml of the extract was evaporated and dissolved in 5ml of 1:1 ethylacetate and a cyclohexane mixture (v:v), (Al-Nasir and Batarseh, 2008).

#### *2.3.5 Plant Extraction*

The wet homogenized samples containing 100g of fruit materials were placed into a 500ml Erlenmeyer flask. Extraction was carried out with 100ml of acetone overnight using a horizontal shaker at a shaking velocity of 220 cycle/min. The liquid/liquid partitioning was performed by adding 15g of NaCl and 100ml cyclohexane, and the mixture was shaken for one hour. The organic layer was decanted into a 250ml Erlenmeyer flask and dried over 15g sodium sulfate. 100ml of the extract was evaporated and dissolved in 5ml of 1:1 ethylacetate and a cyclohexane mixture (v:v), (Al Nasirand Batarseh, 2008).

#### *2.3.6 Sample Cleanup*

The sample solvents were concentrated to near dryness using a rotary evaporator, and the trace of solvents was removed under a gentle nitrogen stream. The alumina was activated overnight at 180oC, then, it was partly deactivated with 2% H2O and shaken for two hours by a horizontal shaker. 10g of the deactivated alumina and 1.0g of dried anhydrous Na2SO4 were loaded on top of the chromatography column to separate the non–polar from the polar constituents of the sample matrix. The analyzed samples were transferred to the alumina Column and eluted with 50ml of n-hexane, then in a rotary evaporator and were concentrated in a gentle nitrogen stream. The sample was divided into four portions each of 1ml into a GC amber vial for analysis as shown in chart 3.2 representing the stage of sample cleaning.

### *2.4 Analysis*

A Schimadzu GC chromatograph model 2010 equipped with a 63Ni electron capture detector was used for the analysis of PCBs. A 30 m DB–5 fused silica capillary column with a 0.25 lm film thickness and a 0.32 mm inner diameter was

used for the quantification of organochlorine compounds (J & W Scientific, USA). Helium (grade 5.5) was employed as carrier gas (1 ml min_1) and nitrogen as make up gas (58 ml min_1). The oven temperature was programmed from 60 _C (1 min) to 160 _C (1 min) at 15 _C min_1, then to 220 _C (5 min) at 5 _C min_1, finally at 3 _C min_1 to 280 _C (10 min). The injector and detector temperatures were maintained at 250 _C and 300 _C, respectively. The splitless injection volume was 1 ll. The Schimadzu Post-Run software was used for data analysis and quantification.

## 3. Results and Discussion

As vegetables and citrus are the main products in the Jordan valley, their quality is of vital importance. To ensure the population health, knowledge of diet quality intake of certain persistent pollutants such as PCBs is of vital importance. [Grassi et al. 2010]. The PCBs residue in both vegetables and pealed citrus fruits in the investigated sites are given below.

### *3.1 Vegetables*

A total of forty-two vegetable samples were collected from the Jordan valley representing four types of vegetables and two types of irrigation water. The concentration of six types of PCBs (PCB52, PCB101, PCB138, PCB153, PCB180, and PCB209) in addition to total PCBs found in the respective vegetables were summarized in terms of minimum, mean, mean, and the percentage of the detected PCBs are shown in Table 1.

**Table 1.** PCBs concentrations in ppb for vegetables collected from sites A and C

| | PCB52 | PCB101 | PCB138 | PCB153 | PCB180 | PCB209 | Σ PCBs | PCB52 | PCB101 | PCB138 | PCB153 | PCB180 | PCB209 | Σ PCBs |
|---|---|---|---|---|---|---|---|---|---|---|---|---|---|---|
| | Tomato (Site C) n=8 | | | | | | | Tomato (Site A) n=8 | | | | | | |
| **Min** | 0.4 | 0.6 | BDL | BDL | BDL | 3.0 | 1.0 | 24.0 | 5.6 | BDL | 9.3 | 1.5 | 19.5 | 1.5 |
| **Max** | 9.2 | 6.0 | BDL | BDL | BDL | 26.9 | 30.6 | 24.0 | 7.9 | BDL | 9.3 | 1.5 | 19.5 | 51.4 |
| **Mean** | 3.4 | 2.4 | BDL | BDL | BDL | 13.4 | 13.4 | 24.0 | 7.1 | BDL | 9.3 | 1.5 | 19.5 | 22.6 |
| **Detection%** | 83 | 83 | ND | ND | BDL | 83 | ND | 20 | 20 | ND | 50 | 20 | 20 | ND |
| | Zucchini (Site C) n=8 | | | | | | | Zucchini (Site A) n=8 | | | | | | |
| **Min** | 5.4 | 18.4 | 0.6 | BDL | 1.0 | 6.8 | 1.6 | 1.7 | 4.5 | 2.8 | BDL | 0.8 | 0.7 | 7.3 |
| **Max** | 5.4 | 18.4 | 0.6 | BDL | 1.0 | 6.8 | 25.2 | 10.3 | 13.5 | 7.0 | BDL | 2.6 | 44.3 | 73.2 |
| **Mean** | 5.4 | 18.4 | 0.6 | BDL | 1.0 | 6.8 | 13.4 | 4.7 | 9.9 | 4.6 | BDL | 1.7 | 22.5 | 27.2 |
| **Detection%** | 20 | 20 | 20 | ND | 20 | 20 | ND | 80 | 60 | 60 | ND | 40 | 40 | ND |
| | Eggplant (Site C) n=8 | | | | | | | Eggplant (Site A) n=8 | | | | | | |
| **Min** | 0.1 | 7.3 | 0.2 | 0.8 | 0.1 | 0.2 | 1.3 | 2.7 | 11.6 | 5.5 | 13.7 | 1.8 | 1.1 | 13.4 |
| **Max** | 1.1 | 11.0 | 0.2 | 0.8 | 7.8 | 0.2 | 18.8 | 58.2 | 74.6 | 5.5 | 24.4 | 1.8 | 25.2 | 104.6 |
| **Mean** | 0.6 | 9.2 | 0.2 | 0.8 | 3.9 | 0.2 | 9.5 | 28.5 | 34.7 | 5.5 | 19.0 | 1.8 | 13.1 | 52.2 |
| **Detection%** | 40 | 40 | 20 | 20 | 40 | 20 | ND | 60 | 60 | 20 | 40 | 20 | 40 | ND |
| | Cucumber (Site C) n=8 | | | | | | | Cucumber (Site A) n=8 | | | | | | |
| **Min** | 0.1 | 0.5 | 0.3 | 0.4 | 0.2 | 0.3 | 0.4 | 3.7 | 0.5 | 0.1 | BDL | 5.5 | BDL | 0.5 |
| **Max** | 0.1 | 0.9 | 0.3 | 0.4 | 0.2 | 0.5 | 1.5 | 3.7 | 2.8 | 0.1 | BDL | 5.5 | BDL | 9.2 |
| **Mean** | 0.1 | 0.6 | 0.3 | 0.4 | 0.2 | 0.4 | 0.9 | 3.7 | 1.6 | 0.1 | BDL | 5.5 | BDL | 4.2 |
| **Detection%** | 14 | 43 | 14 | 14 | 43 | 57 | ND | 25 | 50 | 25 | ND | 25 | ND | ND |

*n represents The number of samples, BDL represents below detection limit, and ND represents Not Determined.*

There was a great variation in the types of PCBs among the vegetable types as well as in the total PCBs concentrations (the sum of individual PCBs in each sample) within each type of vegetable as well as between vegetable types and the irrigation water used. Generally, the total PCBs concentrations were significantly higher for the plants irrigated with KTD water than the same plant species irrigated with mixed water type. This indicates that water quality is the main source of PCBs in the investigated area. For vegetables irrigated with KTD, eggplant showed the highest sum of PCBs concentrations ranging from 13.4 to 104.6 ppb with a mean value of 52.2. On the other hand, cucumber showed the lowest concentration ranging from 0.4-1.5 ppb with a mean value of 0.9 ppb. The high variation in the PCBs residue in the different plant species could be attributed to the physiology of the plants rather than to the irrigation water and soil quality.

In general, the occurrence of different types of PCBs was not congener within each vegetable species as its occurrence and concentrations varied with the plant species at the same site. However, it can be confirmed that PCB52, PCB101 and PCB209 were the most detected PCBs in tomato samples irrigated with KTD as they were detected in more than 83% of the samples.

### *3.2 Citrus*

For citrus, a total number of twenty-one citrus samples were analyzed for six types of PCBs (PCB52, PCB101, PCB138, PCB153, PCB180, and PCB209) in grapefruit, orange, lemon and mandarin. A statistical summary (minimum, maximum and means) of individual PCBs concentrations as well as their sum for four types of citrus are presented in Table 2.

**Table 1.** PCBs concentrations in ppb for different types of citrus fruits collected from the investigated site

| | PCB52 | PCB101 | PCB138 | PCB153 | PCB180 | PCB209 | Σ PCBs | PCB101 | PCB138 | PCB209 | Σ PCBs |
|---|---|---|---|---|---|---|---|---|---|---|---|
| | Grapefruit n=5 | | | | | | | Orange n=5 | | | |
| **Min** | 0.1 | 0.1 | 0.1 | 1.1 | 0.7 | 0.1 | 2.0 | 1.0 | 1.9 | 0.7 | 3.6 |
| **Max** | 0.3 | 6.9 | 7.0 | 1.6 | 4.1 | 0.1 | 13.8 | 29.3 | 1.9 | 9.8 | 9.8 |
| **Mean** | 0.2 | 3.5 | 4.4 | 1.3 | 2.5 | 0.1 | 8.3 | 15.1 | 1.9 | 4.9 | 5.8 |
| **Detection %** | 40 | 40 | 80 | 40 | 80 | 20 | | 40 | 20 | 75 | |
| | Lemon n=5 | | | | | | | Mandarin n=6 | | | |
| | PCB52 | | PCB101 | PCB180 | PCB209 | Σ PCBs | PCB52 | PCB101 | PCB180 | PCB209 | Σ PCBs |
| **Min** | 7.5 | | 22.9 | 1.6 | 74.8 | 11.0 | 1.1 | 37.8 | 0.4 | 2.9 | 5.2 |
| **Max** | 20.2 | | 42.5 | 20.2 | 74.8 | 138.0 | 234.2 | 37.8 | 218.0 | 119.0 | 501.5 |
| **Mean** | 12.8 | | 32.7 | 7.9 | 74.8 | 128.2 | 62.2 | 37.8 | 73.8 | 30.0 | 109.6 |
| **Detection %** | 80 | | 40 | 60 | 20 | ND | 66 | 15 | 50 | 100 | ND |

*n represents The number of samples, BDL represents below detection limit, and ND represents Not Determined.*

Among the citrus samples, lemon showed a mean concentration higher than those of other analyzed citrus samples as its mean concentration was 128.2 ppb ranging from 11.0 to138.0 ppb, followed by mandarin with a mean concentration of 109.6 ppb ranging from 5.2 to 501.5 ppb, followed by grapefruit with a mean concentration of 8.3 ppb ranging from 2.0 to13.8 ppb. Orange showed the lowest concentration of 5.8 ppb ranging from 3.6 to9.8 ppb.

The types of detected PCBs in the analyzed samples varied according to the citrus species. For orange, only three PCBs were detected (PCB101, PCB138, and PCB209), whereas for lemon and mandarin, four types of PCBs were detected (PCB52, PCB101, PCB180, and PCB209). For grapefruit, all the analyzed PCBs were detected. This could be attributed to the physiology of the plant rather than to the environment which was the same for all of the citrus types including the large surface/content ratio of these different citrus species.

The concentration of PCBs in the citrus samples were much lower than that in the vegetables which is due to the sample preparation, as the citrus fruits were pealed before extraction which removed a high quantity of PCBs with the skin.

### *3.3 Irrigation Water*

PCBs were analyzed in twenty-four irrigation water samples (8 samples from each site). The results showed that only few PCBs were found in the irrigation water at low concentrations. At site A, only three types of PCBs were detected, PCB101 was found in only one sample at a concentration of 0.012 ppb, PCB138 was found in two samples at the concentrations of 0.01 and 0.035 ppb, and PCB153 was found in only one sample at a concentration of 0.004 ppb. For site B, only two samples showed a PCB content as it was 0.152 ppb from PCB101 and 0.08 ppb from PCB209. Site C showed a higher variety as four PCBs were detected in the irrigation water. Two out of eight samples showed a PCBs content. PCB101, PCB138, and PCB153 were detected at the concentrations of 0.017,0.062 and 0.019 ppb respectively in one sample. The other sample contained three types of PCBs (PCB101, PCB138 and PCB180) at the concentrations of 0.013, 0.059 and 0.012 ppb respectively. Therefore, the irrigation water is not the source of PCBs in the investigated sites.

### *3.4 Soil*

The concentration of PCBs collected from the three investigated site are summarized in Table 3 in terms of minimum, mean, median, and maximum percentages. Results showed that there is a variation in the abundance and concentration of PCBs among the sites as well as within each site. The highest concentration was found at site A with an average value of the sum of PCBs 108.7 ppb ranging from 9.9 - 373.4 ppb. The most frequent detected PCB was PCB101 as it was detected in all of the analyzed samples. Other PCBS were detected at different frequencies.

**Table 3.** PCBs concentrations in ppb for soils at sites irrigated with different types of irrigation water

| | PCB52 | PCB101 | PCB138 | PCB153 | PCB180 | PCB209 | Σ PCBs |
|---|---|---|---|---|---|---|---|
| **Soil (Site B) n=9** | | | | | | | |
| **Min** | 1.1 | 2.0 | 1.2 | 1.4 | 1.6 | 1.0 | 2.6 |
| **Max** | 34.4 | 7.0 | 1.6 | 4.6 | 1.6 | 1.0 | 15.3 |
| **Mean** | 7.6 | 4.8 | 1.4 | 3.0 | 1.6 | 1.0 | 8.3 |
| **Detection %** | 100 | 56 | 22 | 22 | 11 | 11 | ND |
| **Soil (Site A) n=7** | | | | | | | |
| **Min** | 5.1 | 5.6 | 2.0 | 1.2 | 0.1 | BDL | 9.9 |
| **Max** | 5.1 | 363.6 | 36.6 | 9.7 | 1.0 | BDL | 373.4 |
| **Mean** | 5.1 | 97.9 | 10.0 | 4.5 | 0.7 | BDL | 108.7 |
| **Detection %** | 14 | 100 | 72 | 57 | 57 | ND | ND |
| **Soil (Site C) n=7** | | | | | | | |
| **Min** | 0.7 | 0.4 | 2.8 | BDL | 0.3 | BDL | 0.4 |
| **Max** | 3.9 | 176.5 | 94.0 | BDL | 1.5 | BDL | 107.0 |
| **Mean** | 1.7 | 40.0 | 48.4 | BDL | 0.9 | BDL | 24.2 |
| **Detection %** | 57 | 86 | 29 | ND | 43 | ND | ND |

*n represents The number of samples, BDL represents below detection limit, and ND represents Not Determined.*

The lowest PCBs were detected at site B, as the source of water is mainly fresh groundwater resources. The concentration at this site ranged from 2.6 to 15.3 ppb with an average value of 8.3 ppb. PCB52 was the most detected type as it existed in all of the analyzed samples, whereas PCB180 and PCB209 were detected in only one sample out of the nine analyzed samples.

The concentration of PCBs at site C showed values ranging between site A and site B as the irrigation water is a mixture of the water at site A and site B. The PCBs concentration at this site ranged from 0.4 – 107.0 with an average value of 24.2 ppb. The most frequent PCB was BCB101 which was detected in 86% of the analyzed samples.

The PCBs concentrations in some of the soil samples collected from site A were much higher than those collected from industrialized cities like Moscow. They ranged from 3.1 to 42 ppb [Wilcke et al., 2006], however, the other investigated sites were comparable with the PCBs concentrations in soils irrigated with wastewater at other sites in the world such as Shenyang, China where their concentrations ranged from 4.4-20.14 ppb [Song et al., 2006].

Therefore, it can be concluded that the main source of PCBs in the investigated area was the irrigation water as it was highest at site A and lowest at site B.

## 4. Conclusions

The concentrations of six target PCBs were found to vary according to the type of fruits as well as with the irrigation water. The different plant types showed different concentrations of various PCBs. Among the citrus fruits, lemon showed the highest concentration and orange was the lowest among the analyzed citrus samples. For vegetables, the impact of irrigation water was clear as vegetables irrigated with KTD water showed higher PCBs values than those irrigated with the mixed water. Variation within each type of the target fruits and vegetable was noticed indicating that irrigation water was not the main source of PCBs but other contamination pathways existing in the environment including the atmospheric deposition.

## Acknowledgement

This work was funded by the Research and Innovation Support Fund/ Ministry of Higher Education and Scientific Research, Amman-Jordan, and the authors gratefully acknowledge the funding support.

## References

Al Nasir, F., and Batarseh, M. (2008). Agricultural reuse of reclaimed water and uptake of organic compounds: Pilot study at Mutah University wastewater treatment plant. Jordan Chemosphere, 72: 1203–1214.

Al-Omari, A., Farhan, I., Kandakji, T., Jibril, F. (2019). Zarqa River pollution: impact on its quality, Environ Monit Assess., 191(3):166.

Bakoglu, M., Karademir, A., Ayterk, S. (2004). An evaluation of the occupational health risks to workers in a hazardous waste incinerator. J. Occup. Health, 46(2): 156–164.

Batarseh, M., Kreuzig, R., Al-Nasir, F., Bahadir, M. (2003). Residue Analysis of Organic Pollutants in Sediments from the Amman/Zarqa Area in Jordan. Part II: Organchlorine Compounds. Fresen. Environ. Bull., 12(9): 979–983.

Benanoue, L. (2009). Characterization of volatile and semi-volatile compounds in wasteland fill leaches (2009). Anal. Bioanal. Chem. 393: 1043–1054.

Fandi, K., Qudsieh, I., Muyibi, S., Massadeh, M. (2009). Water Pollution Status Assessment of King Talal Dam, Jordan. Advances in Environmental Biology, 3(1): 92-100.

Franzaring, J and van der Eerden, L. (2000). Accumulation of airborne persistent organic pollutants (POPs) in plants Basic and Applied Ecology, 1(1): 25-30.

Grassi P, Fattore, E., Generoso, C., Fanelli, R., Arvati, M., Zuccato, E. (2010). Polychlorobiphenyls (PCBs), polychlorinated dibenzo-p-dioxins (PCDDs) and dibenzofurans (PCDFs) in fruit and vegetables from an industrial area in northern Italy. Chemosphere;79(3): 292-8.

Jiries, A., Ziadat, O., Lintelmann, J. (2004). The Quality of Drinking Water at Source of West Amman-Jordan. Water International, 29(3): 392-397.

Shahalam, A., Zahra, B.M.A., Jaradat, A. (1998). Wastewater irrigation effect soil, crop and environment: a pilot scale study at IRBID, Jordan. Water Air Soil Pollut., 106: 425–445.

Song, Y.F., Wilk, B.M., Song, X.Y., Gong, P., Zhou, Q.X.,Yang, G.F. (2006). Polycyclic aromatic hydrocarbons (PAHs), polychlorinated biphenyls (PCBs) and heavy metals (HMs) as well as their genotoxicity in soil after long-term wastewater irrigation. Chemosphere, 65(10):1859–1868.

Urlich, P. (2005). Atmospheric aerosols: composition, transformation, climate and health effects. Angew. Chem., 44 (46): 7520–7540.

WHO/IPCS. (1993). Principles for Evaluation of Chemical Effects of the Aged Population. Environmental Health Criteria 144. Geneva: WHO.

Wilcke, W., Martin, K., Grigorij, S.A., Fokin, D., Kaupenjohann, M. (2006). Polychlorinated biphenyls (PCBs) in soils of the Moscow region: concentrations and small-scale distribution along an urban-rural transect. ,Environmental Pollution, 141(2): 327 – 335.

Yahya, R., Tahboub, Mohammad F. Zaater, Dima F. Khater (2017). Semi-volatile organic pollutants in Jordanian surface water, Arabian Journal of Chemistry, 10, 3318-3323

JJEES

JJEES (2019) 10 (4): 252-255
ISSN 1995-6681

Jordan Journal of Earth and Environmental Sciences

# Antimicrobial Activity of Momordica cochinchinensis Seeds and Seeds Aril Extract

Qays Alkhafaji[1], Iqbal Mohammed[2], Shurook Saadedin[3], Salwa Al-Awadei[4], Taif Abedulhussein[3], Ghada AL-Jussani[5]

[1]Kamal al-Samarrai hospital, Fertility Center, infertility treatment and IVF, Iraq
[2]Ministry of Agriculture, office –Horticulture, Iraq
[3]University of Baghdad, Institute of Genetic Engineering and Biotechnology for Postgraduate Studies, Iraq
[4]University of Al-Nahrain, College of Applied Biotechnology, Iraq
[5]The Hashemite University, Faculty of Medicine, Jordan

Received 16 July 2019; Accepted 2 September 2019

**Abstract**

In attempt to investigate the antimicrobial activity of the Gac fruit (Momordica cochinchinensis) seeds' aril, seed extract, and crude seed aril oil against some gram-positive and gram-negative bacteria using microdilution assay, seed arils were extracted using ethanol\ethylacetate (6:4), aqueous extraction of the seeds and crude seed aril oil were used. This study shows that the extract of seed arils exhibited the best antimicrobial activity. The minimum inhibitory concentration (MIC) of the ethanol\ ethylacetate ranges between 0.391 and 3.125mg/ml. The extract showed significant inhibition against all bacteria Bacillus subtilis; Staphylococcus aureus; Micrococcus luteus; Klebsiella pneumonia, and Enterobacter aerogenes. The maximum antibacterial activities were observed against S. aureus by the seed aril extract (0.391 mg/ml), while the crude oil showed no antimicrobial activity in this study. The seed aqueous extract showed inhibition against S. aureus only with the concentration of (12.5 mg/ml). Therefore, the results of this study show that the antibacterial activity of the Gac fruit seed aril extracts can be beneficial for the development of alternative antibacterial sources.



**Keywords:** Antimicrobial activity, G+ bacteria, G- bacteria, Carotenoids, (Momordica cochinchinensis), Microdilution assay.

## 1. Introduction

Momordica cochinchinensis Spreng (gac) from the Cucurbitaceae family is commonly called "Gac fruit" which is an edible plant used as herbal medicine. This plant grows in tropical Asian countries, including Vietnam, Laos, Thailand, China, Bangladesh, and India (Kubola and Siriamornpun, 2011; Kubola et al., 2013). Fruits of M. cochinchinensis are big, denselyaculaeate, green in color and when ripe, become dark orange or red. It is composed of two main parts: a mesocarp and an endocarp. The mesocarp, which makes up nearly 50% of the weight of the fruit, is 1/2" thick, spongy, and orange in color. The endocarp is composed of the soft and sticky arils, with the thickness of about 1-3 mm. This part usually covers the black seed and accounts for around 25% of the fruit weight (Nguyen, 2014; Vuong, 2000).

The Gac plant is high in β-carotene and lycopene, and can be cultivated from seeds or root tubers. It grows as devious vines, and the fruit is a rich nutrient source (Tinrat, et al., 2014).

In recent years, antimicrobial resistance has become a major global problem (Raghunath, 2008). Posing an ever-increasing therapeutic problem. One of the methods to reduce the resistance to antibiotics is by using antibiotic resistance inhibitors from plants. Among the factors contributing to microbial resistance are the indiscriminate use of antimicrobial agents by both healthcare professionals and patients. Therefore, there is a need for developing new antimicrobials drugs ( Okeke, et al. 1999; Mourad, et al., 1993). Scientific evidence supports the hypothesis that plants contain bioactive compounds with medical applications. Recent advancements in drug discanaloovery is based on designing compounds that are analogous to natural plant compounds. (Ghosh, et al., 2012; Begum, et al., 2012; Abreu, et al., 2012).

Innuna (2013) found that the seed aril ethanolic, ether, and aqueous extract had no effect on S. aureus, while the ethanolic extract had a high inhabitation effect on Micrococcus luteus, (Innuna, 2013).

Tinrat et al. (2014) found that E. coli and P. aerginosa were the most susceptible to seed aril ethanoic extracts with a MIC value of 3.125 mg/ ml, while the same extract had a higher MIC value of 6.25 mg/ ml against S. aureus .

Tinrat and Sila-Asna, (2016) studied seed arils' different extracts and oil and found that the hexane extract was significantly better than the acetone and the methanolic extracts with a MIC value of 1.56- 12.50 mg/ml, MIC was 3.125 mg/ml for S. aureus and 1.56 mg/ml for K. pneumoniae, while the MIC for the oil was 100 mg/ml for S. aureus, and there was no effect on K. pneumoniae (Tinrat and Sila-Asna, 2016).

The fruit of M. cochinchinensis contains various bioactive compounds including flavonoids such as rutin, myricetin, luteolin, quercetin, Apigenin, and kaempferol (Raghunath, 2008). carotenoids such as α, β-carotene,zeaxanin, lycopene, lutein, and phenolic compounds such as gallic acid, vanillic acid, ferulic acid, caffeic acid, and proto catechuic acid . The

* Corresponding author e-mail: ghadahmed2000@gmail.com

aim of this study is to evaluate the antibacterial activity of seed arils, seed extract, and crude seed aril oil of the Gac fruit using microdilution assay.

## 2. Materials and Methods

### *2.1 Preparation of Plant Extract*

*2.1.1 Plant Materials:*

The Momordica cochinchinensis seed aril oil with 0.4% lycopene. The Gac seeds were imported from Sabiwe Vietnam Co., Ltd- Vietnam. Seed arils from the Gac fruit were cultivated in Iraq by the researchers.

*2.1.2 Materials Extraction*

The seeds of Gac fruit were ground into a fine powder. Then, 50 g were weighed. The powder was boiled in one liter of water for one hour. The extract was filtrated, and the aforementioned step was repeated twice with the residue. All of the filtrated collection was mixed together. The extract was dried to powder using the Minispray Dryer B-290\ Switzerland modified method.

The seeds' aril was prepared and extracted with Ethanol: Ethyl acetate (6:4v/v) according to the procedures of Saadedin (Saadedin, et al., 2017).

### *2.2 Test Microorganisms*

The antimicrobial activity of the Gac fruit extracts were tested against five bacterial strains (B.subtilis ATCC 6633, S. aureus ATCC 25923, M. luteus ATCC 10240, E. aerogenes ATCC 13048, and K. pneumoniae ATCC 31488).

### *2.3 Preparation of the Inoculum:*

Stock bacterial cultures were maintained at room temperature for two hours. Each strain was streaked on a Müller-Hinton agar plate, and incubated at 37 ºC for twenty-four hours. The inoculum was prepared by emulsifying a minimum of three colonies from those plates in sterile 0.9% NaCl (w/v) till $10^8$ colony forming units (CFU) per ml (0.5 McFarland scale) are formed. For the agar dilution assays, the suspensions were diluted with sterile 0.9% NaCl (w/v) until they reach $10^7$ CFU per ml (working bacterial suspensions) (National Committee for Clinical Laboratory Standards, 2000).

### *2.4 Antibiotics*

The antibiotics were prepared by dissolving standard antibacterial powders of tetracycline from Sigma and vancomycine from Lilly in dimethylsulphoxide (DMSO) (Merck) (Tinrat, 2014).

### *2.5 Sterilization*

The Gac fruit extracts and antibiotics were filtered through a 0.22-l µm membrane filter before use for sterilization (Sousa, et al., 2007).

### *2.6 Minimum Inhibitory Concentration (MIC) Determination*

The antibacterial activity of different parts of the Gac friut extracts was studied using a microdilution method according to the method of (Tinrat, 2014), and MIC values were determined for the bacterial strains. The extracts were dissolved in 10% DMSO, and diluted with a culture broth to a concentration of 100 mg/ml. Further two-fold serial dilutions were performed by the addition of a culture broth to reach the required concentrations18. Ten dilutions (100 - 0.195 mg/ml) were prepared from each extract in test tubes. Then, 0.5 ml of a bacterial suspension ($10^7$ CFU/mL) of the pathogenic strains was added to each concentration of the extracts. The same tests were done at the same time for growth control (Nutrient Broth + inoculums) and sterility control (Nutrient Broth + test sample) and DMSO.

100 µl of each dilution was distributed in 96-well plates, as well as a sterility control and a growth control and antibiotics. All experiments were performed in triplicate and the microdilution 96-well plates were incubated at 37ºC for twenty-four hours. The well with the least concentration of the extract that completely inhibits the growth after twenty-four hours of incubation was recorded as the MIC. The growth of pathogenic strains was identified by optical density (ELISA reader, CLX800-BioTek Instruments). The results were expressed in (mg/ml).

## 3. Results and Discussion

### *3.1 Antimicrobial Activities of Plant Extracts by MIC*

The antimicrobial activities of the Ethanol\ethyl acetate extracts of M. cochinchinensis against five bacterial species were evaluated by observing the microdilution method. The antimicrobial activities of the extracts are shown in Table 1. It was found that all Ethanol\ethyl acetate extracts showed antimicrobial activity against all five bacterial strains with MIC values varying from 0.391 to 3.125 mg/ml . Among the gram-positive ones, the ethanol\ethyl acetate extract of aril had the lowest MIC value (0.391mg/mL) against S. aureus ATCC 25923, and among the gram- negative ones, the lowest MIC value was (1.563mg/mL) against K. pneumoniae ATCC 31488. On the basis of MIC values, S. aureus ATCC 25923, B. subtilis ATCC 6633, M. luteus ATCC 10240 were more sensitive to the extract than E. aerogenes ATCC 13048, K. pneumoniae ATCC 31488. The seed water extract had no microbicidal activity against all pathogenic strains except S. aureus ATCC 25923 with MIC values of 12.5 mg/ml. The MIC values for tetracycline were found at a concentration of 2.0-3.0µg/ml, while that of vancomycine was between 3.125 and 11.12 µg/ml.

**Table 1.** MIC of (Momordica cochinchinensis) extracts against tested microorganisms by microdilution assay.

| Momordica cochinchinensis | Solvent Fraction | | MIC (mg/ml) | | | |
|---|---|---|---|---|---|---|
| | | *Bs+* | *Sa+* | *Ml+* | *Ea-* | *Kv -* |
| **Seeds' aril** | Ethanol\ethylacetate(6:4) | 0.781 | 0.391 | 0.781 | 3.125 | 1.563 |
| **Seed** | aqueous | No effect | 12.5 | No effect | No effect | No effect |
| **Seeds' aril oil** | Crude | No effect | No effect | No effect | No effect | No effect |
| **Tetracycline** | - | 2.32 | 2.0 | 2.34 | 2.71 | 3.0 |
| **vancomycine** | - | 7.89 | 3.125 | 8.01 | 11.12 | 7.58 |

*(B s= Bacillus subtilis); (S a= Staphylococcus aureus); ( Ml= Micrococcus luteus); (Kv= Klebsiella pneumoniae) and (Ea) Enterobacter aerogene*

A comparison of the susceptibility of the extracts towards bacterial strains, Figure (1), shows that S. aureus appeared to be more susceptible to aril extracts than the other strains tested. The different cell-wall composition of each species may be responsible for the different antimicrobial susceptibilities. The cell wall of S. aureus (gram positive bacteria) is composed of peptidoglycan layers combined with the teichoic acid molecules. In gram-negative cell wall, the peptidoglycan layer is much thinner, and there is no teichoic acid. Moreover, an outer membrane closely overlies the peptidoglycan layer so that the membrane and layer comprise the cell wall (Alcamo, 2001).

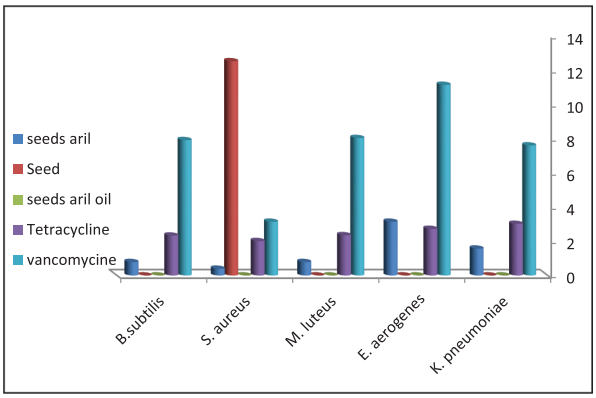


**Figure 1.** Comparison of Antimicrobial Activities of seeds' aril, aqueous seed extract, crude oil and antibiotics against different microorganisms. MIC values varying from 0.391 to 3.125 mg/ml for the plant extract and 2.0-3.0µg/ml, for tetracycline, while that of vancomycine was 3.125 to 11.12 µg/ml.

The data of this study clearly show that the Gac seed aril extract had antibacterial activity against both types of bacteria. The MIC values show that the antibacterial activity depends on the extract concentration. The ethanol\ethyl acetate extracts may contain effective compounds such as asluteolin, quercetin, apigenin, and kaempferol [14] which showed strong antibacterial proparties against a broad range of pathogenic strains[13]. This finding comes in agreement with other studies showing that the ethanolic extract from other species of Cucurbitaceae has antimicrobial activities (Tang, et al., 2010; Badmanaban and Patel, 2009; Bhattacharya, et al., 2010; Kumar and Kammaraj, 2010).

## 4. Conclusions

The antibacterial activity of different extracts of Momordica cochinchinensis Spreng. (Gac fruit) was evaluated using the minimum inhibitory concentration (MIC) method. The seed aril extraction with ethanol\ ethyl acetate showed good activity against the five tested pathogenic strains, including gram-positive and gram-negative bacteria. Staphylococcus aureus ATCC 25923 had the most susceptibility to this extract, while there was no effect of the seed aril crude oil. The aqueous seed extract showed activity against Staphylococcus aureus ATCC25923 only. On the basis of these data, and the data of other researchers, it becomes clear that the activity of the extracts largely depends on the type of the solvent used. This study supports the idea that the Momordica cochinchinensis fruit is likely to be a new antimicrobial source for the pharmaceutical industry.

## Acknowledgement

In this work, the authors would like to thank the Hamdi Mango Center for Scientific Research (HMCSR)/ Department of Cell Line and Culture, University of Jordan for their assistance, guidance, and hosting the research activities within their facilities.

## References

Abreu, A.C., McBain, A.J., Simoes, M. (2012). Plants as sources of new antimicrobials and resistance-modifying agents, Nat. Prod. Rep., 29: 1007–1021.

Alcamo, I.E. (2001). Fundamentals of microbiology. Jones and Bartlett Publishers, Inc., New York, 6th edition.

Badmanaban, R., and Patel, C.N. (2009). Study on anthelmintic and antibacterial activity of the leaf extracts of Lagenaria siceraria. Journal of Global Pharma Technology, 2 (4): 66-70.

Begum, S., Naqvi, S.Q.Z., Ahmed, A., Tauseef, S., Siddiqui, B.S. (2012). Antimycobacterial and antioxidant activities of reserpine and its derivatives, Nat. Prod. Res., 26: 2084–2088.

Bhattacharya, B., Samanta, M. Pal P., Chakraborty, S., Samanta, A. (2010). In vitro evaluation of antifungal and antibacterial activities of the plant Coccinia grandis (L.) voigt (Family-Cucurbitaceae). Journal of Phytology. 2: 52-57.

Ghosh, S., Chisti, Y., Banerjee, U.C. (2012). Production of shikimic acid. Biotech. Advances, 30: 1425–1431.

Innuna, A. (2013) Antimicrobial activity of Gac (Momordica cochinchinensis), Proceeding, Science and Engineering, (2013) 1-6.

Kubola, J., and Siriamornpun, S. (2011). Phytochemical and antioxidant activity of different fruit fraction (Peel, pulp, aril and seed) of thai gac (Momordica cochinchinensis spreng). Food Chemistry. 127(3): 1138-1145.

Kubola, J., Meeso, N., Siriamornpun, S. (2013). Lycopene and beta carotene concentration in aril oil of gac (Momordica cochinchinensis Spreng) as influenced by aril-drying process and solvents extraction Food Research International. 50: 664-669.

Kumar, S.S., and Kammaraj, M. (2010). Analysis of phytochemical constituents and antibacterial activities of Cucumis anguri L. against clinical pathogens. American-Eurasian Journal of Agricultural and Environmental Sciences, 7: 176-178.

Mourad, A.S., Metwally, M., Nour, E.L., Deen, A., Threlfall, E.J., Rowe, B., Mapes T., Hedstrom, R., Bourgeois, A.L., Murphy, J.R. (1993). Multiple-drug resistant Salmonella typhi. Clin and Infect Dis., 17(1):135-136.

National Committee for Clinical Laboratory Standards (2000). Methods for Dilution Antimicrobial Susceptibility Tests for Bacteria That Grow Aerobically; Approved Standard Fifth Edition. NCCLS document M7-A5. NCCLS: Wayne, PA, USA.

Nguyen, P.M. (2014). Investigation the ratios of antioxidant supplementation into the mixture of GAC (Momordica Cochinchinensis spreng) and carrier to get the highest total carotenoid content during drying. International Journal of Multidisciplinary Research and Development, 1(3): 34-40

Okeke, I.N., Lamikaure, A., Edelman, R. (1999). Socioeconomic and Behavioural Factors Leading to Acquired Bacterial Resistance to Antibiotics in Developing Countries. EmergInfect Dis., 5(1): 1-9

Raghunath, D. (2008). Emerging antibiotic resistance in bacteria with special reference to India. J Biosci., 33(4): 593-603.

Saadedin, S.M. K., Mohammed, I.H., Abdullah, S.J. (2017). Solvents extraction efficiency for lycopene and β-carotene of GAC fruit (Momordica cochinchinensis, Spreng) cultivated in Iraq. Bioscience Research, 14(4): 788-800.

Sousa, M., Ousingsawat, J., Seitz, R., Puntheeranurak, S., Regalado, A., Schmidt, A. (2007). An extract from the medicinal plant Phyllanthus acidus and its isolated compounds induce airway chloride secretion: a potential treatment for cystic fibrosis. Mol Pharmacol, 71: 366-76.

Tang, J., Meng, X. , Liu, H., Zhao, J., Zhou, L., Qiu, M., Zhang, X., Yu, Z., Yang, F. (2010). Antibacterial activity of sphingolipids isolated from the stems of cucumber (Cucumis sativus L.). Molecules, 15: 9288-9297.

Tinrat, S. (2014) Comparision of antioxidant and Antimicrobial activities of unripe and ripe fruit extracts of Momordica cochinchinensis Spreng (Gac fruit). Int. J. Pharm. Sci. Rev. Res., 28(1): 75-82.

Tinrat, S., Akkarachaneeyakorn, S., Singhapol, C. (2014). Evaluation of antioxidant and antimicrobial activities of Momordica Cochinchinensis Spreng (Gac fruit) ethanolic extract. International Journal of Pharmaceutical Sciences and Research. 5(8): 3163-3169.

Tinrat, S., and Sila-Asna, M. (2016) Antimicrobial and synergistic effects with antibiotics of Momordica cochinchinensis Spreng (Gac fruit) aril against pathogenic bacteria, Int. J. Pharm. Sci. Rev. Res., 39(2): 286-294

Vuong, L.T. (2000). Underutilized β-carotene-rich crops of Vietnam. Food Nut.Bull., 21: 173-181.

المملكة الأردنية الهاشمية


صندوق دعم البحث العلمي


الجامعة الهاشمية

# المجلة الأردنية
# لعلوم الأرض والبيئة

# JJEES

مجلة علمية عالمية محكمة

المجلد (١٠) العدد (٤)

http:// jjees.hu.edu.jo/

ISSN 1995-6681

# المجلة الأردنية لعلوم الأرض والبيئة

## مجلة علمية عالمية محكمة

**المجلة الأردنية لعلوم الأرض والبيئة: مجلة علمية عالمية محكمة ومفهرسة ومصنفة، تصدر عن عمادة البحث العلمي في الجامعة الهاشمية وبدعم من صندوق البحث العلمي - وزارة التعليم العالي والبحث العلمي، الأردن.**





### ترسل البحوث إلكترونيا إلى البريد الإلكتروني التالي:

**رئيس تحرير المجلة الأردنية لعلوم الأرض والبيئة**

**jjees@hu.edu.jo**



**لمزيد من المعلومات والأعداد السابقة يرجى زيارة موقع المجلة على شبكة الانترنت على الرابط التالي:**

**www.jjees.hu.edu.jo**

المملكة الأردنية الهاشمية صندوق دعم البحث العلمي الجامعة الهاشمية

# JJEES

## المجلة الأردنية لعلوم الأرض والبيئة

المجلد (١٠) العدد (٤)

مجلة علمية عالمية محكمة تصدر بدعم من صندوق دعم البحث العلمي

ISSN 1995-6681 jjees.hu.edu.jo كانون الأول ٢٠١٩